PREPARATION OF POROUS MATERIAL MCM-41 AND ACTIVATED CARBON AS NICKEL CATALYST SUPPORTS FOR *n*-BUTANOL SYNTHESIS

Krittanun Deekamwong

A Thesis Submitted in Partial Fulfillment of Requirements for the Degree of Master of Science in Chemistry

Suranaree University of Technology

Academic Year 2015

การเตรียมวัสดุรูพรุน MCM-41 และถ่านกัมมันต์เพื่อเป็นตัวรองรับตัวเร่งปฏิกิริยานิกเกิลสำหรับการสังเคราะห์ *n*-บิวทานอล

นายกฤตนันท์ ดีคำวงค์

วิทยานิพนธ์นี้เป็นส่วนหนึ่งของการศึกษาตามหลักสูตรปริญญาวิทยาศาสตรมหาบัณฑิต

สาขาวิชาเคมี

มหาวิทยาลัยเทคโนโลยีสุรนารี

ปีการศึกษา 2558

PREPARATION OF POROUS MATERIAL MCM-41 AND ACTIVATED CARBON AS NICKEL CATALYST SUPPORTS FOR *n*-BUTANOL SYNTHESIS

Suranaree University of Technology has approved this thesis submitted in partial fulfillment of the requirements for a Master's Degree.

Thesis Examining Committee

(Asst. Prof. Dr. Sanchai Prayoonpokarach)

Chairperson

(Assoc. Prof. Dr. Jatuporn Wittayakun)

Member (Thesis Advisor)

SUPUNNEE J.

(Dr. Supunnee Junpirom)

Member

Sirinuch Loiha

(Dr. Sirinuch Loiha)

Member

(Prof. Dr. Sukit Limpijumnong)

Vice Rector for Academic Affairs and Innovation

(Prof. Dr. Santi Maensiri)

Dean of Institute of Science

กฤตนันท์ ดีคำวงค์ : การเตรียมวัสดุรูพรุน MCM-41 และถ่านกัมมันต์เพื่อเป็นตัวรองรับตัวเร่งปฏิกิริยานิกเกิลสำหรับการสังเคราะห์ *n*-บิวทานอล (PREPARATION OF POROUS MATERIAL MCM-41 AND ACTIVATED CARBON AS NICKEL CATALYST SUPPORTS FOR *n*-BUTANOL SYNTHESIS) อาจารย์ที่ปรึกษา : รองศาสตราจารย์ ดร.จตุพร วิทยาคุณ, 114 หน้า

วิทยานิพนธ์ฉบับนี้ประกอบไปด้วยงานวิจัยหลัก 4 หัวข้อ ได้แก่ 1) การสังเคราะห์แบบไฮโดรเทอร์มัลและพิสูจน์เอกลักษณ์ของ MCM-41 ที่ประกอบไปด้วยซิลิกอน ([Si]MCM-41) ภายใต้คลื่นไมโครเวฟ 2) การนำ CTA^+ ออกมาจาก [Si]MCM-41 3) การเตรียมถ่านกัมมันต์เพื่อใช้เป็นตัวรองรับตัวเร่งปฏิกิริยา 4) การสังเคราะห์และพิสูจน์เอกลักษณ์ของตัวเร่งปฏิกิริยาบนตัวรองรับเพื่อนำไปใช้สังเคราะห์ *n*-บิวทานอล จากเอทานอล

การศึกษาส่วนแรกเกี่ยวกับการสังเคราะห์ [Si]MCM-41 ภายใต้คลื่นไมโครเวฟ โดยมีอัตราส่วนของ CTAB:SiO_2 กับอัตราส่วนของ NaOH:SiO_2 และเวลาในการตกผลึกที่แตกต่างกันเพื่อเพิ่มคุณภาพของ [Si]MCM-41 จากการทดลองพบว่าปัจจัยที่กล่าวมาข้างต้นนั้นส่งผลให้การสังเคราะห์ด้วยอัตราส่วน 3.34SiO2: 4.46NaOH: 1CTAB ภายใต้คลื่นไมโครเวฟเป็นระยะเวลา 90 นาที มีโครงสร้างแบบเฮกซะกอนัลเรียงตัวอย่างเป็นระเบียบ พื้นที่ผิวสูงและอนุภาคขนาดเล็ก จากการวิเคราะห์ด้วยเทคนิคการเลี้ยวเบนของรังสีเอกซ์ (XRD) การดูดซับและคายซับของแก๊สไนโตรเจน เทคนิคทางความร้อน (TGA) และการกระเจิงแสง (DLS) ตามลำดับ นอกจากนี้เมื่อเปรียบเทียบขนาดอนุภาคของ [Si]MCM-41 ที่สังเคราะห์ภายใต้คลื่นไมโครเวฟจะให้ขนาดเล็กกว่า [Si]MCM-41 ที่สังเคราะห์ภายใต้ความร้อนจากเตาอบทั่วไป

การศึกษาส่วนที่สองเพื่อที่จะลดการใช้พลังงานในการกำจัด CTA^+ จาก [Si]MCM-41 ที่สังเคราะห์ได้ โดยศึกษาบทบาทของตัวกลางในการแลกเปลี่ยนไอออน ชนิดของสารละลายเกลืออุณหภูมิและเวลาในการแลกเปลี่ยนภายใต้การสั่นของคลื่นอัลตราโซนิก ซึ่งพบว่าการแลกเปลี่ยนไอออนด้วยเกลือของแอมโมเนียมที่อุณหภูมิ 30 °C ในเวลา 15 นาทีให้ประสิทธิภาพในการกำจัด CTA^+ สูงมากกว่า 70 % และไม่ทำลายโครงสร้าง [Si]MCM-41 ด้วยการวิเคราะห์ด้วย XRD และ TGA นอกจากนี้การนำ CTA^+ กลับคืนมาจากสารละลายที่ได้จากการสกัดโดยแลกเปลี่ยนไอออนมาแล้วข้างต้นและจากสารละลายในขั้นตอนการสังเคราะห์ [Si]MCM-41 แสดงให้เห็นว่า CTA^+ ที่นำกลับมาได้มีองค์ประกอบอื่นที่ไม่ต้องการ

การศึกษาส่วนที่สามเกี่ยวกับการเพิ่มตำแหน่งความเป็นกรดในถ่านกัมมันต์ของต้นตะขบ (*M. calabura*) ที่คาดการณ์ว่าเป็นตำแหน่งที่ใช้ดูดซับตัวเร่งปฏิกิริยานิกเกิล ทั้งนี้หมู่ฟังก์ชันกรด คุณลักษณะทางพื้นผิวและเสถียรภาพทางความร้อนของตัวอย่างที่เตรียมได้สามารถพิสูจน์ได้ด้วยเทคนิคอินฟราเรดสเปกโทรสโกปี (FTIR) การดูดซับและคายซับของแก๊สไนโตรเจน และ TGA ซึ่งพบว่าตำแหน่งความเป็นกรดเพิ่มขึ้นได้เมื่อผ่านกระบวนการกระตุ้นทางกายภาพภายใต้บรรยากาศแก๊สคาร์บอนไดออกไซด์และภายใต้บรรยากาศแก๊สออกซิเจนตามลำดับ

การศึกษาส่วนสุดท้ายเกี่ยวกับการเตรียมตัวเร่งปฏิกิริยานิกเกิลบนตัวรองรับ [Si]MCM-41 และถ่านกัมมันต์ที่ผ่านการดัดแปรและพิสูจน์เอกลักษณ์ด้วยเทคนิค XRD เทคนิคการคายซับตามอุณหภูมิของแก๊สแอมโมเนียและคาร์บอนไดออกไซด์ และเทคนิคการคายซับตามอุณหภูมิรีดักชันแบบผันกลับ จากนั้นนำมาทดสอบเร่งปฏิกิริยา Guerbet พบว่าตัวเร่งปฏิกิริยาที่สังเคราะห์ขึ้นให้ผลการเร่งปฏิกิริยาต่ำและไม่จำเพาะต่อ *n*-บิวทานอล อย่างไรก็ตาม จากผลการทดลองแสดงให้เห็นว่าการมีอยู่ของตำแหน่งกรด/เบสและโลหะภายในตัวเร่งปฏิกิริยาเดียว สามารถเพิ่มประสิทธิภาพการเร่งปฏิกิริยานี้ได้ประมาณ 2 เท่า

สาขาวิชาเคมี ลายมือชื่อนักศึกษา_____

ปีการศึกษา 2558 ลายมือชื่ออาจารย์ที่ปรึกษา_____

KRITTANUN DEEKAMWONG : PREPARATION OF POROUS MATERIAL MCM-41 AND ACTIVATED CARBON AS NICKEL CATALYST SUPPORTS FOR *n*-BUTANOL SYNTHESIS. THESIS ADVISOR : ASSOC. PROF. JATUPORN WITTAYAKUN, Ph.D. 114 PP.

MCM-41/MICROWAVE/TEMPLATE REMOVAL/EXTRACTION/ION EXCHANGE/ULTRASOUND/ACTIVATED CARBON/NICKEL/*n*-BUTANOL

There are four main topics in this thesis consisting of 1) hydrothermal synthesis of siliceous MCM-41 ([Si]MCM-41) under microwave irradiation and characterization; 2) removal and recovery of templating agent CTA^+ from the as-synthesized [Si]MCM-41; 3) preparation of activated carbon as a catalyst support 4) synthesis and characterization of nickel catalysts on activated carbon and [Si]MCM-41 for the synthesis of *n*-butanol from ethanol.

The first topic involve the synthesis of [Si]MCM-41 under microwave irradiation was studied. Effects of CTAB:SiO_2 mole ratio, NaOH:SiO_2 mole ratio and crystallization time were varied to improve the quality of the [Si]MCM-41. The synthesis by using 3.34SiO2: 4.46NaOH: 1CTAB gel ratio under microwave hydrothermal time of 90 min achieved the high ordering of hexagonal structure, high surface area and small particle size regarding to X-ray diffraction (XRD), N_2 adsorption-desorption, thermogravimetric analysis (TGA) and dynamics light scattering (DLS). Furthermore, [Si]MCM-41 synthesized under microwave irradiation has smaller particle sizes than those obtained from conventional heating.

The second topic dealt with a strategy to reduce energy consumption on CTA^+ removal from the as-synthesized [Si]MCM-41. An inductive role of ion exchange media, type of salt solutions, time and temperature under sonication was revealed by TGA and XRD. The ion exchange condition by using ammonium salt under 30 °C for 15 min gave the percentage of CTA^+ removal more than 70 % and did not destruct the [Si]MCM-41 structure. Furthermore, CTA^+ recovery from the solution after CTA^+ extraction (extracted CTA^+) and from the solution after synthesis of [Si]MCM-41 (waste powder) was studied. The extracted CTA^+ and waste powder contained CTA^+ molecules and unwanted compounds which were oxidized CTAB and siliceous material according to Fourier transform infrared spectroscopy (FTIR) and XRD.

The third topic, activated carbon from charcoal of *M. calabura* wood was modified to increase acid sites which were expected as adsorption site for nickel catalyst. The acid functional groups, surface properties and thermal stability were determined by FTIR, N_2 adsorption-desorption and TGA. Acid sites on the activated carbon were enhanced after treatments under CO_2 and then air zero.

Finally, nickel nanoparticles on [Si]MCM-41 and modified activated carbon were prepared and characterized by XRD, NH_3 temperature-programmed desorption, CO_2 temperature-programmed desorption and inverse-temperature programmed reduction. All of catalyst screening on Guerbet reaction showed a low ethanol conversion and *n*-butanol selectivity. However, the presence of acid/base and metal in a catalyst increased the catalytic activity by twofold.

School of Chemistry Student's Signature_____

Academic Year 2015 Advisor's Signature_____

ACKNOWLEDGEMENT

I would like to thank people who support me on everything. First, I would like to thank my advisor, Assoc. Prof. Dr. Jatuporn Wittayakun who is every kind in many things that I could not write it all. I really appreciate all he's done to help me. Second, I would to thank Prof. Masaki Kawano for his supervision for my short term research at Pohang University of Science and Technology (POSTECH), Republic of Korea even though the work is still in progress and not included in thesis. He gave me the inspiration, ideas and experience in crystallography. Third, I would like to thank Jatuporn's group members and Masaki's group members for being there every time when I needed some help. Finally, I thank my family members who also support me, have me and cheer me up all the time.

A scholarship for my study was from the Thai government through the Development and Promotion of Science and Technology Talents Project (DPST).

Krittanun Deekamwong

CONTENTS

CONTENTS (Continued)

CONTENTS (Continued)

CONTENTS (Continued)

CONTENTS (Continued)

CONTENTS (Continued)

LIST OF FIGURES

LIST OF FIGURES (Continued)

LIST OF FIGURES (Continued)

LIST OF FIGURES (Continued)

LIST OF TABLES

LIST OF TABLES (Continued)

Table **Page**

.

LIST OF SCHEMES

Scheme **Page**

CHAPTER I

INTRODUCTION

1.1 Introduction

To reduce the cost of catalyst production, an inexpensive resource should be employed. For a siliceous mesoporous material MCM-41 ([Si]MCM-41), a conventional synthesis normally uses a muffle furnace as a heating source. In addition to make pores, cetyltrimethylammonium ion (CTA^+) as a template of [Si]MCM-41 is usually degraded by calcination. This process is slow and waste CTA^+. An application of microwave irradiation and ion exchange can accelerate the synthesis and recover CTA^+, respectively (González-Rivera et al., 2014). Therefore, the experimental parameters thru the use of microwave heating source and ion exchange are the interest in this work.to minimize the cost of the [Si]MCM-41 synthesis.

To produce activated carbon as a support, the preparation from an abundant wood is a good candidate. In this work, *M. calabura* wood which is an abundant tree widely seen in Nakhon Ratchasima province, Thailand was used to produce activated carbon by using pyrolysis and gases physical treatment.

The crisis of the energy shortage and environment is currently one of the big problems of the world and also Thailand. It is necessary to seek a way to increase renewable fuel sources. *n*-butanol is the one of renewable alcohol fuel which will be blended in fossils fuels. The improvement of chemical synthesis of *n*-butanol via Guerbet process by using heterogeneous catalyst is promising to take place an

ecological process (Riittonen et al., 2012; Riittonen et al., 2015; Zhang et al., 2013). Therefore, this work used heterogeneous nickel (Ni) catalyst supported on [Si]MCM-41 and activated carbon. The catalysts could catalyze *n*-butanol synthesis from ethanol by using the hydrothermal batch reaction as described by Zhang et al. (2013).

1.2 References

González-Rivera, J., Tovar-Rodr´ıguez, J., Bramanti, E., Duce, C., Longo, I., Fratini, E., Galindo-Esquivela, I.R. and Ferrari-Rivera, C. (2014). Surfactant recovery from mesoporous metalmodified materials (Sn–, Y–, Ce–, Si–MCM-41), by ultrasound assisted ion-exchange extraction and its re-use for a microwave in situ cheap and ecofriendly MCM-41 synthesis. **Journal of Materials Chemistry A**. 2: 7020 – 7033.

Kamiński, W., Tomczak, E. and Górak, A. (2011). Biobutanol - production and purification methods. **Ecological Chemistry and Engineering S**. 18: 31 – 37.

Riittonen, T., Eränen, K., Mäki-Arvela, P., Shchukarev, A., Rautio, A.-R., Kordas, K., Kumar, N., Salmi, T. and Mikkola, J. (2015). Continuous liquid-phase valorization of bio-ethanol towards bio-butanol over metal modified alumina. **Renewable Energy**. 74: 369 – 378.

Riittonen, T., Toukoniitty, E., Madnani, D.K., Leino, A.-R., Kordas, K., Szabo, M., Sapi, A., Arve, K., Wärnå, J. and Mikkola, J.-P. (2012). One-pot liquid-phase catalytic conversion of ethanol to 1-butanol over aluminium oxide - the effect of the active metal on the selectivity. **Catalysts**. 2: 68 – 84.

Zhang, X., Liu, Z., Xu, X., Yue, H., Tian, G. and Feng, S. (2013). Hydrothermal synthesis of 1-butanol from ethanol catalyzed with commercial cobalt powder. **ACS Sustainable Chemistry & Engineering**. 1: 1493 – 1497.

CHAPTER II

LITERATURE REVIEW

2.1 Mesoporous MCM-41

2.1.1 Background

More than 20 years ago, MCM-41 (Mobil Composition of Matter No. 41) was discovered by Mobil research group (Beck et al., 1992). It has a hexagonal array of one-dimensional uniform pores around 2-10 nm in diameter (Meléndez-Ortiz et al., 2013), high surface areas (about 1000 m^2/g), and high thermal stability (Beck et al., 1992). A surfactant is required as a template in the synthesis of MCM-41. Two formation mechanisms of MCM-41 were proposed as shown in Figure 2.1. In pathway 1, the template molecules form rod-shape micelle which further organizes to form hexagonal liquid crystal. Then, silicate ions interact with the positive end of the micelle to produce hexagonal array with silicate layer. Pathway 2, Silicate ions are added to the micelles before the preorganization (Chen et al., 1993). From both pathways, the template molecules are removed by calcination or extraction to produce MCM-41 with cylinderial pores.

.

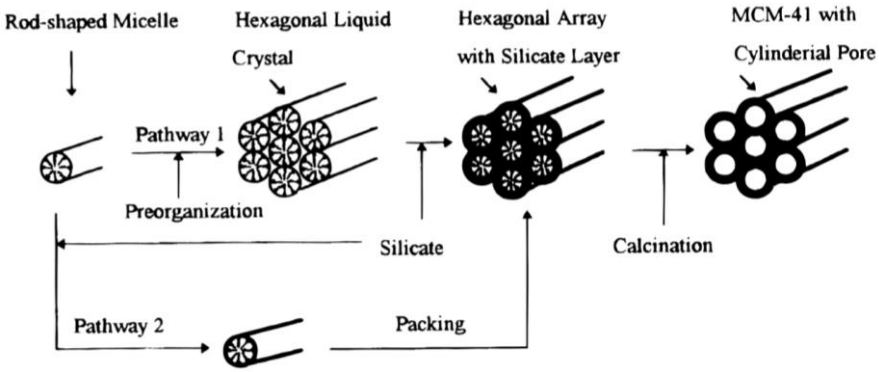

Figure 2.1 Liquid crystal templating mechanism via two possible pathways (Beck et al., 1992).

In order to confirm hexagonal structure with an experimental data, an X-ray powder diffraction pattern of MCM-41 was simulated (Ugliengo et al., 2008). The (100), (110), (200), (210) and (300) planes corresponding to a hexagonal unit cell are obtained in diffraction peaks between 1.0 – 10.0 degree (Figure 2.2). The higher (h00) and (h10) planes resulting in long-range ordering of hexagonal MCM-41 structure was also observed (Cheng et al., 1997).

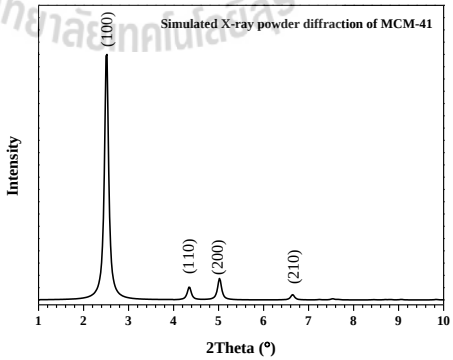

Figure 2.2 Simulated X-ray powder diffraction pattern of MCM-41 (generated by Ugliengo et al., 2008).

2.1.2 Synthesis of MCM-41

There are many studies on improvement of MCM-41 under a conventional hydrothermal method. Two optimal parameters were reported by Cheng et al. (1997). The first parameter is temperature. The hexagonal phase is always observed at 100 °C and transformed to lamellar and amorphous phase at 150 °C as a function of time. The second parameter is the ratio of [CTAB]:[fumed SiO_2] that the ratio of 2.7 gave a high periodic hexagonal structure regarding to relative peak intensity of X-ray diffraction pattern. Liu et al. (2012) investigated an effect of the surfactant size. The longer alkane chain in the range of C_{12} - C_{16} showed the larger pore size and the longer ordering of hexagonal structure. Different media solution and additive influenced the quality of MCM-41 (Liou et al., 2011; Martin et al., 2002; Varache et al., 2015). Moreover, the physical properties of MCM-41 can be modified to suit with its application by changing type of silica source and template, gel composition, pH, and additives (Albuquerque et al., 2005; Cheng et al., 1997; Luechinger et al., 2003; Meléndez-Ortiz et al., 2013).

Although the conventional hydrothermal method produced MCM-41 works with a high quality, it is a slow process with at least 48 h and the surfactant is decomposed during calcination (Ryczkowski et al., 2005). To speed up the process, microwave is applied as a heating source (Bachari and Guerroudj, 2012; Cheng et al., 2005; Gonźalez-Rivera et al., 2014; Jiang et al., 2008; Laha and Gläser, 2007; Park et al., 1998; Park et al., 2004; Shi et al., 2011; Wang et al., 2012). As a result, the MCM-41 synthesis could be achieved in a much shorter time.

According to an expensive cost of surfactant and high energy consumption during calcination, alternative ways were studied to bring the surfactant back to

recycle and minimize the energy. Mild conditions to decompose the template were applied to reduce the energy consumption (Liu et al., 2010; Marcilla et al., 2011; Tian et al., 2002). However, the surfactant was still decomposed and wasted. The solvent extraction method was employed to recover the template for recycle (Gonźalez-Rivera et al., 2014; Hitz and Prins, 1997; Shaghayegh and Zanjanchi, 2014).

2.1.3 Application of MCM-41

With good physical properties and high thermal stability, MCM-41 has been widely employed as a support, catalyst or molecular sieve. Nevertheless, the siliceous MCM-41 has a limitation regarding active function such as acid or base site that makes it not suitable for some catalytic reactions. Therefore, an heteroatom is loaded on surface or incorporated into the framework of MCM-41 to generate active sites (Banchari et al., 2012; Collard et al., 2014; Gunduz and Dogu, 2012; Jiang et al., 2008; Khieu et al., 2009; Wojcieszak et al., 2004; Wang et al., 2003; Wang et al., 2012). The substitution of silicon atoms by other atoms could increase their acid sites (Brønsted or Lewis) and basic sites. Nickel-containing in MCM-41 have been widely used in catalytic reactions such as hydrocracking (Tanggarnjanavalukul et al., 2015; Qin et al., 2015), hydrodeoxygenation (Nash et al., 2016; Tran et al., 2016) and steam reforming (Karnjanakom et al., 2015).

2.2 Activated carbon

Activated carbon is a form of derivative carbon prepared from carbonaceous materials like animal, plant, mineral, and agriculture waste materials (Hassler, 1963). It consists of amorphous and graphite-like microcrystalline structure contributed

porosity and acts as an adsorbent. The arrangement of graphene-like layers in disordered structure can provide the porous structures or free interstices. In addition to graphene framework, activated carbon also contains heteroatoms such as hydrogen, oxygen, nitrogen, and sulfur resulting to change the chemical properties. In 2003, a new representative activated carbon structure called “the basic structural unit (BSU)” was published (Bandosz et al., 2003). BSU consists of the layers of the polyaromatic-like molecules (Figure 2.3).

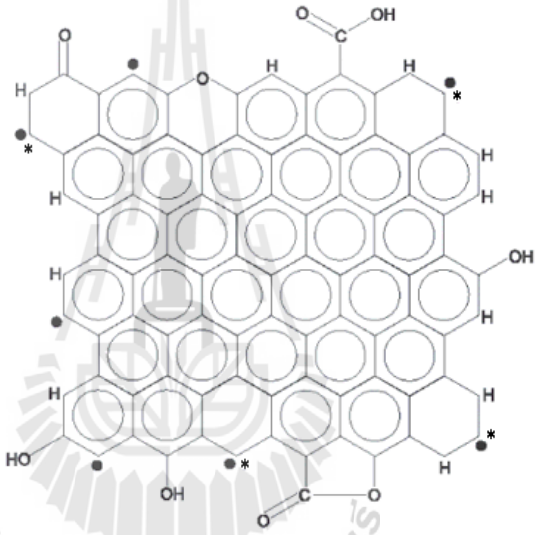

Figure 2.3 Layers of the polyaromatic-like molecules of activated carbon (Mochida et al., 2006).

Typically, activated carbon is prepared via 2 routes. The first route involves pyrolysis or carbonization and activation separately. The second route is a continuous procedure of the two processes. Pyrolysis changes a raw carbonaceous material to charcoal by thermal decomposition of volatile matter in the range of 600 – 1000 °C. There are several kinds of furnace for pyrolysis such as a horizontal or vertical ceramic tube furnace, Iwasaki kiln or Iwate kiln. The properties of charcoal depend on

a heating rate, hold time and atmospheric condition. Then, the charcoal is activated to generate the porosity and the obtained material is called “activated carbon”. Normally, there are two types of activation: (1) the physical activation by gasifying the carbon with an oxidizing agent such as water steam or carbon dioxide at a temperature of about 800 - 1100 °C, (2) the chemical activation by thermal decomposition of the impregnated precursor such as zinc chloride or phosphoric acid at the temperature about 500 – 900 °C (Fiqueredo et al., 1999; Junpirom et al., 2007).

Activated carbon has a high surface area (> 400 m^2/g) and acid/base resistivity. It has been used for gas purification (Rik, 1994; Sircar et al., 1996), carbon dioxide capture (Choi et al., 2009), hydrogen storage (Dillon et al., 1997), water treatment (Gupta et al., 2009; Gupta and Suhas, 2009; Mohand and Pittman Jr., 2007), catalytic hydrogenation (Liu et al., 2015; Merabti et al., 2010; Pierre et al., 2007) and auto hydrogen transfer reaction (Yang et al., 2015).

2.3 *n*-butanol synthesis

In 2015, Department of Alternative Energy Development and Efficiency, Ministry of Energy of Thailand announced the run-on trend of renewable fuels. The use of renewable energy has been growth rapidly more than others. Alcohol as an additive in fuel is now one of the most renewable energy that has recently become a research interest according to the number of published papers and the expansion of the biofuels market (Figure 2.4). Among various alcohols, *n*-butanol shows a high heating value, high flash point and less corrosive (Table 2.1). Moreover, it can be miscible with diesel and gasoline.

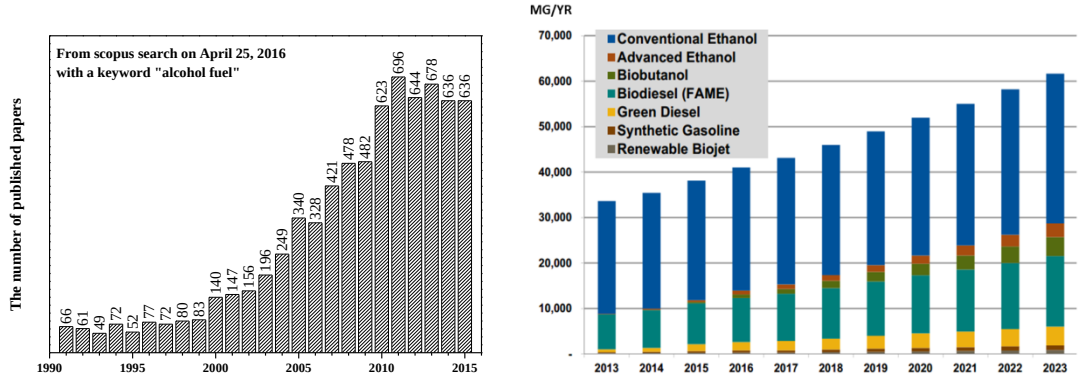

Figure 2.4 (Left) the number of published papers about alcohol fuel from 1991 to 2015 (www.scopus.com), (Right) the prediction of an expanding biofuels market from 2013 to 2023 (Navigant research, 2013).

Table 2.1 Specification of alcohol and conventional fossil fuels (Chao et al., 2011).

	Gasoline	Diesel	Methanol	Ethanol	*n*-Butanol
Cetane number	0-10	40-55	3	8	25
Octane	80-99	20-30	111	108	96
Oxygen content (wt. %)	-	-	50	34.8	21.6
Density at 20 °C (g/mL)	0.72	0.82	0.79	0.79	0.81
Lower heating value (MJ/kg)	42.7	42.5	19.9	26.8	33.1
Viscosity at 40 °C (mm^2/s)	0.6	3.0	0.59	1.08	2.63

n-butanol is generally produced by a biosynthesis using fermentation by bacteria (Volesky and Szczesny, 1983). However, the main issue of this method is the low concentration of biobutanol and toxic metabolic production from the bacteria (Kamiński et al., 2011). Another method to produce *n*-butanol is from ethanol which

can be produced from biomass. There are two proposed pathways. In the first path way, a molecule of ethanol is activated on the catalyst basic sites and condensed with another ethanol molecule by dehydration. In the second process which is known as Guerbet process (Figure 2.5), ethanol is dehydrated to acetaldehyde which is further converted to crotonaldehyde by Aldol condensation. Then, the crotonaldehyde was hydrogenated to *n*-butanol (Sun and Wang, 2014).

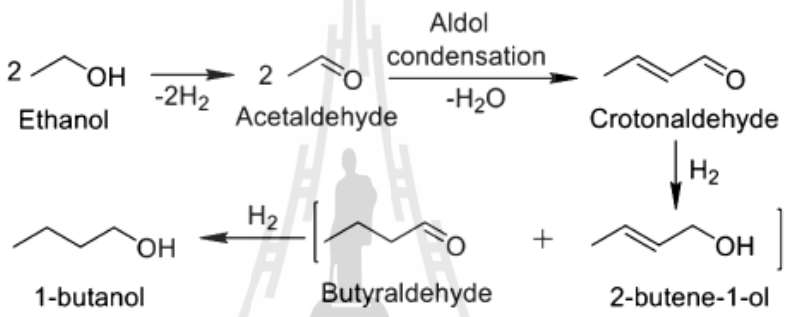

Figure 2.5 Reaction pathways from ethanol to *n*-butanol (Sun and Wang, 2014).

Heterogeneous catalysts for the synthesis of *n*-butanol include modified zeolites, mixed oxides, modified hydroxyapatites, metallic Co, Ni, Fe, and Raney Cu. Catalytic testing for *n*-butanol synthesis from ethanol is widely studied in a fixed bed reactor at atmospheric pressure or under hydrogen pressure which also serves as a hydrogen source at about 500 °C. Most of the results showed about 20-65% selectivity and low conversion, depending on the metal active phase and the basic site on support (Carvalho et al., 2012; Dowson et al., 2013; Jordison et al., 2015; Ndou et al., 2003; Ogo et al., 2012; Tsuchida et al., 2006).

2.4 References

Albuquerque, A., Vautier-Giongo, C. and Pastore, H.O. (2005). Physical chemistry of nanostructured molecular sieves by the study of phase diagrams the case of the cetyltrimethylammonium bromide – tetramethylammonium silicate – water system. **Journal of Colloid and Interface Science.** 284: 687 – 693.

Bachari, K. and Guerroudj, R.M. (2012). Characterization and catalytic properties of nickel-substituted hexagonal mesoporous silica prepared by microwave-hydrothermal method. **Comptes Rendus Chimie**. 15: 317 – 323.

Bandosz, T.J., Biggs, M.J., Gubbins, K.E., Hattori, Y., Liyama, T., Kaneko, K.E, Pikunic, J. and Thomson, K.T. (2003). Molecular models of porous carbons. In L.R. Radovic.(ed.). **Chemistry and Physics of Carbon**. 28: 41 – 228.

Beck, J.S., Vartuli, J.C., Roth, W.J., Leonowicz, M.E., Kresge, C.T., Schmitt, K.D., Chu, C.T.-W., Olson, D.H., Shepparol, E.W., Mc-Cullen, S.B., Higgins, J.B. and Schlenker, J.L. (1992). A new family of mesoporous molecular sieves prepared with liquid crystal templates. **Journal of the American Chemical Society**. 114: 10834 – 10843.

Carvalho, D.L., Avillez, R.R., Rodriguesc, M.T., Borgesa, Luiz E.P. and Appelc, L.G. (2012). Mg and Al mixed oxides and the synthesis of *n*-butanol from ethanol. **Applied Catalysis A: General**. 415 – 416: 96 – 100.

Chao, J., Yaoc, M., Liuc, H., Leed, Chia-Fon F. and Ji, J. (2011). Progress in the production and application of *n*-butanol as a biofuel. **Renewable and Sustainable Energy Reviews**. 15: 4080 – 4106.

Chen, C-Y., Burkett, S.L., Li, H-X. and Davis, M.E. (1993). Studies on mesoporous materials II. Synthesis mechanism of MCM-41. **Microporous Materials**. 2: 27 – 34.

Cheng, C.-E., Cheng, H.-H., Wu, L.-L. and Chengm, B.-W. (2005). Synthesis and characterization of nanoscale aluminosilicate mesoporous materials by microwave irradiation. **Surface Science and Catalysis**. 156: 113 – 118.

Cheng, C.-F., Park, D.H. and Klinowski, J. (1997). Optimal parameters for the synthesis of the mesoporous molecular sieve [Si]-MCM-41. **Journal of the Chemical Society, Faraday Transactions**. 93(1): 193 – 197.

Choi, S., Drese, J.H. and Jones, C.W. (2009). Adsorbent materials for carbon dioxide capture from large anthropogenic point sources. **ChemSusChem.** 796 – 854.

Collard, X., Li, L., Lueangchaichaweng, W., Bertrand, A., Aprile, C. and Pescarmona, P.P. (2014). Ga-MCM-41 nanoparticles: Synthesis and application of versatile heterogeneous catalysts. **Catalysis Today**. 235: 184 – 192.

Dillon, A.C., Jones, K.M., Bekkedahl, T.A., Kiang, C.H., Bethune, D.S. and Heben M.J. (1997). Storage of hydrogen in single-walled carbon nanotube. **Nature.** 386: 377 – 379.

Deekamwong, K. (2016). **Alcohol fuel from 1991 to 2016** [on-line]. Available: http://www.scopus.com.

Dowson, George R.M., Haddow, M.F., Lee, J., Wingad, R.L. and Wass, D.F. (2013). Catalytic conversion of ethanol into an advanced biofuel unprecedented selectivity for *n*-butanol. **Angewandte Chemie International Edition**. 52: 9005 – 9008.

Fiqueredo, J.L., Pereira, M.F. R., Freitas, M.M.A. and Órfão, J.J.M. (1999). Modification of the surface chemistry of activated carbons. **Carbon.** 37: 1379 – 1389.

Gonźalez-Rivera, J., Tovar-Rodr´ıguez, J., Bramanti, E., Duce, C., Longo, I., Fratini, E., Galindo-Esquivela, I.R. and Ferrari-Rivera, C. (2014). Surfactant recovery from mesoporous metalmodified materials (Sn–, Y–, Ce–, Si–MCM-41), by ultrasound assisted ion-exchange extraction and its re-use for a microwave in situ cheap and ecofriendly MCM-41 synthesis. **Journal of Materials Chemistry A**. 2: 7020 – 7033.

Gunduz, S. and Dogu, T. (2012). Sorption-enhanced reforming of ethanol over Ni- and Co-incorporated MCM-41 type catalysts. **Industrial & Engineering Chemistry Research**. 51(26): 8796 – 8805.

Gupta, V.K. and Suhas. (2009). Application of low-cost adsorbents for dye removal – A review. **Journal of Environmental Management**. 90: 2313 – 2342.

Gupta, V.K., Carrott, P.J.M. and Ribeiro Carrott, M.M.L. (2009). Low-Cost Adsorbents: Growing Approach to Wastewater Treatment—a Review. **Environmental Science and Technology.** 10: 783 – 842.

Hassler, J.W. (1963). **Activated Carbon**. New York. Chemical Publishing.

Hitz, S. and Prins, R. (1997). Influence of template extraction on structure, activity, and stability of MCM-41 catalysts. **Journal of Catalysis**. 168: 194 – 206.

Jiang, T., Tang, W., Zhao, Q. and Yin, H. (2008). Effect of Ni-doping on the pore structure of pure silica MCM-41 mesoporous molecular sieve under microwave irradiation. **Colloids and Surfaces A: Physicochemical and Engineering Aspects**. 315: 299 – 303.

Jordison, T.L., Lira, C.T. and Miller, D.J. (2015). Condensed-phase ethanol conversion to higher alcohols. **Industrial & Engineering Chemistry Research**. 54: 10991 – 11000.

Junpirom, S., Tangsathitkulchai, C. and Tangsathitkulchai, M. (2007). Preparation of activated carbons from longan seed by physical and chemical methods (in Thai). **Suranaree Journal of Science and Technology.** 14(1): 63 – 76.

Kamiński, W., Tomczak, E. and Górak, A. (2011). Biobutanol - production and purification methods. **Ecological Chemistry and Engineering S**. 18: 31 – 37.

Karnjanakom, S., Guan, G., Asep, B., Du, X., Hao, X., Samart, C. and Abudala, A. (2015). Catalytic steam reforming of tar derived from steam gasification of sunflower stalk over ethylene glycol assisting prepared Ni/MCM-41. **Energy Conversion and Management**. 98: 359 – 368.

Khieu, D.Q., Quang, D.T., Lam, T.D., Phu, N.H., Lee, H.J. and Kim, J.S. (2009). Fe-MCM-41 with highly ordered mesoporous structure and high Fe content: synthesis and application in heterogeneous catalytic wet oxidation of phenol. **Journal of Inclusion Phenomena and Macrocyclic Chemistry**. 65(1 – 2): 73 – 81.

Kirk, R.E. and Othmer, D.F. (1978). **Encyclopedia of Chemical Technology**. New York. John-Wiley and Sons.

Laha, S.C. and Gläser, R. (2007). Characterization and catalytic performance of [Cr] MCM-41 and [Cr] MCM-48 prepared by either classical or microwave heating. **Microporous and Mesoporous Materials**. 99: 159 – 166.

Liou, T.-H. (2011). A green route to preparation of MCM-41 silicas with well-ordered mesostructure controlled in acidic and alkaline environments. **Chemical Engineering Journal**. 171(3): 1458 – 1468.

Liu, C., Wang, X., Lee, S., Pfefferle, L.D. and Haller, G.L. (2012). Surfactant chain length effect on the hexagonal-to-cubic phase transition in mesoporous silica synthesis. **Microporous and Mesoporous Materials**. 147(1): 242 – 251.

Liu, Y., Gu, Y., Hou, Y., Yang, Y., Deng, S. and Wei, Z. (2015). Hydrophobic activated carbon supported Ni-based acid-resistant catalyst for selective hydrogenation of phthalic anhydride to phthalide. **Chemical Engineering Journal**. 275: 271 – 280.

Liu, Y., Pan, Y., Wang, Z.-J., Kuai, P. and Liu, C.-J. (2010). Facile and fast template removal from mesoporous MCM-41 molecular sieve using dielectric-barrier discharge plasma. **Catalysis Communications**. 11: 551 – 554.

Luechinger, M., Frunz, L., Pringruber, G.D. and Prins, R. (2003). A mechanistic explanation of the formation of high quality MCM-41 with high hydrothermal stability. **Microporous and Mesoporous Materials.** 64(1 – 3): 203 – 211.

Machado, C. (2010). Butanol production and use as biofuel. **BIO V Seninario Latioamericano y del Caribe de Biocombustibles**.

Marcilla, A., Beltran, M., Gómez-Siurana, A., Martinez, I. and Berenguer, D. (2011). Template removal in MCM-41 type materials by solvent extraction. **Chemical Engineering Research and Design**. 89: 2330 – 2343.

Meléndez-Ortiz, H.I., Mercado-Silva, A., García-Cerda, L.A., Castruita, G. and Perera-Mercado, L.A. (2013). Hydrothermal synthesis of mesoporous silica MCM-41 using commercial sodium silicate. **Journal of the Mexican Chemical Society**. 57(3): 73 – 79.

Merabti, R., Banchari, K., Halliche, D., Rassoul, Z. and Saadi, A. (2010). Synthesis and characterization of activated carbon-supported copper or nickel and their catalytic behavior towards benzaldehyde hydrogenation. **Reaction Kinetics Mechanisms and Catalysis.** 101: 195 – 208.

Mochida, I., Yoon, S.-H. and Qiao, W. (2006). Catalysts in syntheses of carbon and carbon precursors. **Journal of the Brazilian Chemical Society**. 17(6): 1059 – 1073.

Mohan, D. and Pittman Jr., C. (2007). Arsenic removal from water/wastewater using adsorbents – A critical review. **Journal of Hazardous Materials.** 142: 1 – 53.

Nash, C.P., Ramanathan, A., Ruddy, D.A., Behl, M., Gjersing, E., Griffin, M., Zhu, H., Subramaniam, B., Schaidle, J.A. and Hensley, J.E. (2016). Mixed alcohol dehydration over Brønsted and Lewis acidic catalysts. **Applied Catalysis A: General**. 510: 110 – 124.

Navigant Research. (2013). The expanding biofuels market [on-line]. Available: http://nenmore.blogspot.com/2013_04_01_archive.html.

Ndou, A.S., Plint, N. and Coville, N.J. (2003). Dimerisation of ethanol to butanol over solid-base catalysts. **Applied Catalysis A: General**. 251: 337 – 345.

Ogo, S., Onda, A., Iwasa, Y., Hara, K., Fukuoka, A. and Yanagisawa, K. (2012). 1-Butanol synthesis from ethanol over strontium phosphate hydroxyapatite catalysts with various Sr/P ratios. **Journal of Catalysis**. 296: 24 – 30.

Park, S.-E., Chang, J.-S., Hwang, Y.K., Kim, D.S., Jhung, S.H. and Hwang, J.S. (2004). Supramolecular interactions and morphology control in microwave synthesis of nanoporous materials. **Catalysis Surveys from Asia**. 8(2): 91 – 110.

Park, S.-E., Kim, D.S., Chang, J.-S. and Kim, W.Y. (1998). Synthesis of MCM-41 using microwave heating with ethylene glycol. **Catalysis Today**. 44: 301 – 308.

Perrard, A., Gallezot, P., Joly, J.-P., Durand, R., Baljo, C., Coq, B. and Trens, P. (2007). Highly efficient metal catalysts supported on activated carbon cloths: A catalytic application for the hydrogenation of D-glucose to D-sorbitol. **Applied Catalysis A: General**. 331: 100 – 104.

Qin, J., Li, B., Zhang, W., Lv, W., Han, C. and Liu, J. (2015). Synthesis, characterization and catalytic performance of well-ordered mesoporous Ni-MCM-41 with high nickel content. **Microporous and Mesoporous Materials**. 208: 181 – 187.

Riittonen, T., Toukoniitty, E., Madnani, D.K., Leino, A.-R., Kordas, K., Szabo, M., Sapi, A., Arve, K., Wärnå, J. and Mikkola, J.-P. (2012). One-pot liquid-phase catalytic conversion of ethanol to 1-butanol over aluminium oxide - the effect of the active metal on the selectivity. **Catalysts**. 2: 68 – 84.

Rik, R. (1994). Using activated carbon for gas/air purification. **Chemical Processing.** 57(11): 53 – 58.

Ryczkowski, J., Goworek, J., Gac, W., Pasieczna, S. and Borowiecki, T. (2005). Temperature removal of templating agent from MCM-41 silica materials. **Thermochimica Acta**. 434: 2 – 8.

Schulz, M. and Clark, S. (2011). Vehicle emissions and fuel economy effects of 16% butanol and various ethanol blended fuels (E10, E20, and E85). **Journal of ASTM International**. 8: 1 – 19.

Shaghayegh, J. and Zanjanchi, M.A. (2012). A simple and fast sonication procedure to remove surfactant templates from mesoporous MCM-41. **Ultrasonics Sonochemistry**. 19: 1087 – 1093.

Shi, Y., Wang, S. and Ma, X. (2011). Microwave preparation of Ti-containing mesoporous materials. Application as catalysts for transesterification. **Chemical Engineering Journal**. 166: 744 – 750.

Sircar, S., Golden T.C. and Rao, M.B. (1996). Activated carbon for gas separation and storage. **Carbon**. 1: 1 – 12.

Sun, J. and Wang, Y. (2014). Recent advances in catalytic conversion of ethanol to chemicals. **ACS Catalysis**. 4: 1078 – 1090.

Tanggarnjanavalukul, C., Donphai, W., Witoon, T., Chareonpanich, M. and Limtrakul, J. (2015). Deactivation of nickel catalysts in methane cracking reaction: Effect of bimodal meso–macropore structure of silica support.**Chemical Engineering Journal** 262: 364 – 371.

Tian, B., Yang, H., Liu, X., Xie, S., Yu, C., Fan, J., Tua, B. and Zhao, D. (2002). Fast preparation of highly ordered nonsiliceous mesoporous materials via mixed inorganic precursors. **Chemical Communications**. 17: 1824 – 1825.

Tran, N.T.T., Uemura, Y., Chowdhury, S. and Ramli, A. (2016). Vapor-phase hydrodeoxygenation of guaiacol on Al-MCM-41 supported Ni and Co catalysts. **Applied Catalysis A: General**. 512: 93 – 100.

Tsuchida, T., Sakuma, S., Takeguchi, T. and Ueda, W. (2006). Direct synthesis of *n*-butanol from ethanol over nonstoichiometric hydroxyapatite. **Industrial & Engineering Chemistry Research**. 45: 8634 – 8642.

Ugliengo, P., Sodupe, M., Musso, F., Bush, I.J., Orlando, R. and Dovesi, R. (2008). Realistic models of hydroxylated amorphous silica surfaces and MCM-41 mesoporous material simulated by large-scale periodic B3LYP calculations. **Advanced Materials**. 20(23): 4579 – 4583.

Varache, M., Bezverkhyy, T., Saviot, L., Bouyer, F., Baras, F. and Bouyer, F. (2015). Optimization of MCM-41 type silica nanoparticles for biological applications: Control of size and absence of aggregation and cell cytotoxicity. **Journal of Non-Crystalline Solids**. 408: 87 – 97.

Volesky B. and Szczesny, T. (1983). Bacterial conversion of pentose sugars to acetone and butanol. **Advances in Biochemical Engineering/Biotechnology**. 27: 101 – 118.

Wang, S., Shi, Y. and Ma, X. (2012). Microwave synthesis, characterization and transesterification activities of Ti-MCM-41. **Microporous and Mesoporous Materials**. 156: 22 – 28.

Wang, Y., Ohishi, Y., Shishido, T., Zhang, Q., Yang, W., Gup, Q., Wan, H. and Takehira, K. (2003). Characterizations and catalytic properties of Cr-MCM-41 prepared by direct hydrothermal synthesis and template - ion exchange. **Journal of Catalysis**. 220(2): 347 – 357.

Wojcieszak, R., Monteverdi, S., Mercy, M., Nowak, I., Ziolek, M. and Bettahar, M.M. (2004). Nickel containing MCM-41 and AlMCM-41 mesoporous molecular sieves characteristics and activity in the hydrogenation of benzene. **Applied Catalysis A: General**. 268(1 – 2): 241 – 253.

Yang, C. and Meng, Z.Y. (1993). Bimolecular condensation of ethanol to 1-butanol catalyzed by alkali cation zeolites. **Journal of Catalysis**. 142: 37 – 44.

Yang, H., Cui, X., Dai, X., Deng Y. and Shi, F. (2015). Carbon-catalysed reductive hydrogen atom transfer reactions. **Nature Communications**. 6: 6478 – 6488.

Zhang, X., Liu, Z., Xu, X., Yue, H., Tian, G. and Feng, S. (2013). Hydrothermal synthesis of 1-butanol from ethanol catalyzed with commercial cobalt powder. **ACS Sustainable Chemistry & Engineering**. 1: 1493 – 1497.

CHAPTER III

CHARACTERIZATION OF SILICEOUS MCM-41 SYNTHESIZED BY MICROWAVE-ASSISTED HYDROTHERMAL METHOD

3.1 Abstract

Siliceous mesoporous material [Si]MCM-41 was synthesized by microwave-assisted hydrothermal method with various gel composition and hydrothermal time. The characteristic and physical properties of samples were investigated by powder X-ray diffraction (XRD), N_2 adsorption-desorption and dynamics light scattering (DLS). A thermal stability was studied by thermogravimetric analysis (TGA). The optimum synthesis included $3.34SiO_2$:4.46NaOH: CTAB: $1.16H_2SO_4$:$225H_2O$ of gel composition and 90 min of hydrothermal time. The CTAB and NaOH concentration strongly influenced the hexagonal structure. The duration of hydrothermal time resulted to particle size variation. However. the particle size of [Si]MCM-41 synthesized under microwave irradiation was smaller than that under the conventional heating.

3.2 Introduction

3.2.1 Mesoporous MCM-41

MCM-41 has been normally synthesized by hydrothermal method with a heating source from an electric oven and time is 48 h. To reduce the resource of hydrothermal synthesis and maintain the quality of MCM-41, several methods have been investigated. For example, the synthesis at room temperature was investigated (Meléndez-Ortiz et al., 2013). The properties of resulting products were slightly different from those of traditional process. However, the reaction time was long at the low temperature and pressure provided the low kinetic reaction.

A fast synthesis of Al-MCM-41 could be done in less than 1 h by microwave-assisted hydrothermal method at 150 °C (Wu et al. (1996). The results showed high quality hexagonal mesoporous structure with 900 – 1000 $m^2.g^{-1}$ of surface area. The microwave irradiation can vibrate solvent molecules and ion species in the gel composition to generate internal heat. With the internal heat source, the formation mechanism might be different. Researchers paid attention to expand the study by changing microwave power and dielectric constants of co-solvent (Bachari and Guerroudj, 2012; Cheng et al., 2005; Gonźalez-Rivera et al., 2014; Jiang et al., 2008; Laha and Gläser, 2007; Park et al., 1998; Park et al., 2004; Shi et al., 2011; Wang et al., 2012). However, the effect of the gel composition and crystallization time on crystallinity, particle size and surface properties relatively have not been explored. Such effect might play an important role during the crystallization process comparing to synthesize under an electric oven.

To reduce the energy consumption in the synthesis, the study herein explored the synthesis of siliceous MCM-41 ([Si]MCM-41) was synthesized under a

microwave irradiation ([Si]MCM-41 (MW)) with different CTAB:SiO_2 mole ratios (0.025 – 0.400), NaOH:SiO_2 mole ratios (1.0 – 2.0) and crystallization times (15 – 180 min).

3.3 Experimental

3.3.1 Synthesis of [Si]MCM-41 by microwave-assisted hydrothermal method

[Si]MCM-41 was synthesized by microwave-assisted hydrothermal method as described in the literature (Cheng et al., 1997; Jiang et al., 2008). The gel composition was prepared at room temperature by using a silica gel (Merck) as a silica source, cetyltrimethylammonium bromide (CTAB, ACROS) as a template, sodium hydroxide (NaOH, Carlo Erba) as an alkaline precursor, and 3 M sulfuric acid (diluted from 96% H_2SO_4, Carlo Erba) as a pH adjusting agent.

To study an effect of gel composition, CTAB was dissolved in 20 mL deionized water. Then, a solution containing 3.551 g of SiO_2 in 40 mL NaOH solution was added within 1 h under stirring. After 18 h the gel pH was adjusted to 9 - 10 by 3 M H_2SO_4 within 30 min. After a continuous stirring for 2 h, the resulting gel with total volume of 60 mL was transferred into a 100-mL Teflon-lined microwave vessel, closed and heated with a heating rate 5 °C/min to 100 °C and held for 90 min in a Microwave MARs 6-One Touch. The temperature was monitored by an IR sensor with an adjustable power output (1200 W). After cooling to room temperature, the mixture was filtered. The solid product was washed with deionized water and dried at 80 °C. This sample was named “As-synthesized [Si]MCM-41 (MW)”. For further characterization, some portion of sample was calcined at 550 °C for 6 h and named “[Si]MCM-41 (MW)”. To study the effect of hydrothermal time, the best gel

composition which produces the highest relative crystallinity from the previous study was treated under microwave irradiation for 15 – 180 min.

3.3.2 Synthesis of [Si]MCM-41 by conventional hydrothermal method

For comparison, the gel prepared by the method above was crystallized in an oven at 100 °C for 72 h., cooled to room temperature. The mixture was filtered. The solid product was washed with deionized water and dried at 80 °C. For further characterization, some portion of sample was calcined at 550 °C for 6 h and named "[Si]MCM-41 (C)".

3.3.3 Characterization

The samples were characterized by X-ray diffraction (XRD, Bruker D8 Advance) using Cu tube with 0.01 degree of 2 theta step size and 0.5 s step time. The d spacing of (100) plane was calculated by Equation 3.1 (Cheng et al., 2007).

$$d_{100} = \frac{n\lambda}{2\sin\theta} \tag{3.1}$$

Where (d_{100}) is d spacing of (100) plane, n is a positive integer (equal 1), λ is the wavelength of X-ray (1.5418 Å) and θ is the angle between the incident beam and the (100) plane (Cheng et al., 2007).

The dimension of unit cell (a_0) was calculated by Equation 3.2. Where (d_{100}) is the spacing of (100) plane from Equation 3.1 (Cheng et al., 2007).

$$a_0 = \frac{2}{\sqrt{3}} \cdot d_{100} \tag{3.2}$$

Nitrogen adsorption-desorption isotherm was obtained by N_2 adsorption-desorption analysis (Micromeritics ASAP 2010). Surface area and pore size were determined by the Brunauer–Emmett–Teller (BET) and Barrett-Joyner-Halenda (BJH) method, respectively. The wall thickness was determined by Equation 3.3 (Cheng et al., 2007).

$$W_t = a_0 - \text{pore diameter} \tag{3.3}$$

Where W_t is the wall thickness, a_0 is the size of unit cell from Equation 3.2 and pore diameter refers to pore size by BJH method (Cheng et al., 2007).

The thermal stability was determined by thermogravimetric analysis (TGA–DTA, TA Instrument/ SDT2960). The sample was loaded into an alumina pan and suspended to the TGA balance. The heating rate was 20 °C/min from 40 to 1100 °C under the N_2 atmosphere. Particle size distribution was measured by dynamic light scattering (Malvern Zetasizer ZS30). 0.01 g of sample was dispersed on 10 mL ethanol under sonication for 1 h (Liu et al., 2009).

3.4 Results and discussion

3.4.1 Characterization of [Si]MCM-41 (MW)

3.4.1.1 Effect of CTAB:SiO_2 ratio

The XRD patterns of [Si]MCM-41 (MW) with CTAB:SiO_2 ratio of 0.025 – 0.400 are shown in Figure 3.1. The diffraction peak corresponding to (100) plane was observed in 0.0250 – 0.300 ratio. The diffraction peaks corresponding to (110) and (200) planes were obtained in 0.050 – 0.300 ratio. The peaks corresponding to (210) and (300) planes, respectively, were observed from the samples from 0.100 – 0.300 ratio. The d_{100} and a_0 values are shown in Table 3.1. The gel ratio 0.050, 0.100 and 0.200 produced MCM-41 with the same size of unit cell. The small amount of surfactant concentration might not be sufficient to interact with silicate resulting to an uncompleted hexagonal structure. In contrast, the broad peak at 2.58 and 4.40 degree were observed from the sample synthesized with the gel ratio 0.400. This XRD pattern implied a non-ordering mesoporous material proposed in AlMCM-41 under a conventional heating (Kresge and Roth, 2013; Beck et al., 1996). The increase of the CTAB:SiO_2 ratio could lead to a formation of other phases such as MCM-48 and MCM-50 (Figure 3.2).

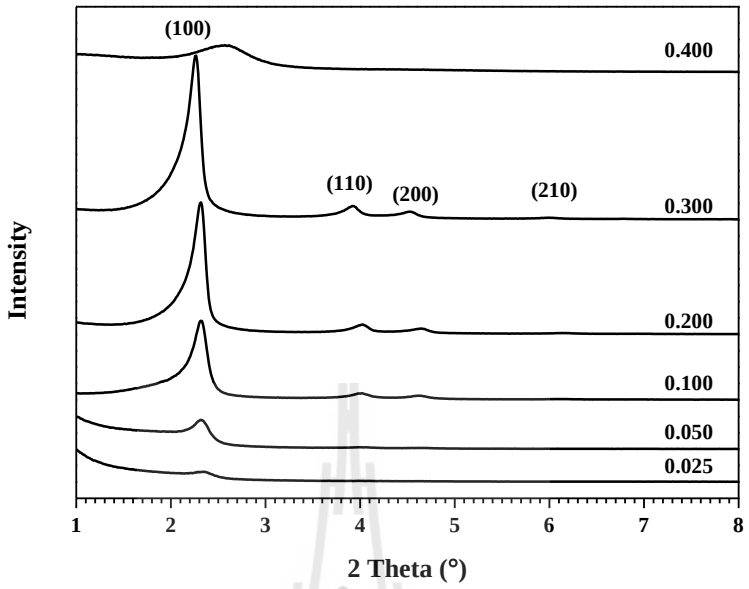

Figure 3.1 XRD patterns of [Si]MCM-41 (MW) from different CTAB:SiO_2 ratios.

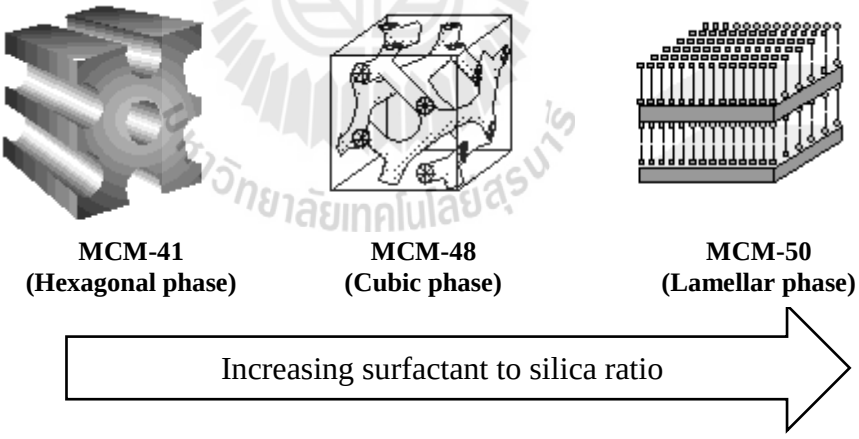

Figure 3.2 The trend of phase change with CTAB:SiO_2 (adapted from Kresge et al., 2013).

Table 3.1 d_{100} and a_0 of [Si]MCM-41 (MW) with different CTAB:SiO_2 ratios.

CTAB:SiO_2	d_{100} (Å)	a_0 (Å)
0.400	-	-
0.300	39.06	45.10
0.200	38.21	44.12
0.100	38.21	44.12
0.050	38.21	44.12
0.025	38.05	43.93

N_2 adsorption-desorption isotherms of [Si]MCM-41 (MW) from different CTAB:SiO_2 ratios are shown in Figure 3.3. All samples showed type IV isotherm. The adsorption at $P/P_0 < 0.3$ corresponded to a monolayer adsorption. The sample with an increase of CTAB:SiO_2 ratios had the larger volume adsorbed (V_a) and corresponding BET surface area (Table 3.2). The second inflection at P/P_0 between 0.3 and 0.4 is a characteristic of mesopores. The hysteresis loop was not observed indicating isotherm type IVc that nitrogen desorbed on mesoporous material without pore condensation. The interaction between nitrogen gas and surface of mesopores was equal or less than that of the interaction between N_2 molecules (Rouquerol et al, 1999). The sharper slope of this region implied the more uniform pores. As a result, the 0.300 ratio showed the narrowest mesopores. According to the full width of half maximum (FWHM) peak of pore size distribution (Figure 3.4), the pore diameter was smaller with a lower of CTAB:SiO_2 ratio The lower FWHM peak corresponded to the more uniform pore. The BJH pore diameter increased with an

increase of CTAB:SiO_2 ratio from 0.025 – 0.200 and stopped by 0.300. Regarding to unit cell, the change from 0.200 – 0.300 ratio was due to an increase of wall thickness (Table 3.3).

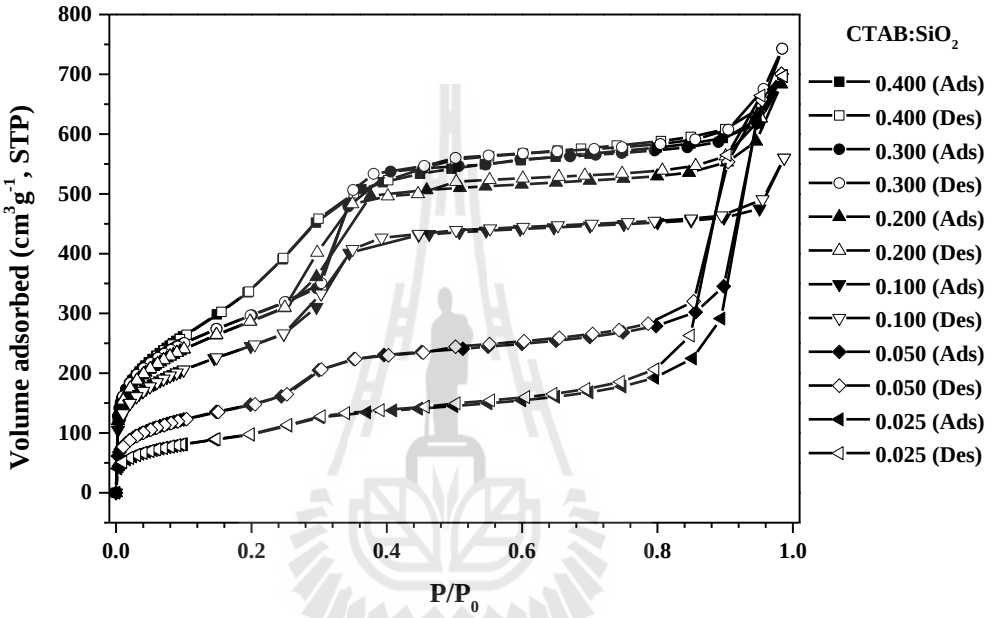

Figure 3.3 N_2 adsorption-desorption isotherms of [Si]MCM-41 (MW) from different CTAB:SiO_2 ratios; adsorption (filled) and desorption (empty).

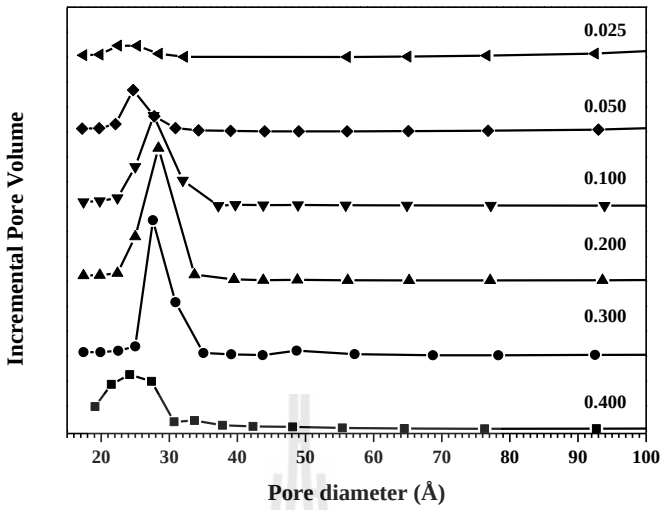

Figure 3.4 Pore size distribution by BJH method of [Si]MCM-41 (MW) from different CTAB:SiO_2 ratios.

Table 3.2 BET surface area, pore diameter of [Si]MCM-41 (MW) with different CTAB:SiO_2 ratios by N_2 adsorption-desorption analysis.

CTAB:SiO_2	BET surface area ($m^2.g^{-1}$)	Pore diameter (Å)
0.4000	1385	24.50
0.3000	1047	28.00
0.2000	1065	28.00
0.1000	914	27.80
0.0500	575	25.00
0.0250	372	24.00

BET surface area of [Si]MCM-41 was expected to relate with the relative XRD intensity of the (100) plane because of the extent of mesoporous. The plot of BET surface area and XRD peak intensity of [Si]MCM-41 (MW) with different CTAB:SiO_2 ratios is shown in Figure 3.5. The relationship was divided into 3 situations. First, BET surface area increased with the peak intensity in the range of 0.025 – 0.200 ratio. Second, the surface area did not change significantly in the range of 0.200 – 0.300 ratio. Third, the surface area increased but the peak intensity decreased. In the last case, a non-ordering of hexagonal structure or interpenetration channel of mesostructured (3D) such as KIT-1 and MCM-48 might form to give a high surface area (Ryoo et al., 1997).

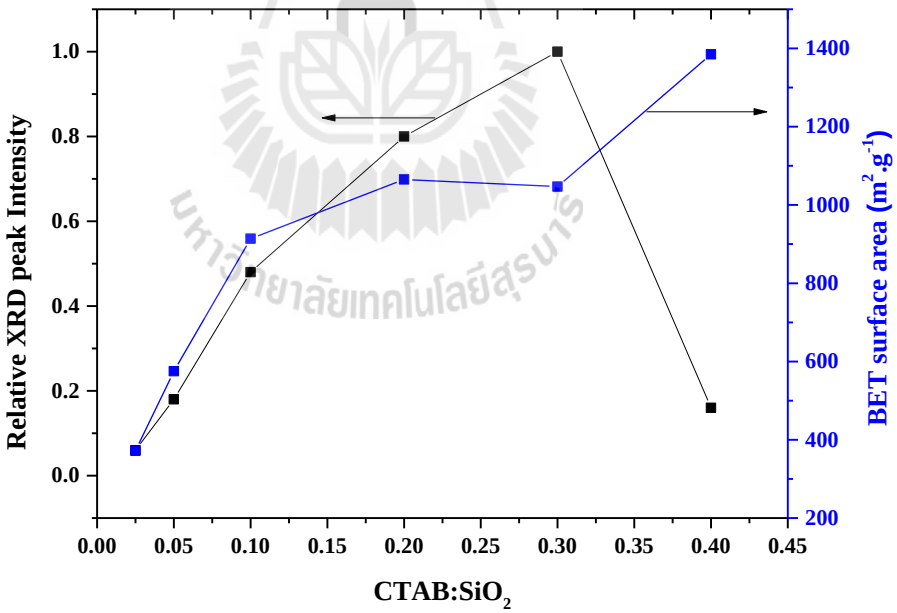

Figure 3.5 The Plot between relative XRD peak intensity versus BET surface areas of [Si]MCM-41 (MW) from different CTAB:SiO_2 ratios.

Table 3.3 Wall thickness (W_t) of [Si]MCM-41 (MW) from different CTAB:SiO_2 ratios.

CTAB:SiO_2	W_t (Å)
0.400	15.01
0.300	17.10
0.200	16.12
0.100	16.32
0.050	19.12
0.025	19.93

Considering the quality of MCM-41 based on the results from XRD and N_2 adsorption-desorption analysis, the CTAB:SiO_2 ratio of 0.300 was the best condition for the synthesis of [Si]MCM-41 under microwave irradiation.

3.4.1.2 Effect of NaOH:SiO_2 ratio

The XRD pattern of [Si]MCM-41 (MW) with NaOH:SiO_2 ratio of 1.0, 1.3 and 2.0 are shown in Figure 3.7. The five characteristic peaks of MCM-41 were observed from the samples with the ratio of 1.3 and 1.0. Only a broad peak around 2.8 degree was observed from the sample with the ratio of 2.0. In this case, the peak appeared at a lower degree compared to the samples from the 1.3 to 1.0 ratios referring to a unit cell expanding by increasing of wall thickness (Park et al., 2012). Na^+ can affect to charge density of interface between surfactant and silicate ions and disturb the formation of mesophase. Moreover, the wall thickness increased under a strong basic solution (Cheng et al., 2007). Since the sample from the ratio of 1.0 gave

the highest XRD peak intensities, this ratio was further employed to understand the effect of hydrothermal time.

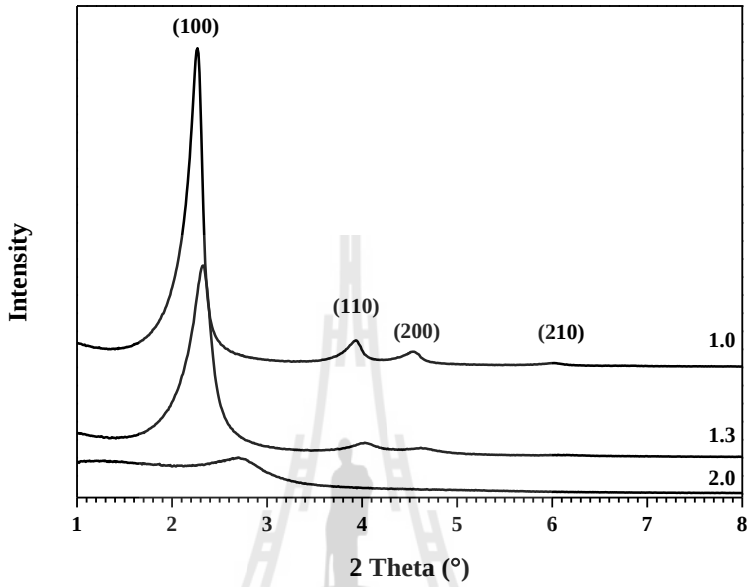

Figure 3.6 XRD patterns of [Si]MCM-41 (MW) from different $NaOH:SiO_2$ ratios.

Table 3.4 a_0 of [Si]MCM-41 (MW) with different $NaOH:SiO_2$ ratios.

$NaOH:SiO_2$	a_0 (Å)
2.0	-
1.3	43.84
1.0	45.10

3.4.1.3 Effect of hydrothermal time under microwave irradiation

The XRD patterns of [Si]MCM-41 (MW) with different hydrothermal times are shown in Figure 3.8. All five diffraction peaks of MCM-41 were observed from the sample treated by hydrothermal process for 15 min. The

sample with a longer hydrothermal time had the higher of peak intensity and a shift to a high degree inferring to the unit cell expanding (Table 3.5). In general, the hydrolysis and polymerization steps depend on the hydrothermal time. The hexagonal mesoporous phase did not transform to other phases under microwave irradiation in the study period.

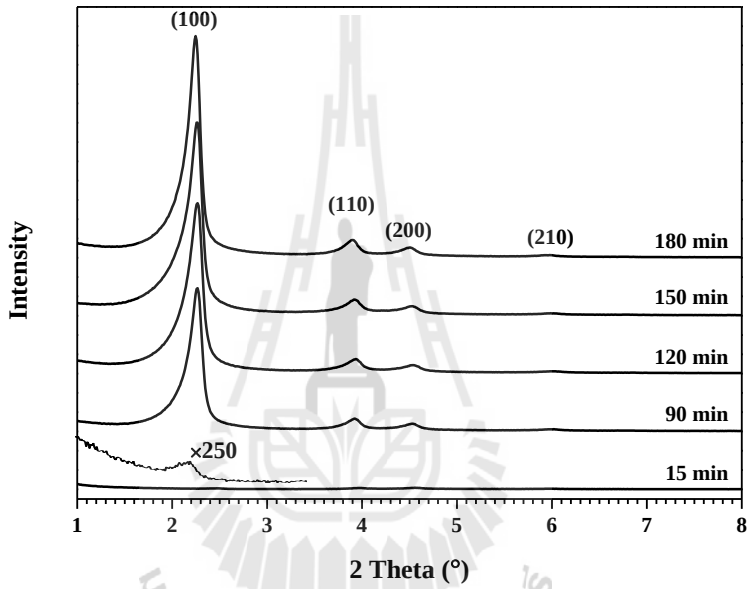

Figure 3.7 XRD patterns of [Si]MCM-41 (MW) from different hydrothermal times.

Table 3.5 a_0 of [Si]MCM-41 (MW) from different hydrothermal times.

Hydrothermal time (min)	a_0 (Å)
15	40.77
90	44.80
120	45.00
150	45.00
180	45.30

N_2 adsorption-desorption isotherms of [Si]MCM-41 (MW) from different NaOH:SiO_2 ratio are shown in Figure 3.9. At $P/P_0 > 0.3$ inflection, all samples exhibited the characteristic of mesoporous material with isotherm type IVc as mentioned in section 3.4.1.1. All samples had similar surface area (see Table 3.6) and BJH pore size distributions (see Figure 3.10). Comparing with previous works as shown in Table 3.7, BET surface area at 100 °C condition for 90 min of this work is higher value than that of Song et al. (2004) and Laha and Gläser (2007) work. Moreover, BET surface area of the samples from the condition higher than 100 °C with either a long or short time was similar. Thus, the higher hydrothermal temperature was not suitable in terms of energy consumption. Therefore, hydrothermal time of 90 min was the best condition in this study providing a high BET surface area and uniform mesopores diameter.

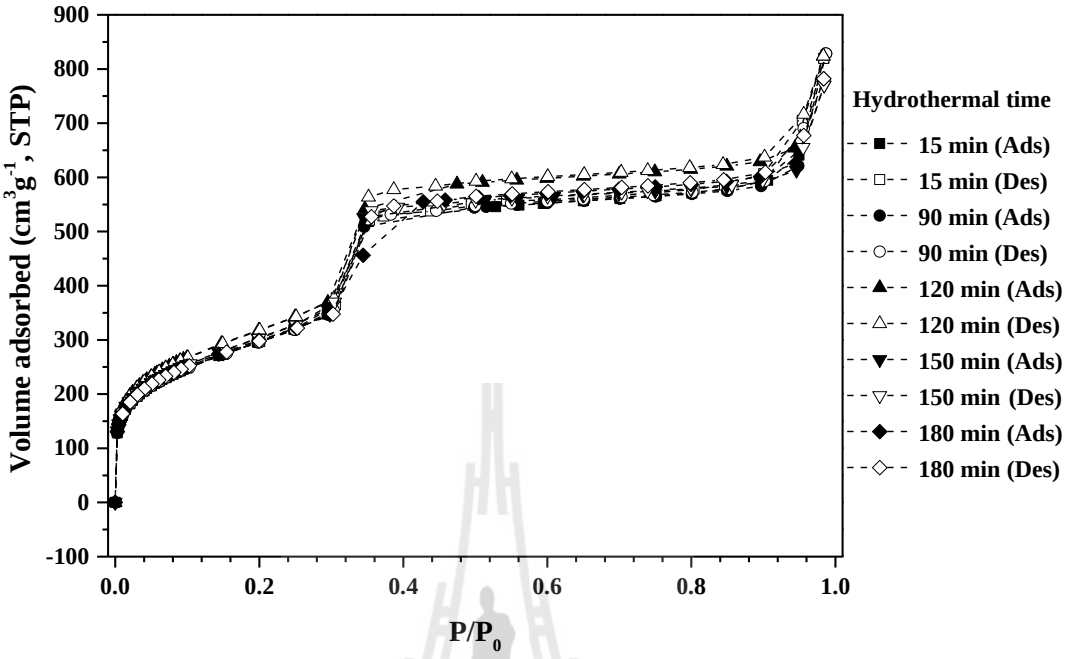

Figure 3.8 N_2 adsorption-desorption isotherms of [Si]MCM-41 (MW) from different hydrothermal times; adsorption (filled) and desorption (empty).

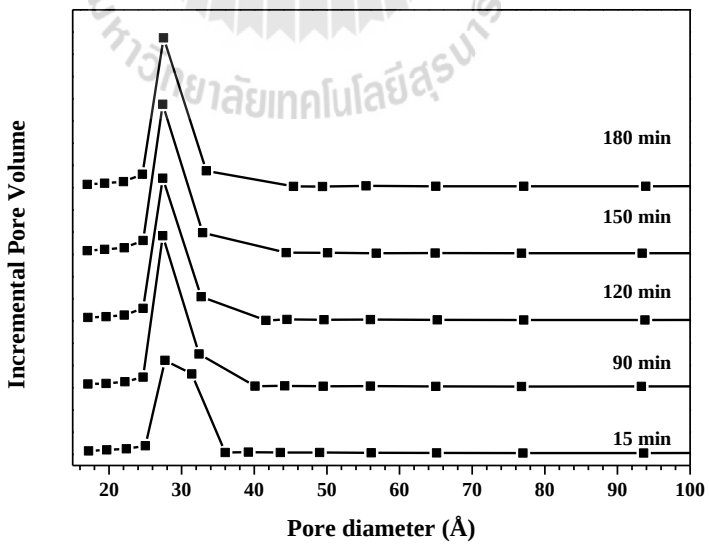

Figure 3.9 Pore size distributions by BJH method of [Si]MCM-41 (MW) from different hydrothermal times.

Table 3.6 BET surface area and pore diameter of [Si]MCM-41 (MW) from different crystallization times by N_2 adsorption-desorption data analysis.

Crystallization time (min)	BET surface area ($m^2.g^{-1}$)	Pore diameter (Å)
15	1066	28.0
90	1138	27.4
120	1064	27.4
150	1067	27.4
180	1093	27.4

Table 3.7 Comparison of heating conditions and surface area of MCM-41 from this work and literatures.

Material	Under microwave irradiation		BET surface area ($m^2.g^{-1}$)	Reference
	Heating (°C)	Time (min)		
Al-MCM-41	150	80	900-1000	Wu and Bein, 1996
[Si]MCM-41	120	60	1020	Park et al., 1998
[Si]MCM-41	100	120	1148	Song et al., 2004
Al-MCM-41	180	>60	800	Cheng et al., 2005
[Si]MCM-41	100	120	1196	Laha and Gläser, 2007
[Si]MCM-41	100	120	NR	González-Rivera et al., 2014
[Si]MCM-41	100	90	1138	This work

The following hypothesis explained the phenomena that the peak intensity was not proportional to the BET surface area. Generally, the peak intensity can be related to particle size (crystallize size) by Scherrer's equation. When the crystal size is large, the peak intensity is high (Monshi et al., 2012). To support this hypothesis, the particle size distributions are shown in Figure 3.11. The particle size tended to increase in the range of 90 – 180 min. Therefore, BET surface area was not improved by the longer hydrothermal time.

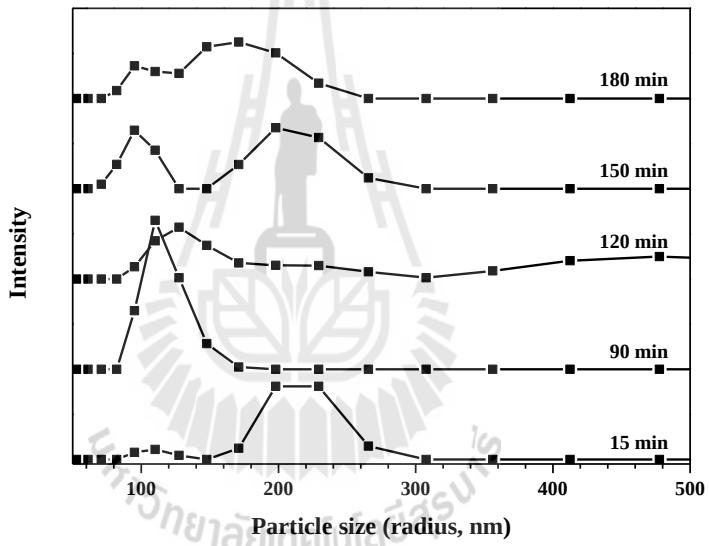

Figure 3.10 Particle size distribution by dynamics light scattering of [Si]MCM-41 (MW) from different hydrothermal times.

3.4.1.4 Thermal stability of MCM-41

A further study on a thermal stability was performed. The TGA thermogram of [Si]MCM-41 (MW) from the optimum condition, namely, CTAB to SiO_2 ratio = 0.300, NaOH:SiO_2 ratio = 1.0 and microwave-assisted hydrothermal time = 90 min is showed in Figure 3.11. The first weight loss from the 40 to 100 °C (2.5%)

corresponded to a removal of physisorbed waters. The second in the range of 150 to 600 °C (1.5%) was attributed to a decomposition of trace amounts of CTAB molecules. The third in the range of higher temperature (1.8%) corresponded to a water removal from silanol groups (-Si-OH) via condensation (Hajjami et al., 2015). The results showed that sample had high thermal stability.

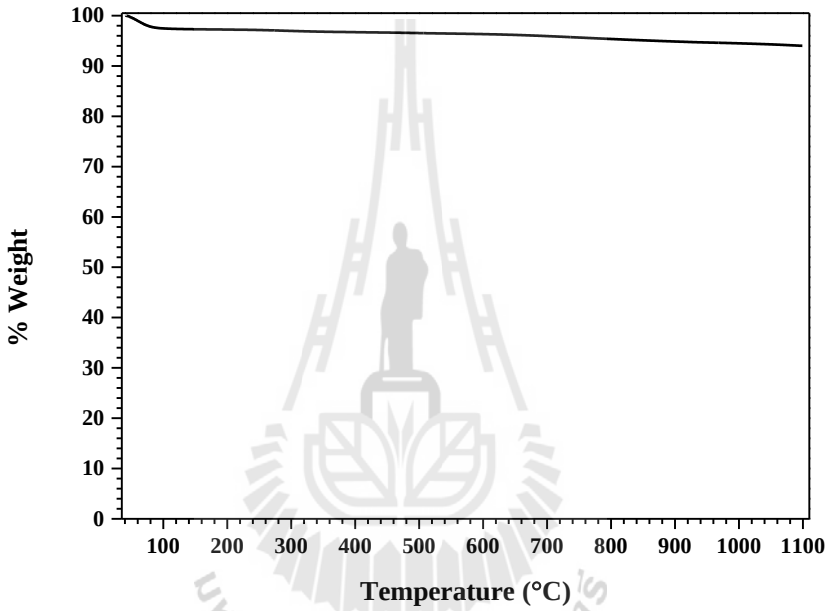

Figure 3.11 TGA thermogram of optimum [Si]MCM-41 (MW).

3.4.2 Comparison between [Si]MCM-41 (MW) and [Si]MCM-41 (C)

From the gel ratio $3.34SiO_2$:4.46NaOH:1CTAB:$1.16H_2SO_4$:$225H_2O$, [Si]MCM-41 (MW) and [Si]MCM-41 (C) were crystallized under microwave irradiation at 100 °C for 3 h and in an oven at 100 °C for 72 h, respectively. The XRD patterns of the products from both syntheses both samples are shown in Figure 3.12. Both samples showed characteristic peaks of MCM-41 but with different intensity. The peaks of Si]MCM-41 (MW) had lower intensity than [Si]MCM-41 (C). This

observation was in contrast with particle size distribution. From Figure 3.13 [Si]MCM-41 (MW) had less amount of large particles than [Si]MCM-41 (C). Therefore, [Si]MCM-41 from microwave-assisted hydrothermal time for 180 min was better than under conventional heating based on the less amount of small particle size.

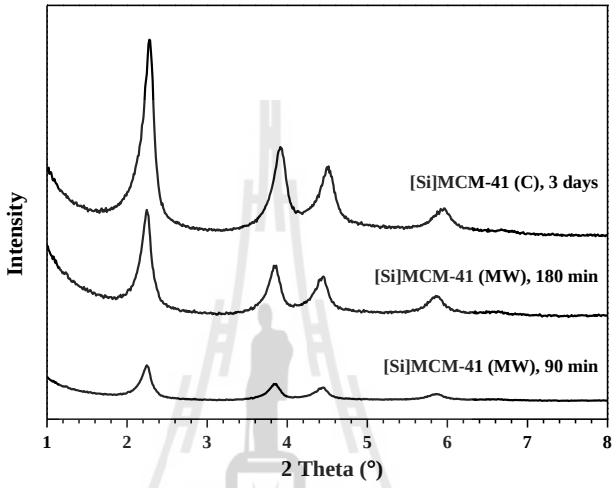

Figure 3.12 XRD patterns of [Si]MCM-41 (MW) and [Si]MCM-41 (C).

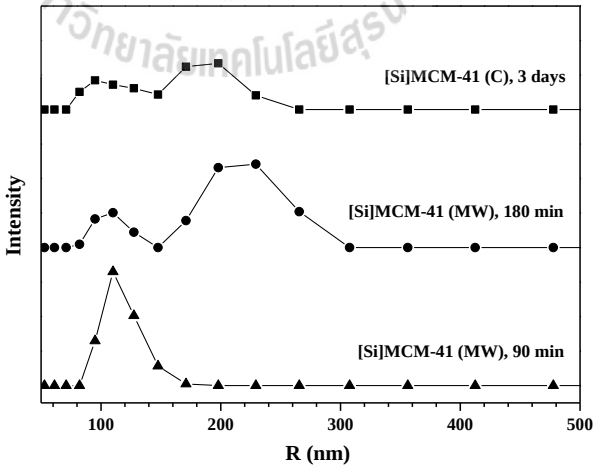

Figure 3.13 Particle size distribution by dynamics light scattering of [Si]MCM-41 (MW) and [Si]MCM-41 (C).

3.5 Conclusions

Siliceous MCM-41 has been synthesized from under microwave irradiation. The insufficient of CTAB concentration resulted to uncompleted MCM-41 structure. On the other hands, the excess CTAB concentration would transfer MCM-41 to non-periodic mesoporous materials. The different $NaOH:SiO_2$ ratio in the range of 1.0 – 1.3 affect to mesopore wall thickness related to degree of polymerization and hydrolysis. About crystallization time, the formation of hexagonal structure began at 15 min and become to be unifrom at 90 min. Therefore, the synthesis condition of $3.34SiO_2$:4.46NaOH:1CTAB:$1.16H_2SO_4$:$225H_2O$ mole ratio at 100 °C for 90 min is the best in this work. Regarding to the relative XRD diffraction peak intensity, N_2 adsorption-desorption analysis and thermogravimetric analysis and dynamics light scattering, the obtained MCM-41 had $a_0 \approx 44.80$ Å, uniform pore diameter of 27.40 Å, BET surface area of 1138 $m^2.g^{-1}$ and high thermal stability of 1100 °C. Moreover, the MCM-4 synthesized under microwave irradiation had the amount of small particle size more than under conventional heating.

3.6 References

Bachari, K. and Guerroudj, R.M. (2012). Characterization and catalytic properties of nickel-substituted hexagonal mesoporous silica prepared by microwave-hydrothermal method. **Comptes Rendus Chimie**. 15: 317 – 323.

Cheng, C.-E., Cheng, H.-H., Wu, L.-L. and Chengm, B.-W. (2005). Synthesis and characterization of nanoscale aluminosilicate mesoporous materials by microwave irradiation. **Surface Science and Catalysis**. 156: 113 – 118.

Cheng, C.-F., Chou, S.-H., Cheng, P.-W., Cheng, H.-H. and Yak, H.-K. (2007). Control of wall thickness and extraordinarily high hydrothermal stability of nanoporous MCM-41 silica. **Journal of the Chinese Chemical Society.** 54: 35 – 40.

Cheng, C.-F., Park, D.H. and Klinowski, J. (1997). Optimal parameters for the synthesis of the mesoporous molecular sieve [Si]-MCM-41. **Journal of the Chemical Society, Faraday Transactions**. 93(1): 193 – 197.

Gonźalez-Rivera, J., Tovar-Rodríguez, J., Bramanti, E., Duce, C., Longo, I., Fratini, E., Galindo-Esquivela, I.R. and Ferrari-Rivera, C. (2014). Surfactant recovery from mesoporous metalmodified materials (Sn–, Y–, Ce–, Si–MCM-41), by ultrasound assisted ion-exchange extraction and its re-use for a microwave in situ cheap and ecofriendly MCM-41 synthesis. **Journal of Materials Chemistry A**. 2: 7020 – 7033.

Hajjami, M., Ghorbani, F., Rahimipanah, S. and Roshani S. (2015). Efficient preparation of Zr(IV)-salen grafted mesoporous MCM-41 catalyst for chemoselective oxidation of sulfides to sulfoxides and Knoevenagel condensation reactions. **Chinese Journal of Catalysis.** 11: 1852 – 1860.

Jiang, T., Tang, W., Zhao, Q. and Yin, H. (2008). Effect of Ni-doping on the pore structure of pure silica MCM-41 mesoporous molecular sieve under microwave irradiation. **Colloids and Surfaces A: Physicochemical and Engineering Aspects**. 315: 299 – 303.

Kresge C.T. and Roth W.J. (2013). The discovery of mesoporous molecular sieves from the twenty year perspective. **Chemical Sociaty Reviews.** 2: 3663 – 3670.

Laha, S.C. and Gläser, R. (2007). Characterization and catalytic performance of [Cr] MCM-41 and [Cr] MCM-48 prepared by either classical or microwave heating. **Microporous and Mesoporous Materials**. 99: 159 – 166.

Liu, X., Sun, H., Chen, Y., Yang, Y. and Borgna, A. (2009). Preparation of spherical large-particle MCM-41 with a broad particle-size distribution by a modified pseudomorphic transformation**. Microporous and Mesoporous Materials**. 121: 73 – 78.

Meléndez-Ortiz, H.I., Mercado-Silva, A., García-Cerda, L.A., Castruita, G. and Perera-Mercado, L.A. (2013). Hydrothermal synthesis of mesoporous silica MCM-41 using commercial sodium silicate. **Journal of the Mexican Chemical Society**. 57(3): 73 – 79.

Monshi, A., Foroughi, M.R. and Monshi, M.R. (2012). Modified scherrer equation to estimate more accurately nano-crystallite size using XRD. **World Journal of Nano Science and Engineering.** 2: 154 – 160.

Park, S.-E., Chang, J.-S., Hwang, Y.K., Kim, D.S., Jhung, S.H. and Hwang, J.S. (2004). Supramolecular interactions and morphology control in microwave synthesis of nanoporous materials. **Catalysis Surveys from Asia**. 8(2): 91 – 110.

Park, S.-E., Kim, D.S., Chang, J.-S. and Kim, W.Y. (1998). Synthesis of MCM-41 using microwave heating with ethylene glycol. **Catalysis Today**. 44: 301 – 308.

Park, J., Han, Y. and Kim, H. (2012). Formation of mesoporous materials from silica dissolved in various NaOH concentrations: effect of pH and ionic strength**. Journal of Nanomaterials.** 2012: 1 – 10.

Rouquerol, F., Rouquerol, J., Llewellyn, P., Sing, K.S.W. and Maurin, G. (2013). Adsorption by powders and porous solids: principles, methodology and applications. United States of America, **Academic Press**.

Ryoo, R., Kim, J.M., Shin, C.H. and Lee, J.Y. (1997). Synthesis and hydrothermal stability of a disordered mesoporous molecular sieve. **Studies in Surface Science and Catalysis**. 105: 45 – 52.

Shi, Y., Wang, S. and Ma, X. (2011). Microwave preparation of Ti-containing mesoporous materials. Application as catalysts for transesterification. **Chemical Engineering Journal**. 166: 744 – 750.

Song, M.-G., Kim, J.-Y., Cho, S.-H. and Kim, J.-D. (2004). Rapid Synthesis of Mesoporous Silica by an Accelerated Microwave Radiation Method. **The Korean Journal of Chemical Engineering.** 21: 1224 – 1230.

Beck, J.S. and Vartuli, J.C. (1996). Recent Advances in The Synthesis, Characterization and Applications of Mesoporous Molecular Sieves. **Solid State & Materials Science**. 1: 78 – 87.

Wang, S., Shi, Y. and Ma, X. (2012). Microwave synthesis, characterization and transesterification activities of Ti-MCM-41. **Microporous and Mesoporous Materials**. 156: 22 – 28.

Wu, C.-G. and Bein, T. (1996). Microwave synthesis of molecular sieve MCM-41. **Chemical Communications**. 925 – 926.

CHAPTER IV

REMOVAL AND RECOVERY OF CETYLTRIMETHYLAMMONIUM ION FROM AS-SYNTHESIZED SILICEOUS MCM-41 FROM MICROWAVE-ASSISTED METHOD

4.1 Abstract

Cetyltrimethylammonium (CTA^+) bromide is a template in the synthesis of siliceous MCM-41 ([Si]MCM-41) which is normally removed by calcination. An alternative removal method which makes CTA^+ recycle possible is an ion exchange extraction. An effect of solvent polarity and type of salt under sonication was studied at various time and temperature. The efficiency of CTA^+ removal was estimated by thermogravimetric analysis (TGA) and X-ray diffraction technique (XRD). CTA^+ removal by NH_4Cl in methanol 70% under sonication at 30 °C for 15 min showed the high efficiency. Moreover, the CTA^+ recovery from solvent in an extracted solution from ion exchange (extracted CTA^+) and a solution after hydrothermal treatment (waste powder) were carried out by solvent evaporation. The mixture compounds are presented in both sample regarding to Fourier transform infrared spectroscopy technique (FTIR) and XRD results.

4.2 Introduction

Cetyltrimethylammonium (CTA^+) bromide is a quaternary ammonium with one chain of C16 alkane and three methyl groups. It is a surfactant which can be used as a template in the synthesis of siliceous MCM-41 ([Si]MCM-41) to form micelle and lead to a formation of highly uniform mesopores. The void of mesopores will be generated after the CTA^+ removal, commonly by calcination (Ryczkowski et al., 2005). The removal by calcination decomposes CTA^+, consumes energy and makes the synthesis of MCM-41 costly.

Various decomposition methods have been employed with mild conditions to minimize energy consumption to remove CTA^+, for example, microwave- or photo-assisted oxidation with a mild thermal treatment (Keene et al., 1998; Chen et al., 2014), dielectric-barrier discharge plasma technique at room temperature (Liu et al., 2010). Although those methods lowered the energy consumption, the CTA^+ was still lost and wasted.

Another method to remove and recover CTA^+ from MCM-41 at mild conditions is solvent and/or ion exchange extraction. As shown in Scheme 4.1, CTA^+ cations interacting with siloxy anions on the mesopore wall by electrostatic force (Chen et al., 2014) could be extracted by a solvent based on solubility principle or exchanged by smaller molecules based on ion exchange efficiency. Schmidt et al. (1994) investigated the impact of template extraction under magnetic stirring on the structure of MCM-41 with different Si/Al ratios. They concluded that templates had stronger interaction on the surface of Al-MCM-41 than that of siliceous MCM-41. Hitz and Prins (1997) studied on CTA^+ ion exchange on Al-MCM-41 by various acids, salts or small quaternary ammonium in alcohol. They concluded that the extraction under

acidic alcohol solution gave a high yield and stable Al-MCM-41. The more polar solvent was proved to be the more efficient for CTA^+ removal method. Different cation sizes directly affect the removal efficiency related to ion mobility between bulk solution and CTA^+ containing Al-MCM-41 on surface. Moreover, MCM-41 structure could be depolymerized under basic solution. Since then, many researchers began to investigate on the other properties related to solvent or ion exchange extraction parameters, for example temperature, duration and solution components (Gomes Jr. et al., 2005; Marcilla et al., 2010; Du et al., 2011; Aripad et al., 2012). Moreover, agitation by sonication was used to increase the removal efficiency (Shaghayegh and Zanjanchi, 2014; Jabariyan et al., 2012). However, most of those works was done on Al-MCM-41 and the effect of media species and solvents on siliceous MCM-41 were not clearly understood. Thus, this work aimed to investigate CTA^+ removal by ion exchange extraction under sonication with various salt solution, time and temperature.

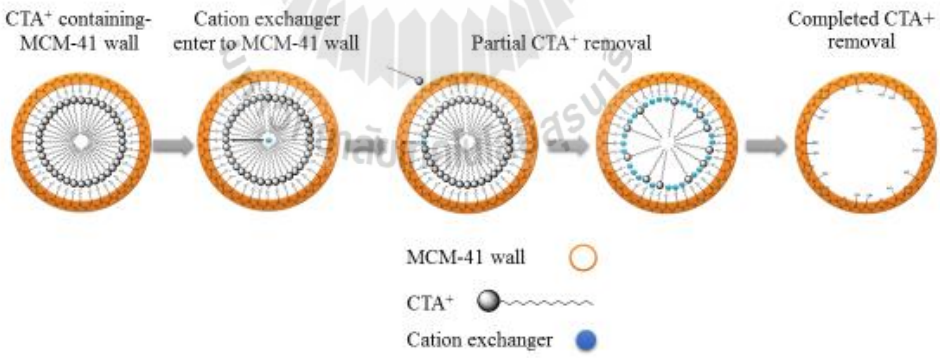

Scheme 4.1 Representation of silica-surfactant interfaces of [Si]MCM-41 and ion-exchange process.

Before the study on CTA^+ removal efficiency, thermal decomposition of CTA^+ in as-synthesized MCM-41 was first determined.

Herein, CTA^+ was removed from siliceous MCM-41 by ultrasound-assisted ion exchange method in various salt solutions. The salts were either alkaline or organic in neutral, acidic and basic condition. Before that an effect of solvent polarity was studied to see the possibility to avoid using methanol which is toxic. Temperature and sonication period were varied.

After extraction, CTA^+ was recovered by evaporation. Moreover, CTA^+ was recovered from the solution from hydrothermal treatment. This solution was generally disposed. Therefore, the additional study on CTA^+ recovery from this solution was set up to see the probable recycling by water evaporation.

4.3 Experimental

4.3.1 CTA^+ removal

Siliceous MCM-41 was synthesized by hydrothermal method under microwave heating with $3.34SiO_2$: $4.46NaOH$:1CTAB:$1.16H_2SO_4$: $225H_2O$ mole ratio as mentioned in Chapter III. The sample was named [Si]MCM-41 (MW). CTA^+ removal from the as-synthesized [Si]MCM-41 (MW) was performed by extraction under sonication. First, methanol or water was used to see effect of solvent polarity. An aqueous or methanolic solution containing NH_4Cl was employed at 60 °C for 30 min. Then the better solvent was used though the next of the study. Various salts were used including $NaNO_3$, NaCl, NaBr, NaOAc, KNO_3, KCl, KOAc, KH_2PO_4, NH_4NO_3, NH_4Cl and NH_4OAc. A typical run was modified from González-Rivera et al. (2014) as follows: the as-synthesized [Si]MCM-41(MW) (0.2 g) and 40 mL of 40 mM salt solution were loaded in a 50-mL centrifuge tube. The mixture was sonicated using an Elmasonic E30H at 27 kHz at 60 °C for 60 min. After sonication, the mixture was

cooled down, separated by centrifugation, washed once with the solvent and dried at 80 °C overnight. The obtained solid sample was named "detemplated [Si]MCM-41 (MW)". The extraction was done under various time (15 – 120 min) and temperature (30 – 60 °C).

4.3.2 CTA^+ recovery

Solvent in the extracted solution was removed by rotary evaporator at 60 °C and dried in an open air at 40 °C. The obtained precipitate was named "Extracted CTA^+".

CTA^+ was also recovered from the hydrothermal solution obtained by centrifugation. It was dried at 80 °C and named "Waste powder".

4.3.3 Characterization

The amount of remaining template in the detemplated [Si]MCM-41 (MW) was determined by thermogravimetric and differential thermogravimetric analysis (TGA–DTA, TA Instrument/ SDT2960) in a flow of air zero (21%O_2 in N_2 balance) with a flow rate 100 mL/min and heating rate 20 °C/min from 40 to 600 °C. The CTA^+ removal efficiency was estimated with Equation 4.1 according to the weight loss from the TGA thermogram in the temperature range 150 – 375 °C.

$$\%\,CTA^+\,removal = \frac{\%\,weight\ loss\ of\ sample_0 - \%\,weight\ loss\ of sample_i}{\%\,weight\ loss\ of\ sample_0} \times 100 \qquad (4.1)$$

Where $sample_0$ is an as-synthesized [Si]MCM-41 (MW) and $sample_i$ is a detemplated [Si]MCM-41 (MW).

The detemplated [Si]MCM-41 (MW) was characterized by X-ray diffraction (XRD, Bruker D8). The extracted CTAB and wasted powder were characterized by FTIR spectroscopy and XRD.

4.4 Results and discussion

4.4.1 TGA analysis of as-synthesized [Si]MCM-41 (MW)

Figure 4.1 shows the percent weight loss of as-synthesized [Si]MCM-41 (MW). The changes were divided into 4 regions according to the work by Ryczkowski et al. (2005) from an analysis by an on-line mass spectrometer. The weight loss from the beginning to 150 °C (3.69%) corresponded to the removal of physisorbed water. The loss between 150 °C and 320 °C (34.67%) was attributed to combustion of quaternary ammonium ions. The next loss between 320 °C and 375 °C (7.42%) corresponded to further combustion of hydrocarbon chain residue. The final range from 375 °C to 600 °C (4.91%) corresponded to dehydroxylation from silanol groups (-Si-OH). Consequently, the weight loss between 150 °C and 375 °C (42.09%) was used as a comparison to other samples.

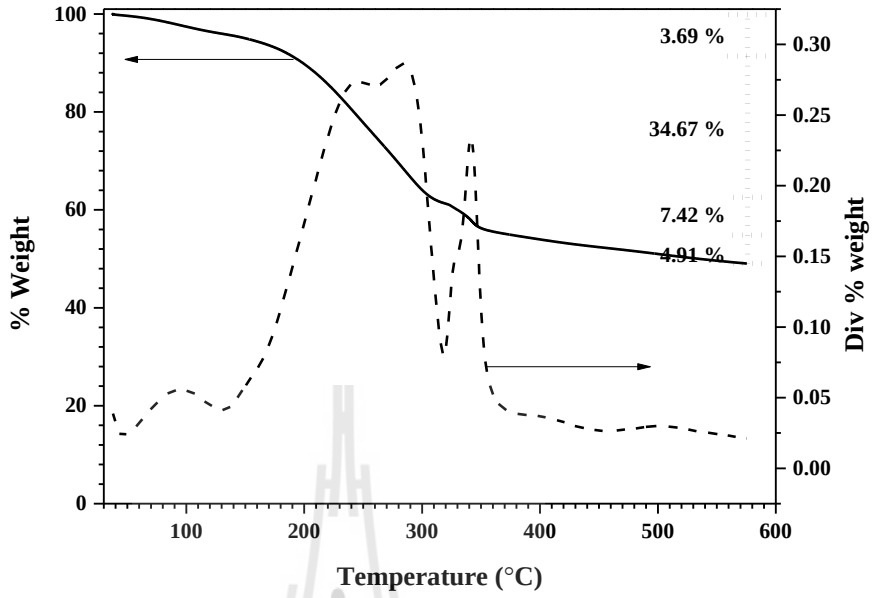

Figure 4.1 TGA thermogram of as-synthesized [Si]MCM-41 (MW), Solid line, % weight; dashed line, Div % weight.

4.4.2 Effect of solvent polarity on CTAB removal

The thermograms of detemplated [Si]MCM-41 (MW) after extraction with water and methanol containing NH_4Cl salt are compared in Figure 4.2. The weight losses were 39.14 wt.% and 13.24 wt.% respectively. The more weight loss from water extraction meant the more amount of CTA^+ remained and lower CTA^+ removal efficiency. Therefore, the CTA^+ removal by aqueous solution was not as effective as methanolic solution. The higher removal efficiency by methanol was explained by Jabariyan et al. (2012). The micelles of CTA^+ could be disrupted by alcohol (Figure A5 in Appendix). In addition, the lower solubility of CTAB (3.64 g/100 g) in water than NH_4Cl (41.4 g/100 g) indicated that CTA^+ preferred to remain in mesopores

rather than water. Hence, methanol solution was selected for further study on an ion-exchange.

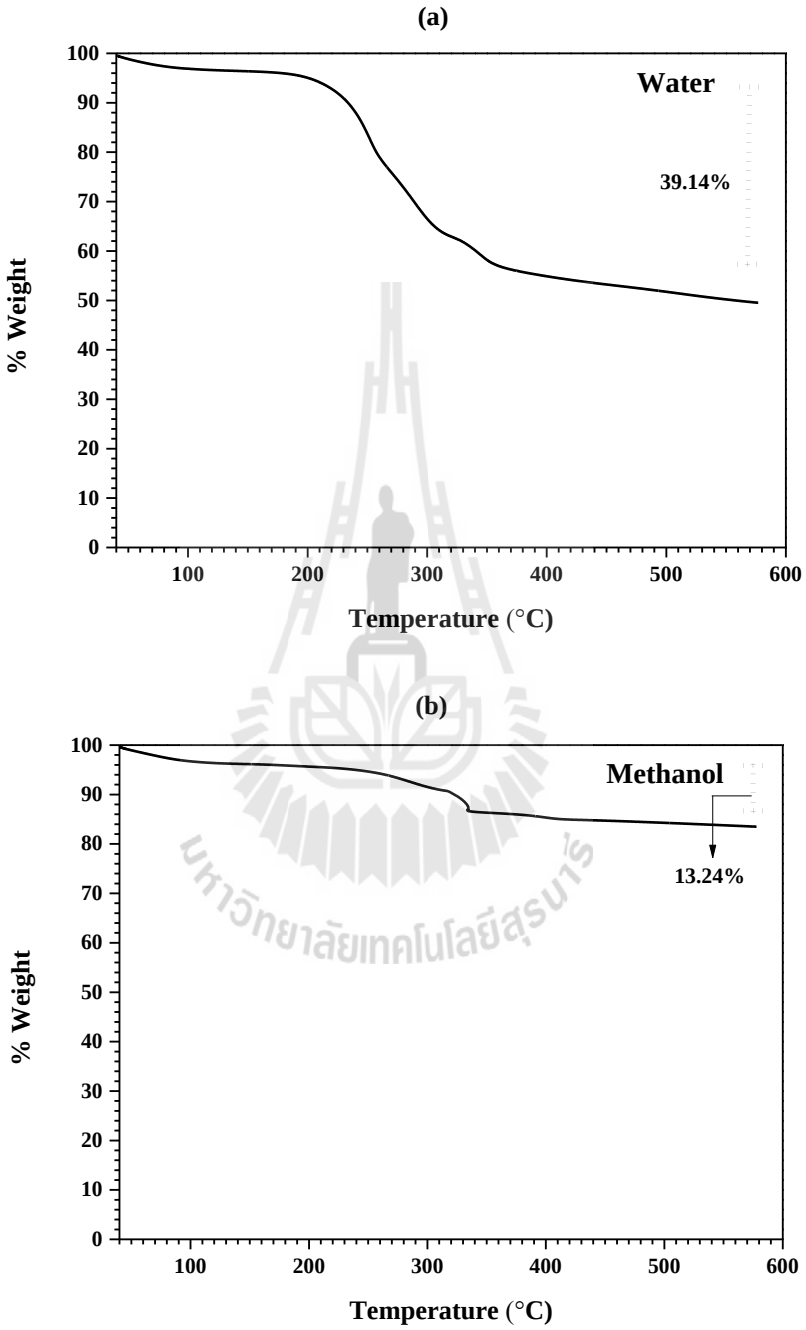

Figure 4.2 Thermograms of detemplated [Si]MCM-41 (MW) after the extraction with water (a) and methanol (b) containing NH_4Cl salt.

4.4.3 Effect of nitrate salt with different cations

The thermograms of detemplated [Si]MCM-41 (MW) after extraction with nitrate salts of different cations (NH_4^+, Na^+ and K^+) in methanol are shown in Figure 4.3. The percent CTA^+ removals are summarized in Table 4.1, respectively. The high CTA^+ removal was obtained from $NaNO_3$ and NH_4NO_3 methanolic solutions. Based on ion exchange principle (Harland, 1994) and mobility of ions in MCM-41 pore containing CTA^+ micelles, the quaternary ammonium ion size of NH_4NO_3 is smaller than that of CTA^+ resulting in an easy exchange. A further confirmation on the effect of cation size of nitrate salts was performed by comparing Na^+ or K^+ (ion size 1.16 Å and 1.52 Å, respectively). CTA^+ removal by Na^+ solution was higher than that by K^+ solution, consistent with the ion size. A study on Na^+ and K^+ cation salts with different anions was also carried out. The results can be found in appendix A. However, both ions were not appropriate to CTA^+ removal because they led to structure collapse (Appendix A). Thus, the further study was focused on ammonium salts.

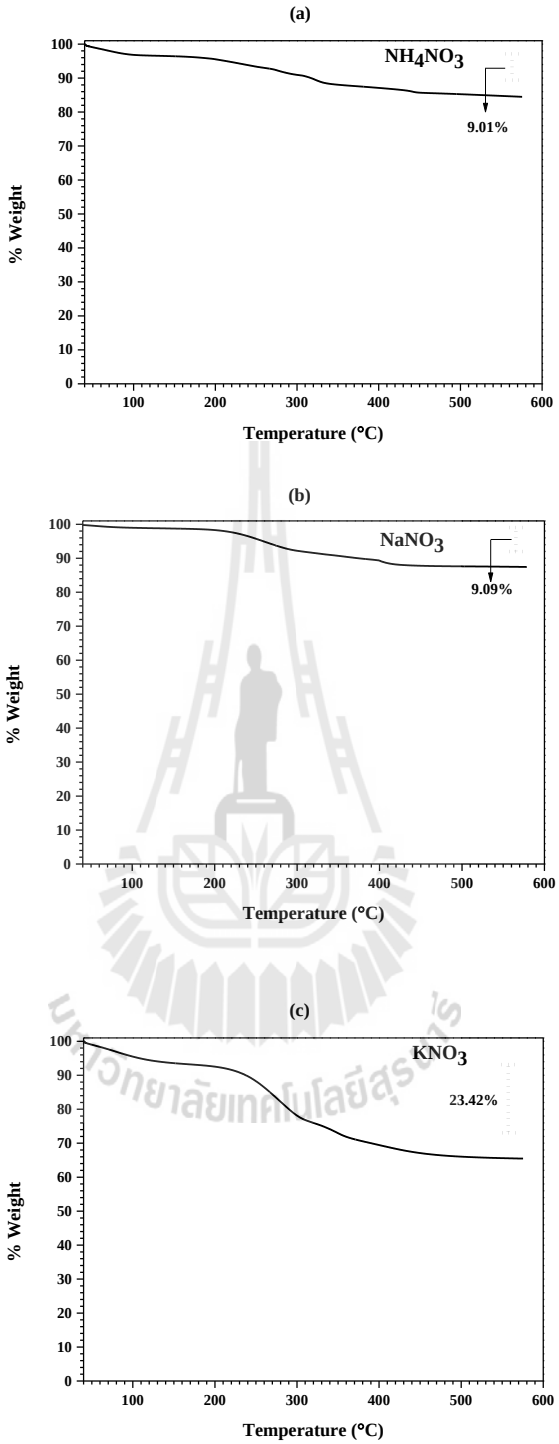

Figure 4.3 Thermograms of detemplated [Si]MCM-41 (MW) after the extraction with nitrate salts of different anions ((a) NH_4^+, (b) Na^+ and (c) K^+).

Table 4.1 The percent weight loss and corresponding to CTA^+ removal of detemplated [Si]MCM-41 (MW) after the extraction with nitrate salts of different cations (NH_4^+, Na^+ and K^+).

	% Weight loss	% CTA^+ removal
$NaNO_3$	9.09	78.40
KNO_3	23.43	44.33
NH_4NO_3	9.01	78.59

The detemplated [Si]MCM-41 (MW) samples after extraction with nitrate salts of different cations in methanol were characterized by XRD and the XRD patterns are shown in Figure 4.4. The 3 main diffraction peaks of the (100), (110) and (200) plane was compared as an indication of structure stability. The samples showed the main diffraction peak with different position and intensity. The sample extracted with NH_4NO_3 solution showed the peak of (100) plane at 2.20 degree. The peak shift compared to as-synthesized sample corresponded to siloxy condensation (Andrade et al., 2000). The peak of (100) plane from the treatment with $NaNO_3$ and KNO_3 solution shifted to 2.35 and 2.45 degree with low intensity possibly due to collapse of mesopores or grafting of alkaline metal oxide on the mesopore wall (Hitz and Prins, 1997). Regarding to the XRD results, NH_4^+ cation was the most suitable for CTA^+ removal.

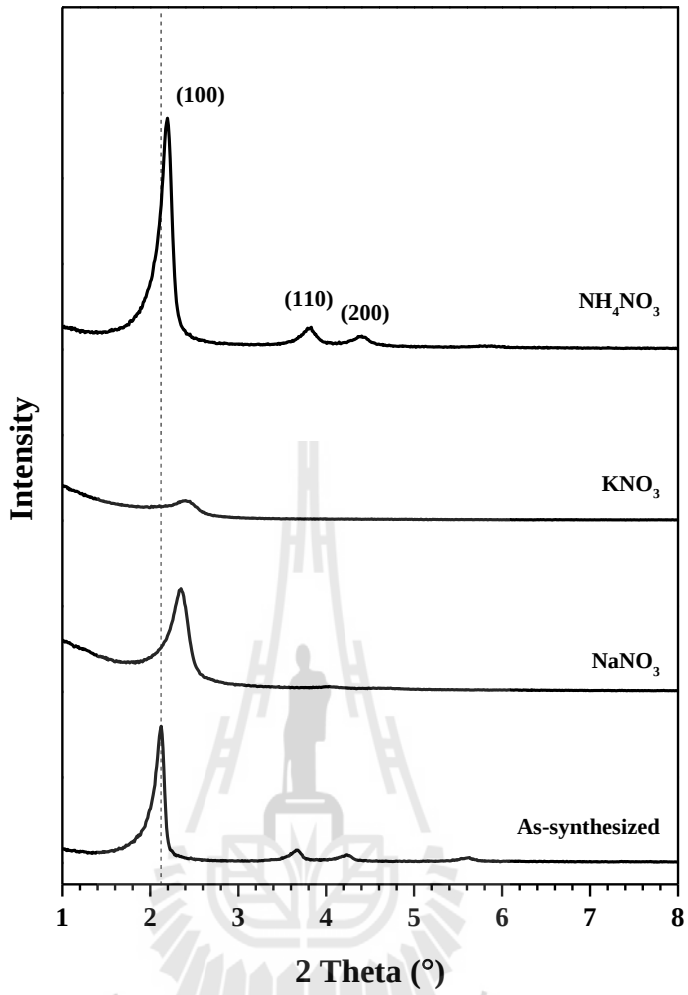

Figure 4.4 XRD patterns of detemplated [Si]MCM-41 (MW) after the extraction with nitrate salts of different cations (NH_4^+, Na^+ and K^+).

4.4.4 Effect of ammonium salt with different anions

The TGA of detemplated [Si]MCM-41 (MW) after the extraction with ammonium salts containing different anions (NO_3^-, Cl^- and OAc^-) are shown in Figure 4.5. The percent CTA^+ removals are summarized in Table 4.2, respectively. All samples had a similar weight loss around 77% CTA^+ removal indicating that the type of anions had no significantly effect on the removal efficiency.

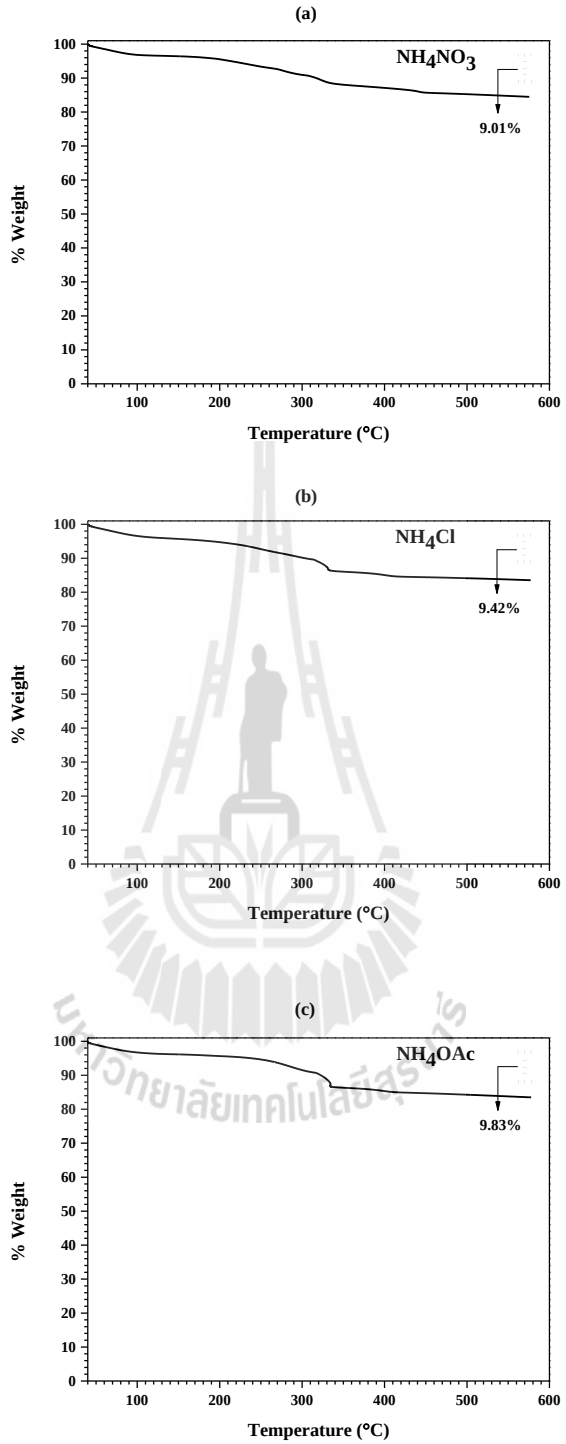

Figure 4.5 Thermograms of detemplated [Si]MCM-41 (MW) after the extraction with ammonium salts of different anions ((a) NO_3^-, (b) Cl^- and (c) OAc^-).

Table 4.2 The percent weight loss and corresponding to CTA^+ removal of detemplated [Si]MCM-41 (MW) after the extraction with ammonium salts of different anions (NO_3^-, Cl^- and OAc^-).

	% Weight loss	% CTA^+ removal
NH_4NO_3	9.01	78.59
NH_4Cl	9.42	77.85
$NH_4(OAc)$	9.83	76.65

Figure 4.6 shows XRD pattern of the detemplated [Si]MCM-41 (MW) samples after the extraction with ammonium salts of different anions (NO_3^-, Cl^- and OAc^-). The main diffraction peak of all samples did not shift significantly implying that the use of ammonium salts similar degree of siloxy condensation. Nevertheless, the appearance of similarity and high intensity of main peak indicated that mesopores are not collapse. Hence, NH_4Cl solution is slightly better than other solution regarded to the quality MCM-41 structure.

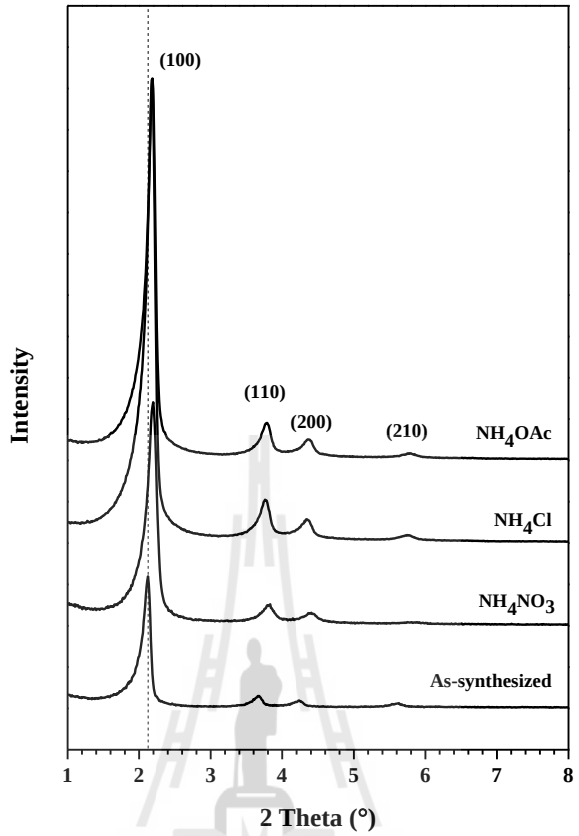

Figure 4.6 XRD patterns of detemplated [Si]MCM-41 (MW) after the extraction with ammonium salts of different anions (NO_3^-, Cl^- and OAc^-).

4.4.5 Effect of sonication time and temperature

The thermograms of detemplated [Si]MCM-41 (MW) after extraction with NH_4Cl methanolic solution under sonication at varying time and temperature are shown in Figure 4.7 and 4.8. At 60 °C, the CTA^+ removal efficiency slightly increased with time. The slight increase indicated that 15 min was sufficient. The longer time allowed the more opportunity for the exchange (Hua et al., 2001). Meanwhile, the temperature close to boiling point of methanol kinetically facilitated the more ion exchange (Jabariyan et al., 2012). However, energy consumption was

concerned. The percent CTA^+ removal was divided by time and temperature to compare the unit-by-unit as shown in Table 4.3 and 4.4. The sonication at 30°C for 15 min achieved the highest CTA^+ removal efficiency.

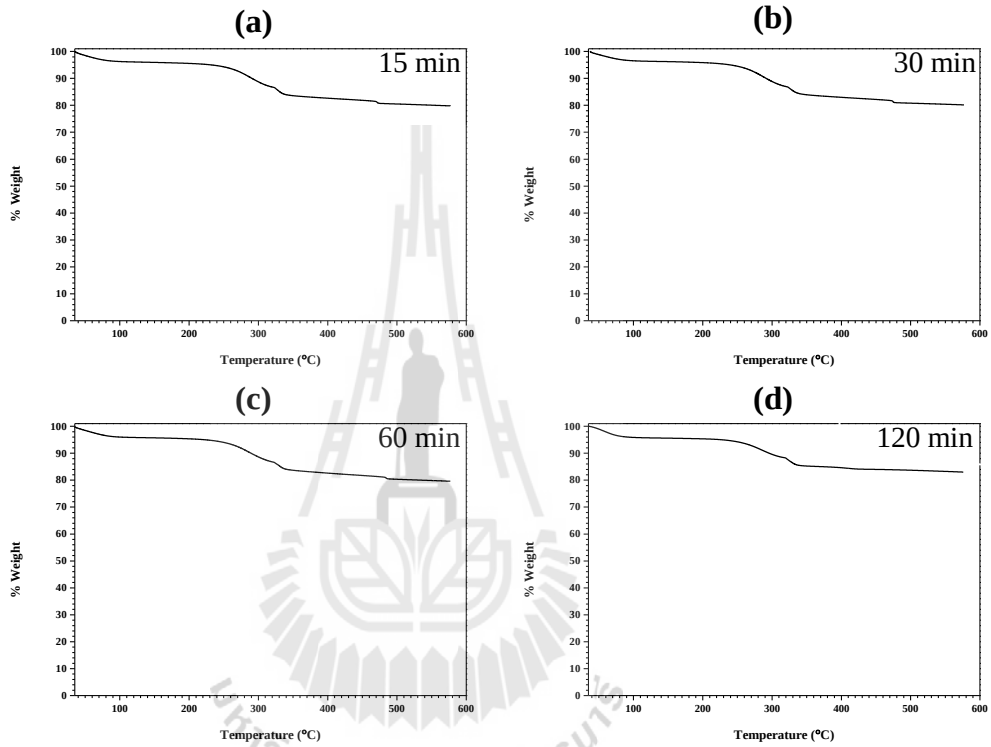

Figure 4.7 Thermograms of detemplated [Si]MCM-41 (MW) after the extraction with NH_4Cl under sonication at 60 °C for (a) 15 min, (b) 30 min, (c) 60 min and (d) 120 min.

Table 4.3 The percent weight loss and corresponding to CTA^+ removal of detemplated [Si]MCM-41 (MW) after the extraction with NH_4Cl under sonication at 60 °C with varying time.

Time (min)	% CTA^+ removal	% CTA^+ removal per min
15	70.54	4.7
30	71.49	2.4
60	74.82	1.3
120	77.67	0.65

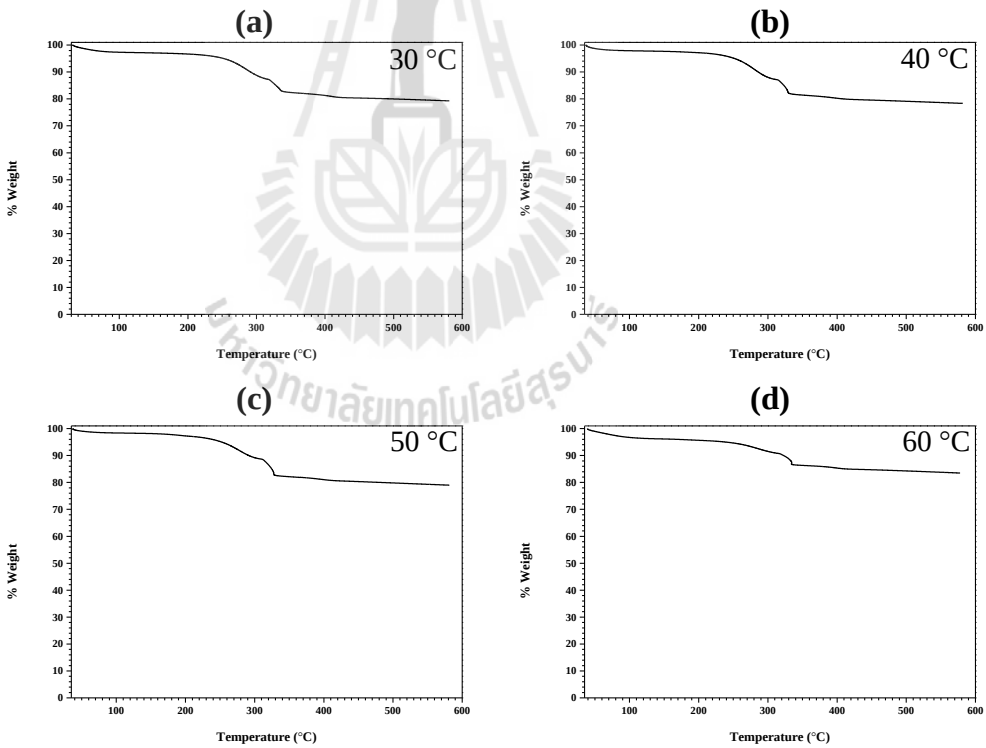

Figure 4.8 Thermograms of detemplated [Si]MCM-41 (MW) after the extraction with NH_4Cl under sonication for 30 min at (a) 30 °C, (b) 40 °C, (c) 50 °C and (d) 60 °C.

Table 4.4 The percent weight loss and corresponding to CTA^+ removal of detemplated [Si]MCM-41 (MW) after the extraction with NH_4Cl under sonication for 30 min at varying temperature.

Temperature (°C)	% CTA^+ removal	% CTA^+ removal per °C
30	61.04	2.0
40	61.51	1.5
50	65.84	1.3
60	71.49	1.2

4.4.6 Template recovery

FTIR spectrum and assignment of extracted CTA^+, waste powder are shown in Figure 4.9 and Table 4.5. The characteristic FTIR spectra of extracted CTA^+, waste powder are similar to pure CTAB. However, some ammonium groups in the extracted CTA^+ might be oxidized by radical species generated under sonochemical reactions (Okitsu et al., 2004) to nitrogen oxide species. Moreover, CTAB molecules and siliceous material remained in the waste powder. The vibration corresponding to external linkage of double four-membered rings (D4R), double five-membered rings (D5R), or double six-membered rings (D6R), and pore opening vibrations were observed from the waste powder after calcination indicating to mixture siliceous materials which is not MCM-41.

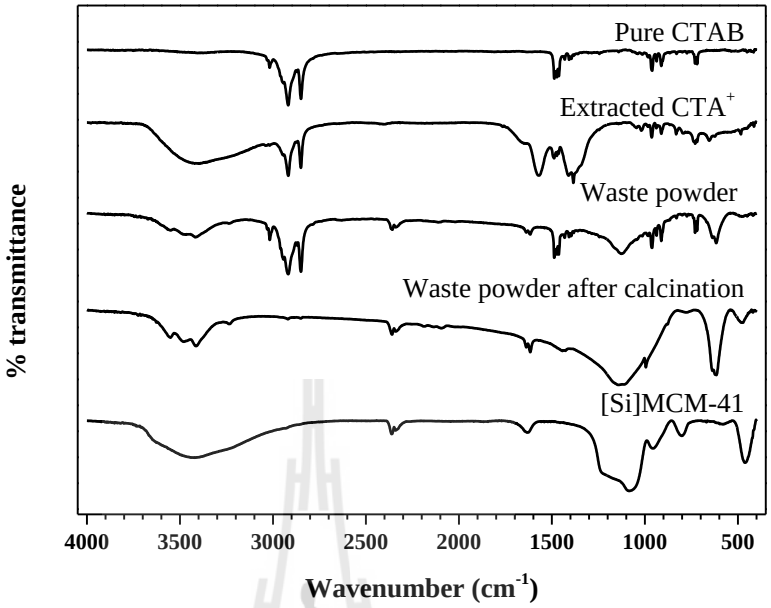

Figure 4.9 FTIR spectra of pure CTAB, extracted CTA^+, waste powder, waste powder after calcination, and [Si]MCM-41.

Table 4.5 Wavenumber and assignment in FTIR spectra of pure CTAB, extracted CTA^+, waste powder, waste powder after calcination, and [Si]MCM-41.

Wavenumber (cm^{-1})	Assignments	Reference
3500	-Si-OH	Jomekian et al., 2012.
3000	$-N(CH_3)_3$	Viana et al., 2012.
2920	$-CH_3$	Gonźalez-Rivera et al., 2014.
2850	$-CH_2$	Gonźalez-Rivera et al., 2014.
1620	$R-NH^{3+}$	Ryczkowski et al., 2005.
1560,1380	-N-O	Shapiro, 1969.
1490-1380	C-H of alkylammonium ion	Ariapad et al., 2012.
1090, 970	SiO_4 stretching	Gonźalez-Rivera et al., 2014.
725	In-plan symmetrical vibration	Ryczkowski et al., 2005.
650-500	External linkage vibrations DR	Li and Wu, 2003.
465	SiO_4 bending	Gonźalez-Rivera et al., 2014.
420-300	Pore opening vibrations on lattice	Li and Wu, 2003.

Data from XRD was used to support the FTIR result. XRD patterns of pure CTAB, extracted CTA^+, waste powder and waste powder after calcination are shown in Figure 4.10 and 4.11. The XRD pattern of extracted CTA^+ and waste powder contained characteristic peaks of CTAB. However, XRD pattern of waste powder after calcination seem to be mixture siliceous materials.

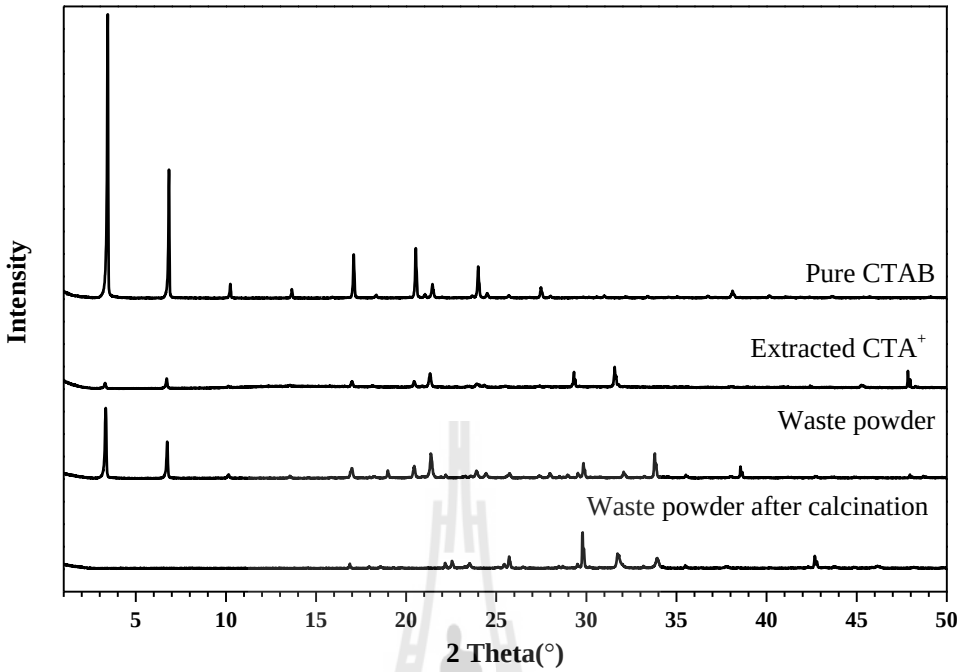

Figure 4.10 XRD patterns of pure CTAB, extracted CTA^+, waste powder and waste powder after calcination.

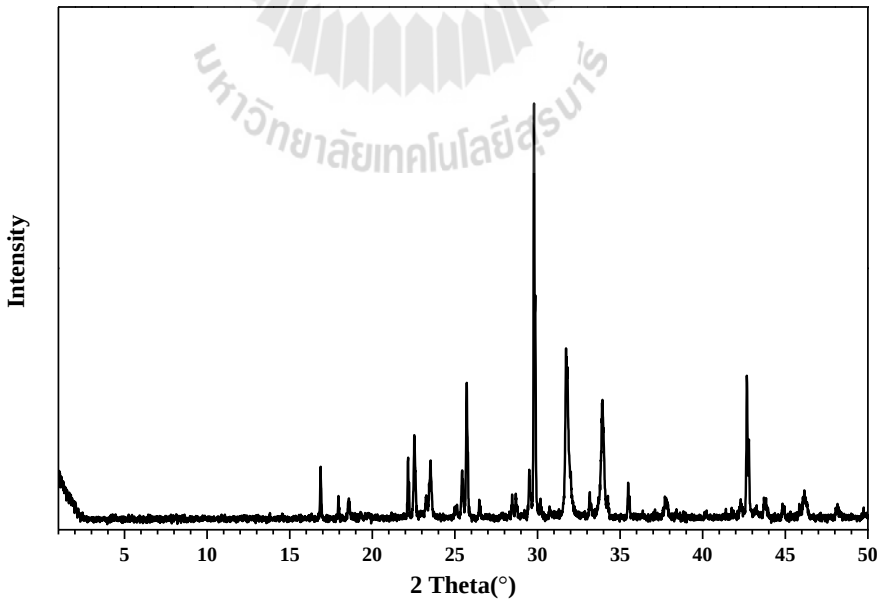

Figure 4.11 XRD pattern of waste powder after calcination (Zoom).

4.5 Conclusions

From all ion exchanges study in various salts, it showed CTA^+ removal about 30-78%. The extraction in the presence of NH_4Cl is the best condition allowed up to 77% of CTA^+ removal. From XRD results, the characteristic peaks of MCM-41 in different ion-exchange extraction conditions were obtained and concluded that 1) cation-exchanges with CTA^+ were compatible with ion exchange principle ordered by $Na^+ > K^+ > NH_4^+$. 2) Alkaline metal ions were not recommended. 3) Different anions of ammonium salts were not significantly different for efficient CTA^+ removal. However, the acidic solution gave high CTA^+ removal percentage and saved MCM-41 structure. The efficient CTA^+ removal increased with increasing time and temperature. However, an ion exchange at 30 °C for 15 minute was suitable for good efficient CTA^+ removal by reducing energy consumption.

The extracted CTA^+ had some characteristic of pure CTAB by FTIR and XRD. They were probably partially oxidized under thermal treatment. One compound in waste powder was CTA^+.

4.6 References

Ariapad, A., Zanjanchi, M.A. and Arvand, M. (2012). Efficient removal of anionic surfactant using partial template-containing MCM-41. **Desalination**. 284: 142 – 149.

Chen, L., Jiang, S., Wang, R., Zhang, Z. and Qiu, S. (2014). A novel, efficient and facile method for the template removal from mesoporous materials. **Chemical Research in Chinese Universities**. 30: 894 – 899.

Du, P.D., Khieu, D.Q. and Hoa, T.T. (2011). Removal of organic template from mesoporous MCM-41. **Journal of Science, Hue Univertity**. 69: 35 – 41.

Gomes Jr. W.A., Cardoso, L.A.M., Gonzaga, A.R.E, Aguiar, L.G. and Andrade, H.M.C. (2005). Influence of the extraction methods to remove organic templates from Al-MCM-41 molecular sieves. **Materials Chemistry and Physics**. 93(1): 133 – 137.

Gonźalez-Rivera, J., Tovar-Rodr´ıguez, J., Bramanti, E., Duce, C., Longo, I., Fratini, E., Galindo-Esquivela, I.R. and Ferrari-Rivera, C. (2014). Surfactant recovery from mesoporous metalmodified materials (Sn–, Y–, Ce–, Si–MCM-41), by ultrasound assisted ion-exchange extraction and its re-use for a microwave in situ cheap and ecofriendly MCM-41 synthesis. **Journal of Materials Chemistry A**. 2: 7020 – 7033.

Harland, C.E. (1994). Ion Exchange: Theory and Practice, first ed., Cambridge: Royal Society of Chemistry, United Kingdom.

Hitz, S. and Prins, R. (1997). Influence of template extraction on structure, activity, and stability of MCM-41 catalysts. **Journal of Catalysis**. 168: 194 – 206.

Hua, Z.-L., Shi, J.-L., Wang, L. and Zhang, W.-H. (2001). Preparation of mesoporous silica films on a glass slide: surfactant template removal by solvent extraction. **Journal of Non-Crystalline Solids.** 292: 177 – 183.

Jabariyan, S. and Zanjanchi, M.A. (2012). A simple and fast sonication procedure to remove surfactant templates from mesoporous MCM-41. **Ultrasonics Sonochemistry**. 19: 1087 – 1093.

Jiang, T., Tang, W., Zhao, Q. and Yin, H. (2008). Effect of Ni-doping on the pore structure of pure silica MCM-41 mesoporous molecular sieve under microwave irradiation. **Colloids and Surfaces A: Physicochemical and Engineering Aspects**. 315: 299 – 303.

Jomekian, A., Mansoori, S.A.A., Bazooyar, B. and Moradian, A. (2012). Enhancement in thermal and hydrothermal stabilities of novel mesoporous MCM-41. **Journal of Porous Materials.** 19: 979 – 988.

Keene, M.T., Gougeon, R.D.M., Denoyel, R., Harris, R.K., Rouquerol, J. and Llewellyn, P. (1999). Calcination of the MCM-41 mesophase: mechanism of surfactant thermal degradation and evolution of porosity. **Journal of Materials Chemistry**. 9: 2843 – 2850.

Liu, Y., Pan, Y., Wang, Z.-J., Kuai, P. and Liu, C.-J. (2010). Facile and fast template removal from mesoporous MCM-41 molecular sieve using dielectric-barrier discharge plasma. **Catalysis Communications**. 11: 551 – 554.

Li, C. and Wu, Z. (2003). Microporous Materials Characterized by Vibrational Spectroscopies. **Chinese Academy of Sciences**, China.

Marcilla, A., Beltran, M., Gómez-Siurana, A., Martínez, I. and Berenguer, D. (2010). Evaluation of the efficiency of solvent extraction for template removal in the synthesis of MCM-41 type materials to be used as tobacco additives for smoke toxicity reduction. **Applied Catalysis A: General.** 378: 107 – 113.

Okitsu, K., Nakamura, H., Takenaka, N., Bandow, H., Meada, Y. and Nagata, Y. (204). Sonochemical reaction occurring in organic solvents: reaction kinetics and reaction site of radical trapping with 1,1-diphenyl-2-picrylhydrazyl. **Research on Chemical Intermediatesa**. 30(7): 763 – 774.

Ryczkowski, J., Goworek, J., Gac, W., Pasieczna, S. and Borowiecki, T. (2005). Temperature removal of templating agent from MCM-41 silica materials. **Thermochimica Acta**. 434: 2 – 8.

Schmidt, R., Akporiaye, D., Stöcker, M. and Ellestad, O.H. (1994). Synthesis of Al-containing MCM-41 materials: template interaction and removal. **Studies in Surface Science and Catalysis**. 84: 61 – 68.

Shapiro, R.H. (1969). Spectral Exercises in Structural Determination of Organic Compounds, first ed., **Holt, Rinehart and Winston**, United States of America.

Viana, R.B., Silva, A.B.F. and Pimentel, A.S. (2012). Infrared spectroscopy of anionic, cationic, and zwitterionic surfactants. **Advances in Physical Chemistry**. 2012: 1 –14.

Zanjanchi, M.A. and Jabariyan, S. (2014). Application of ultrasound and methanol for the rapid removal of surfactant from MCM-41 molecular sieve. **Journal of the Serbian Chemical Society**. 79(1): 25 – 38.

CHAPTER V

PREPARATION OF ACTIVATED CARBON AS A CATALYST SUPPORT

5.1 Abstract

The charcoal was prepared from *M. calabura* wood by an Iwazaki furnace kiln. It was employed as a starting material for activated carbon under CO_2 treatment. The surface modification of activation was performed to create adsorption site by air zero treatment. The polyaromatic-like structure and their functional groups were characterized by FTIR and CHNO analysis. The thermal stability was carried out by TGA analysis. The surface area of sample was estimated by BET from N_2 adsorption-desorption analysis. The experiment concluded that activated carbon after modification had higher acid functional group than the parent charcoal. The BET surface area decreased after modification. However, the thermal stability did not change after CO_2 treatment.

5.2 Introduction

Activated carbon is widely used as a catalyst support because it has a high surface area, acid/base resistivity and low cost of production. Typically, the activated carbon is prepared from a wood by pyrolysis and physical/chemical treatment. The layers of

the polyaromatic-like molecules contain acid/base functional group. Junpirom et al. (2007) investigated the surface modification by chemical and physical treatment

They concluded that air zero physical treatment was a suitable and environmental friendly method to increase the acid sites on surface of activated carbon. Generally, those acid functional groups of surface activated carbon surface are adsorption sites for cation (Azzi Rios et al., 2003; Vasu et al., 2008) (Figure 5.1). Then, the Ni cations could be reduced to form nanoparticles on activated carbon. Therefore, the surface modification was studied.

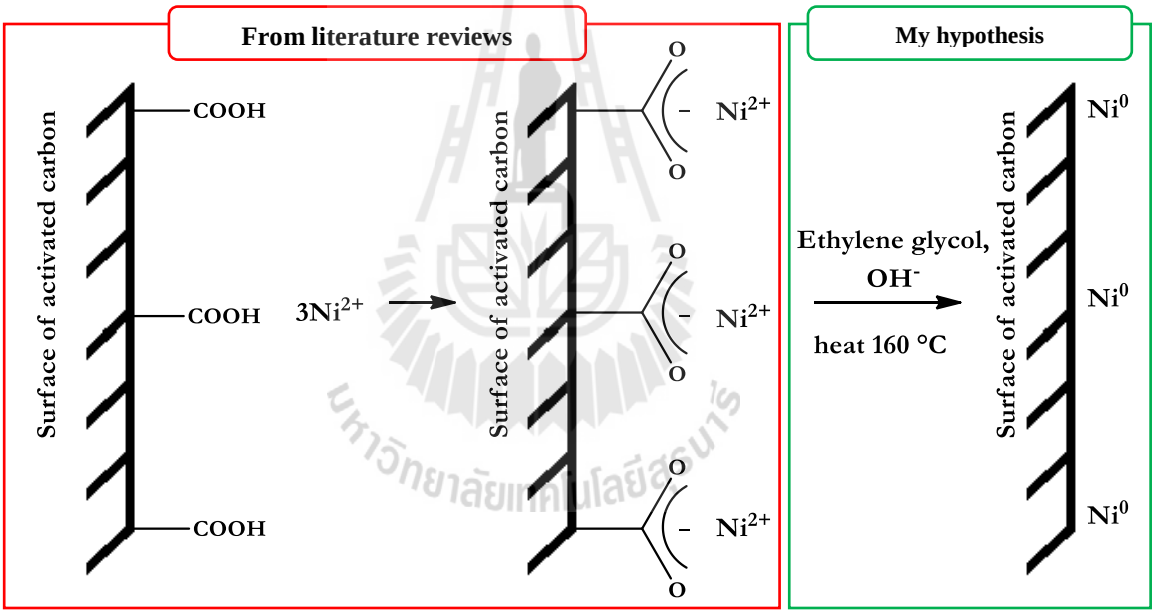

Figure 5.1 Interaction between Ni^{2+} and surface of activated carbon and the expected benefit of acid sites for Ni catalyst.

In this work, the charcoal was prepared by pyrolysis in an Iwazaki kiln from a wood from the plant named "*M. calabura*" from Nakhon Ratchasima province, Thailand. Then, the charcoal was activated by CO_2 physical treatment in a horizontal

tube furnace. After that air zero physical treatment was performed to increase acid site (Figure 5.2).

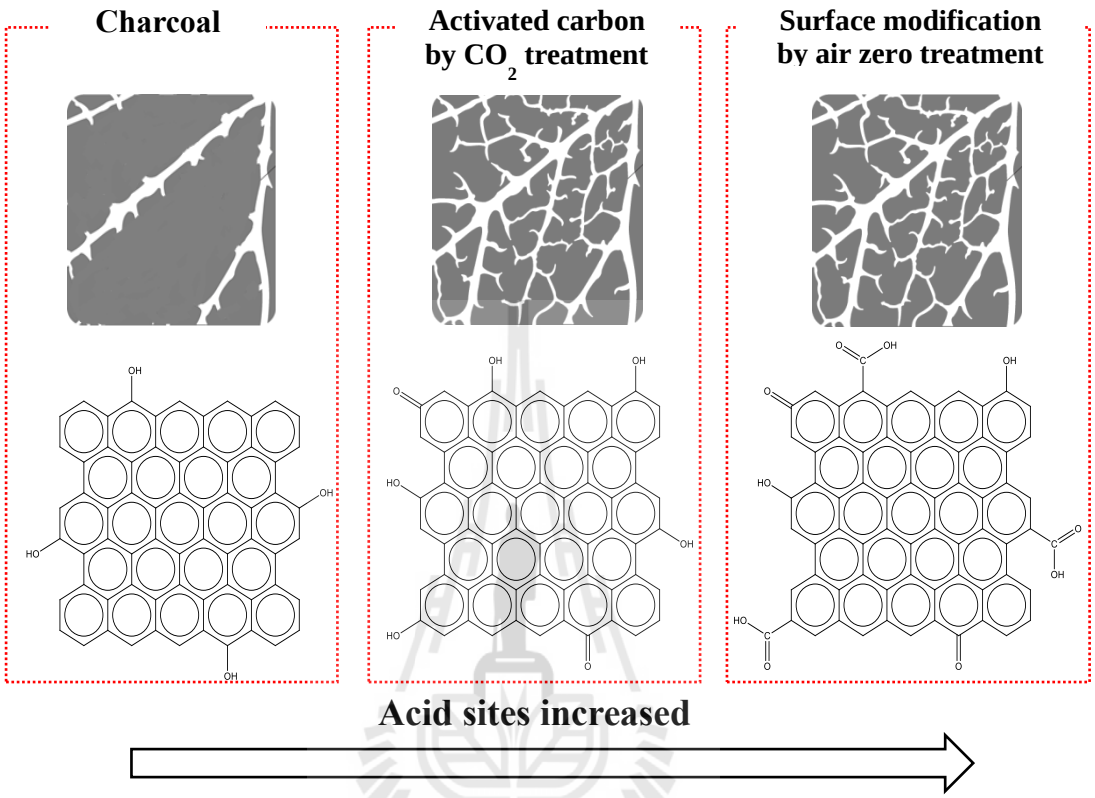

Figure 5.2 Strategy to increase acid sites on activated carbon.

5.3 Experimental

5.3.1 Preparation of charcoal by an Iwazaki furnace

The *M. calabura* wood with diameter about 1 inch was collected from a local field near the university. It was cut to the size about 5-10 × 80 cm and dried in air under sunlight for 30 days. The pyrolysis of *M. calabura* trunk was carried out in an Iwazaki furnace (shown in Figure 5.3) at Energy Ashram, Appropriate Technology Association in Pakchong District, Nakhon Ratchasima. The furnace was built with a 200-litre oil tank connected with an asbestos tube and steel condenser. The optimum

temperature and air flow was controlled by adjusting a gap in the front of the furnace. After about 8-12 h, the gap was closed and the furnace was cooled down to ambient temperature. The obtained charcoal was collected.

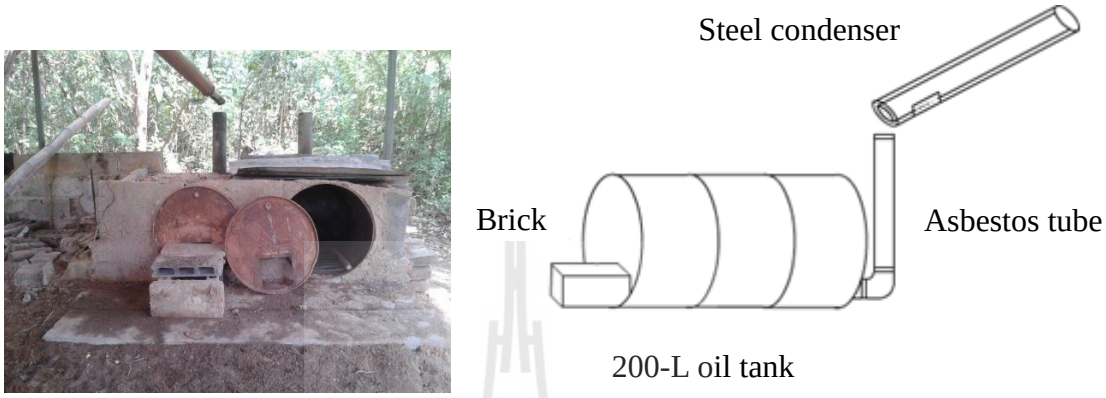

Figure 5.3 (Left) An Iwazaki furnace at Ashram, Appropriate Technology Association, (Right) scheme of an Iwazaki furnace.

5.3.2 Preparation of activated carbon by CO_2 physical treatment

The charcoal of *M. calabura* was activated by CO_2 physical treatment in the horizontal tube furnace (Junpirom et al., 2006). About 2 g of charcoal was crushed and sieved to average particle sizes between 2.1 mm – 0.714 µm, loaded in two ceramic boats and placed at the center of the furnace. It was heated from room temperature to 800 °C with a heating rate of 20 °C/min under 100 mL/min N_2 flow followed by 100 mL/min CO_2 flow (Linde Gas, 99.95%) for 1 h. Finally, the furnace was turned off and cooled to the ambient temperature under N_2 flow. The obtained sample was name “AC”.

5.3.3 Modification of activated carbon surface by air zero physical treatment

The surface of activated carbon was modified by physical treatment in the horizontal tube furnace (Junpirom et al., 2007). About 2 g of activated carbon was crushed and sieved to average particle sizes between 2.1 mm – 0.714 µm, loaded in two ceramic boats and placed at the center of the furnace. It was heated from room temperature to 250 °C with a heating rate of 20 °C/min under 100 mL/min N_2 flow followed by 100 mL/min air zero (21% O_2 in N_2 balance) flow for 24 h. Finally, the furnace was turned off and cooled to the ambient temperature under N_2 flow. The obtained sample was name “Mod AC”.

5.3.4 Characterization of activated carbon and modified activated carbon

Functional groups of samples were determined by FTIR spectroscopy (PerkinElmer, Spectrum GX). N_2 adsorption-desorption isotherm was obtained from a Micromeritics, ASAP 2010. The surface area was calculated by the Brunauer–Emmett–Teller (BET) method.

Thermal stability of material was investigated by thermogravimetric and differential thermogravimetric analysis (TGA–DTA, TA Instrument/ SDT2960) in a flow of N_2 (100 mL/min), heating rate 20 °C/min from 40 to 900 °C. The chemical composition was determined by CHNO elemental analysis (Leco, TruSpec Micro CHNO).

5.4 Results and discussion

5.4.1 Characterization of charcoal, activated carbon and modified activated carbon

FTIR spectrum of the charcoal, AC and Mod AC and peaks assignment are shown in Figure 5.1. In charcoal sample, the aromatic C-C bond corresponding to aromatic carbon of polyaromatic-like structure and O-H bond was observed. After activation, the presence of carbonyl groups is observed and C-C bond was retained (Hesas et al., 2013). Then, the O-H groups were displayed together with carbonyl groups in Mod AC (Hesas et al., 2013). Moreover, all sample showed C=N bond (Aboud et al., 2015). Therefore, it could be implied that C-OH was transformed to C=O after activation and then converted to COOH after surface modification regarding to the presence of both C=O and C-OH functional groups.

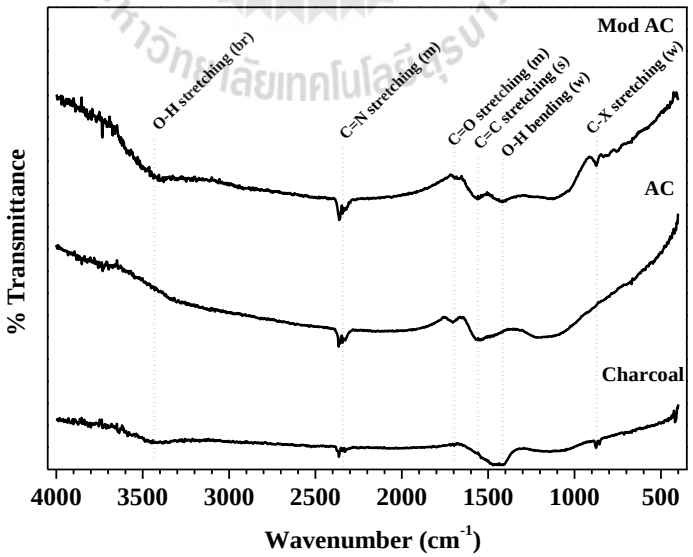

Figure 5.4 FTIR spectra of charcoal, AC and Mod AC; Intensity: br=broad, w=weak, m=medium and s=strong.

The elemental compositions of the charcoal, AC and Mod AC are shown in Table 5.1. The low value of carbon to oxygen (C/O) ratio implied the high amount of acid site. Therefore, the approximated acid sites were increased after activation and modification (Ngernyen et al., 2005).

Table 5.1 Elemental composition of charcoal, AC and Mod AC.

	C (%)	H (%)	N (%)	O (%)	C/O	C/N
Charcoal	83.185	2.929	0.792	6.294	13.22	104.9
AC	82.284	1.531	1.180	10.680	7.705	69.69
Mod AC	74.790	2.492	0.737	10.090	7.412	101.4

The thermogrgams and % weight derivatives of AC and Mod AC are shown in Figure 5.5. The first weight loss at below 100 °C corresponded to a removal of physisorbed water. The second weight loss between 100 – 700 °C referred to the decomposition of surface functional group. The last weight loss at high temperature about 700 °C corresponded to decomposition of activated carbon (Peng et al., 2014). The gradual weight loss probably attributed to the decomposition of surface functional groups. According to the slope, the AC and Mod AC were thermally stable up to 400 °C and 550 °C, respectively. Thus, both samples were suitable as catalyst supports for a reaction condition below those temperatures.

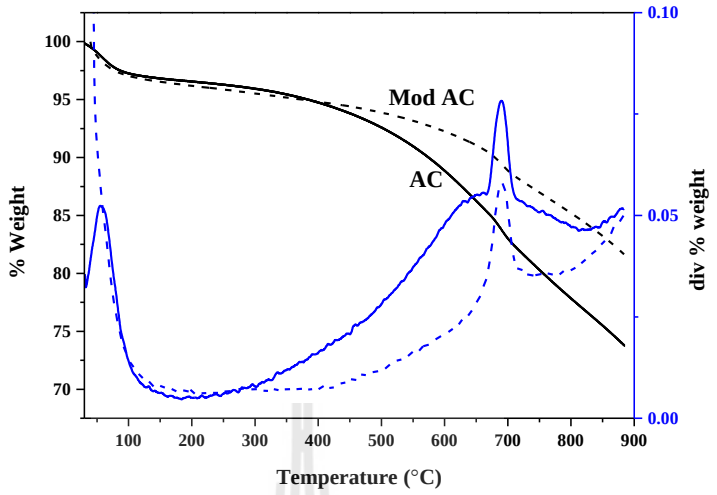

Figure 5.5 Thermograms of AC (solid line) and Mod AC (dashed line).

N_2 adsorption-desorption isotherms of AC and Mod AC are shown in Figure 5.6. The adsorption at $P/P_0 < 0.1$ corresponded to monolayer adsorption (Hesas et al., 2013). After modification, Mod AC had a lower volume adsorbed (V_a) and lower BET surface area (Table 5.2). The modification could cause collapse of pores. It was also possible that the presence of functional groups, such as hydroxyl, carboxyl blocked N_2 to enter the pore (Ngernyen et al., 2005).

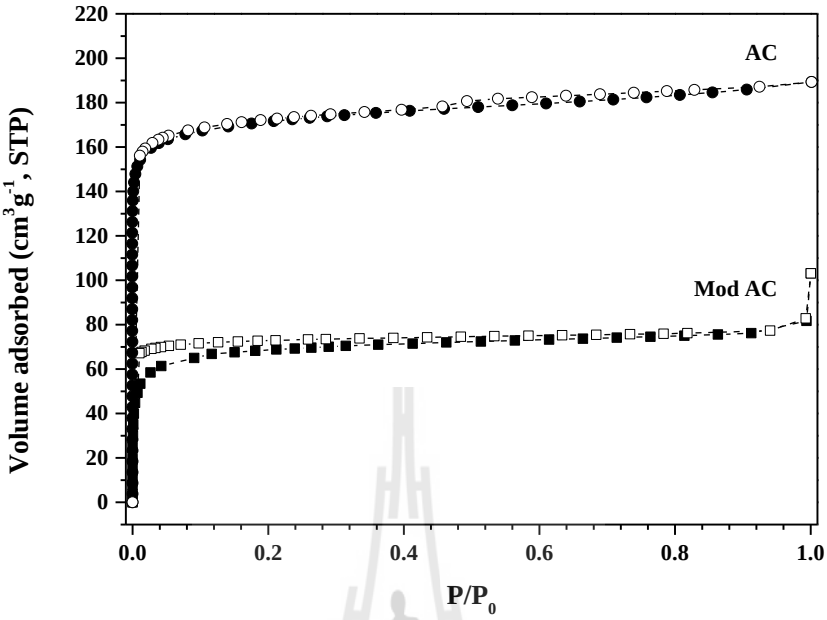

Figure 5.6 N_2 adsorption-desorption isotherms of AC and Mod AC; adsorption (filled) and desorption (empty).

Table 5.2 BET surfaces area by N_2 adsorption-desorption analysis.

	BET surface area ($m^2.g^{-1}$)
AC	412
Mod AC	170

5.5 Conclusions

Activated carbon was prepared from charcoal of *M. calabura* wood by CO_2 physical treatment. It was further modified by air zero physical treatment. Regarding to FTIR and CHNO analysis, oxygen containing functional groups referred to acid sites increased after activation and modification. Moreover, Both AC and Mod AC showed high thermal stability. However, the surface area of modified activated carbon decreased because of pore blocking by the present of functional group.

5.6 References

Aboud, M.F.A., ALOthman, Z.A., Habila, M.A., Zlotea, C., Latroche, M. and Cuevas, F. (2015). Hydrogen storage in pristine and d10-block metal-anchored activated carbon made from local wastes. **Energies**. 8: 3578 – 3590.

Hesas, R.H., Arami-Niya, A., Daud, W.M.A.W. and Sahu, J.N. (2013). Preparation and characterization of activated carbon from apple waste by microwave-assisted phosphoric acid activation: application in methylene blue adsorption. **BioResources**. 8(2): 2950 – 2966.

Junpirom, S., Tangsathitkulchai, C. and Tangsathitkulchai, M. (2007). Preparation of activated carbons from longan seed by physical and chemical methods (in Thai). **Suranaree Journal of Science and Technology.** 14(1): 63 – 76.

Ngernyen, Y., Tangsathitkulchai, C. and Tangsathitkulchai, M. (2005). The modification of acidic surface functionality of wood-based activated carbon. **Suranaree Journal of Science and Technology.**

Peng, G., Steib, M., Gramm, F., Ludwig, C. and Vogel, F. (2014). Synthesis factors affecting the catalytic performance and stability of Ru/C catalysts for supercritical water gasification. **Catalysis Science & Technology.** 4(9): 3329 – 3339.

CHAPTER VI

SYNTHESIS AND CHARACTERIZATION OF NICKEL CATALYSTS ON ACTIVATED CARBON AND MCM-41 FOR THE SYNTHESIS OF *n*-BUTANOL FROM ETHANOL

6.1 Abstract

The objective of this part is to prepare nickel catalyst on activated carbon by precipitation and on [Si]MCM-41 by impregnation, and characterize by several methods. Nickel nanoparticles and nickel incorporated MCM-41 were also prepared by microwave-assisted hydrothermal method for comparison. The structure, acidity and basicity were analyzed by XRD, NH_3-TPD and CO_2-TPD, respectively. Nickel species on both supports were nanoparticles. The catalytic screening of Guerbet reaction to produce *n*-butanol from ethanol conversion was performed under autogeneous pressure at 240 °C for 6 h. The nickel supported on activated carbon and MCM-41 had higher ethanol conversion than unsupported nickel nanoparticle.

6.2 Introduction

In the future, *n*-butanol could become a main part of the biofuels especially for transportation according to their high heating value, high flash point, low oxygen content and miscibility with diesel and gasoline. Currently, a commercial method to produce *n*-butanol is a fermentation process from food. However a production capacity, competition with food and toxicity from bacteria are concerned (Kaminski et al., 2011). Several researches have been shifted the process to a chemical reaction of ethanol from biomass in the presence of a heterogeneous catalyst. Recently, Riittonen et al. (2012) studied a one-pot liquid-phase reaction and concluded that Ni metallic form supported on Al_2O_3 had higher catalytic activity than Pt, Pd, Ag and Co. Then Zhang et al. (2013) revealed a simple and environmental friendly method to produce *n*-butanol by Guerbet process with Co metal powder in a hydrothermal batch reactor at 240 °C and autogenous pressure; a good yield and high selectivity were obtained. Although a good reaction pathway of *n*-butanol was developed (Zhang et al., 2013), the catalyst is still expensive. This problem could be solved by dispersing the metal active phase on porous materials.

Nickel supported and incorporated in MCM-41 were prepared for catalytic reactions involving hydrogen transfer (Karnjanakom et al., 2015; Nash et al., 2016; Tanggarnjanavalukul et al., 2015; Tran et al., 2016; Qin et al., 2015; Wojcieszak et al., 2004). Activated carbon is a porous material which is widely used as a support for nickel catalyst (Fidalgo et al., 2010; Rios et al., 2003; Vasu et al., 2008; Wojcieszak et al., 2006; Yao et al., 2008). Thus, nickel on both porous materials could give high nickel active sites. This property could help to upgrade the catalytic activity on Guerbet process.

Therefore, nickel catalysts supported on MCM-41 and activated carbon were introduced for the synthesis of *n*-butanol by ethanol conversion via Guerbet process. The modified activated carbon which contained the high amount of hydroxyl group was used to adsorb nickel ion by impregnation and further reduced by ethylene glycol. The catalytic testing was carried out in a batch reactor under an autogenous pressure at 240 °C.

6.3 Experimental

6.3.1 Synthesis of nickel nanoparticle

Nickel nanoparticles were synthesized by a method modified from Zhang et al. (2004) and Motuzas et al. (2014). A mixture with OH^-:Ni^{2+} of 4:1 was prepared by dissolving from 0.3553 g of nickel acetate tetrahydrate (98+%, Strem chemicals) and 2.2373 g of sodium hydroxide (Carlo Erba) in 60 mL of ethylene glycol (Carlo Erba). The resulting solution was transferred into a 100 mL microwave vessel, closed and heated via microwave irradiation in a Microwave MARs 6-One Touch in which the temperature is monitored by IR sensor with an adjustable power output (300 W). The temperature was fixed at 180 °C, heating rate 5 °C/min and duration of 15 minutes. After cooling to room temperature, the precipitate was filtered, washed with ethanol and dried at 160 °C. The obtained sample was named “Nickel nanoparticle”.

6.3.2 Preparation of nickel nanoparticles supported on MCM-41 by impregnation (nanoNi/MCM-41 (IMP))

Nickel nanoparticle supported on MCM-41 was prepared by impregnation method. Colloidal nickel nanoparticle from section 6.3.1 was suspended in ethanol

and slowly dropped on calcined [Si]MCM-41 (1 g) and stirred for 24 h. The supported Ni catalysts were dried at 160 °C overnight, and named “nanoNi/MCM-41 (IMP)”. The loading of Ni was 10 wt.%.

6.3.3 Synthesis of nickel incorporated MCM-41 under microwave irradiation (Ni-MCM-41)

The gels of NiMCM-41 was prepared by using a silica gel as a silicon source (Merck), cetyltrimethylammonium bromide (CTAB, ACROS) as a template, sodium hydroxide (NaOH, Carlo Erba) as an alkaline solvent, and 3 M sulfuric acid (diluted from 96% H_2SO_4, Carlo Erba) as a pH adjusting agent. CTAB was dissolved in 20 mL deionized water. Then, a solution containing 3.551 g of SiO_2 in 40 mL NaOH solution was added within 1 h under stirring. After a continuous stirring for 2 h, a 1nickel precursor solution was added. After 18 h the gel pH was adjusted to 9-10 by 3 M H_2SO_4 within 30 min. After a continuous stirring for another 2 h, the resulting gel with total volume of 60 mL was transferred into a 100-mL microwave vessel, closed and heated under microwave irradiation in a Microwave MARs 6-One Touch. The temperature was fixed at 100 °C, heating rate 5 °C/min for 180 min. After cooling to room temperature, the precipitate was filtered, washed with deionized water, dried at 80 °C and calcined at 550 °C for 6 h and named “Ni-MCM-41”. For a comparison, siliceous MCM-41 was synthesized by the same procedure without adding nickel precursor solution. The obtained sample was named “[Si]MCM-41 (MW)”. The characterizations of Ni-MCM-41 sample were shown in appendix B.

6.3.4 Preparation of nickel supported on modified activated carbon by precipitation (nanoNi/Mod AC)

One gram of modified activated carbon (from Chapter V) was dispersed in a 0.3553 g of nickel acetate tetrahydrate in 30 mL of ethylene glycol to allow nickel adsorbs on the surface for 12 h. Then, 2.2373 g of sodium hydroxide in 30 mL of ethylene glycol producing the OH^-:Ni^{2+} mole ratio of 4:1 was added. The 10% weight of Ni^{2+} was expected. The resulting solution with total volume of 60 mL was transferred into a 100 mL microwave vessel, closed and heated via a Microwave MARs 6-One Touch. The temperature was fixed at 180 °C, heating rate 5 °C/min and duration of 15 min. After cooling to room temperature, the precipitate was filtered, washed with ethanol and dried at 160 °C. The obtained sample was named "nanoNi/Mod AC".

6.3.5 Characterization

Nickel nanoparticle was characterized by X-ray diffraction. The crystalline size (D) was calculated by using the Scherrer's equation (Eq 6.1). MCM-41 phase of all catalyst was confirmed by X-ray diffraction. Functional group was determined by Fourier Transform Infra-red (FTIR) technique.

$$D = \frac{0.89\lambda}{\beta \cos\theta} \tag{6.1}$$

Where λ is wavelength (1.5418 Å), β is full width at half maximum (FWHM) of the peak, and θ is the Bragg's angle of the XRD peak from the main diffraction peak.

Acidity of sample was determined by NH_3 temperature-programmed desorption (NH_3-TPD) in a Belcat-B equipped with a thermal conductivity detector. A sample amount of 250 mg was packed in a tubular U-shaped quartz cell, preheated at 550 °C in a He flow (50 mL/min) for 120 min to eliminate physisorbed species and cooled to 50 °C. Then a constant flow of 30 mL/min of 5% vol. NH_3/Ar gas mixture was introduced over the samples for 30 min to achieve saturation. After that the sample was purged with He for 30 min at 100 °C to remove physisorbed NH_3. The TPD measurement was performed from 100 – 800 °C with a heating rate 10 °C/min. The relative number of acid sites was calculated from the peak area.

Basicity of sample was determined by CO_2 temperature programmed desorption (CO_2-TPD), also in a Belcat-B instrument. A sample amount of 250 mg was packed in a tubular U-shaped quartz cell, preheated at 550 ºC in a He flow (50 mL/min) for 120 min to eliminate physisorbed species and cooled to 50 °C. Then a constant flow of 30 mL/min of 5% vol. CO_2/Ar gas mixture was introduced over the samples for 30 min to achieve saturation. After that the sample was purged with He for 30 min at 100 °C to remove physisorbed CO_2, the TPD measurement was performed from 100 – 800 °C with a heating rate 10 °C/min. The relative number of basic sites was calculated from the peak area.

6.3.6 Catalytic performance on hydrothermal synthesis of *n*-butanol from ethanol

Catalytic reaction was done in a 450 mL of Parr 5500 compact reactor with the following procedure. The starting reagent solution containing 150 mL of ethanol, 4.2 g of $NaHCO_3$, 70 mL of water, and 0.4 g of catalyst was added into the autoclave,

sealed, placed in a furnace and heated to 240 °C for 6 h. The final autogenous pressure in the autoclave was around 55 bars as measured by a digital pressure gauge. After each test, the autoclave was quenched to room temperature by water-cooling.

Products were analyzed by a gas chromatograph equipped with flame ionization detector (GC-FID, Agilent G1530A) equipped DB-wax (polyethylene glycol) column. The 0.5 mL of sample and 0.1 mL of *n*-heptanol as an internal standard were diluted in 25 mL of water. The sample (0.1 µL) was injected with a 50:1 split mode. The injection and FID detector temperature were 180 °C and 100 °C, respectively. The temperature was programmed from 100 °C, ramp to 120 °C at 4 °C/min, and then to 180 °C at 30 °C/min for 1 min.

The concentration of ethanol was determined from a standard curve produced by the ratio of peak height of ethanol and *n*-heptanol with various %volume of ethanol (Appendix B). Then the conversion of ethanol was calculated by Equation 6.2 (Riittonen et al., 2015).

$$\text{Conversion of ethanol } (\%) = \left(\frac{C_0 - C_i}{C_0} \right) \times 100 \qquad (6.2)$$

Where C_0 is the initial concentration of ethanol and C_i is measured concentration of ethanol after catalytic reaction.

The *n*-butanol selectivity was estimated from the ratio of peak height of *n*-butanol and *n*-heptanol.

6.4 Results and discussion

6.4.1 Nickel nanoparticle

The XRD pattern of nickel nanoparticles is shown in Figure 6.1. The main diffraction peaks at 44.4, 51.8 and 76.2 degree were assigned to (100), (200) and (220) planes of metallic nickel form (Zhang et al., 2004). The sample did not show the peaks at 32.9, 38.5, and 51.7 degree corresponding to $Ni(OH)_2$ as intermediate phase, and the peaks at 37.2, 43.3 and 62.9 degree corresponding to NiO (Motuzas et al., 2014; Dharmaraj et al., 2006). Nickel nanoparticles were synthesized successfully at 180 °C in 15 min. Thus, the crystalline size calculated by Scherrer's equation was about 32 nm with 0.46 degree of FWHM. The adapted method of nickel nanoparticle was improved by using a shorter time and lower temperature than that of original method (Motuzas et al., 2014; Zhang et al., 2004).

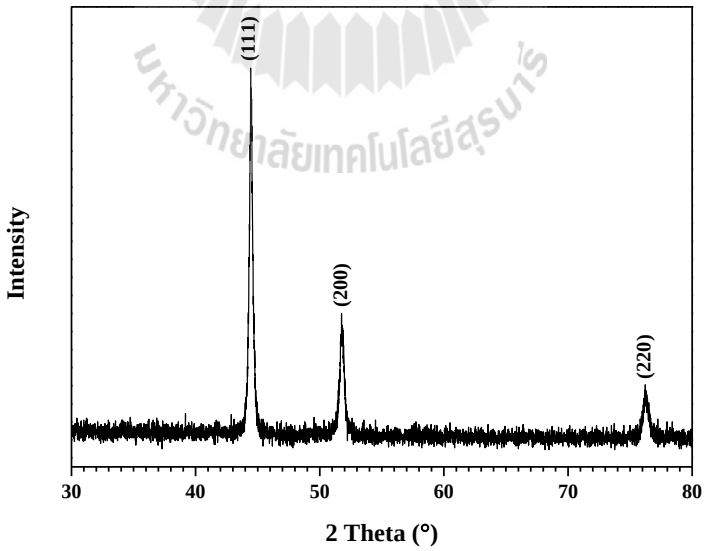

Figure 6.1 XRD pattern of nickel nanoparticles.

6.4.2 nanoNi/MCM-41 (IMP)

The XRD pattern of nanoNi/MCM-41 (IMP) was divided to two ranges. The first range is a characteristic of MCM-41. The main diffraction peak of (100) plane of MCM-41 structure was observed (Figure 6.2a) indicating that MCM-41 pores did not collapse after nickel impregnation. However, the low intensity of the (100) plane together with the disappearing of other diffraction peaks indicated that mesopores lost some periodicity. The XRD pattern in the second range is shown in Figure 6.2b. Peaks of nickel nanoparticle were still observed. The crystalline size was about 45 nm by Scherrer's equation with 0.33 degree of FWHM.

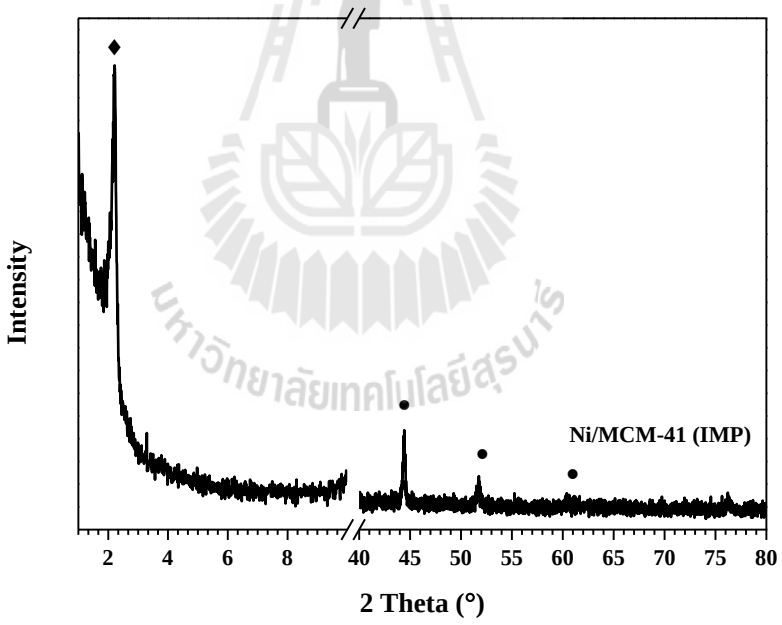

Figure 6.2 XRD patterns of [Si]MCM-41 (♦) and nickel nanoparticles (•) in nanoNi/MCM-41 (IMP) sample.

6.4.3 Ni/Mod AC

The XRD pattern of nickel phase on modified activated carbon is shown in Figure 6.3. Nickel XRD pattern was similar to nickel nanoparticle. The crystalline size was about 50 nm by Scherrer's equation with 0.30 degree of FWHM.

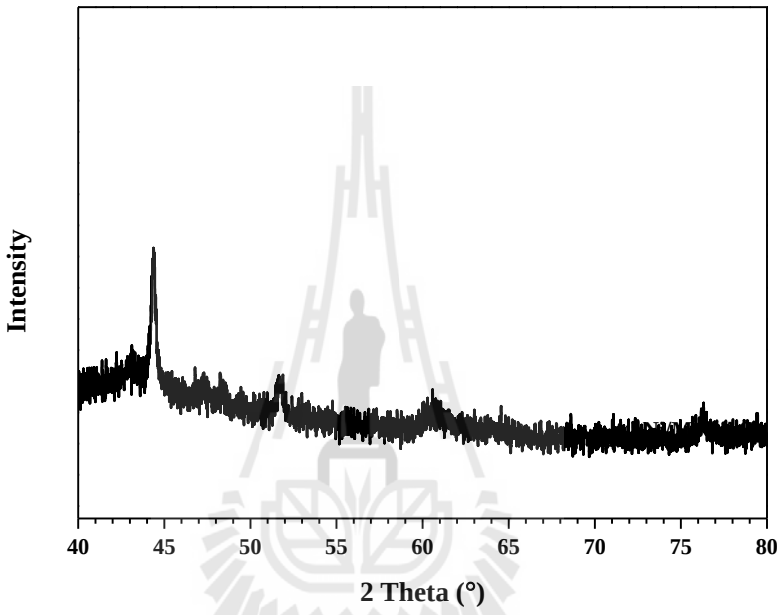

Figure 6.3 XRD patterns of nickel nanoparticles (•) in Ni/Mod AC.

6.4.4 Catalyst screening on Guerbet reaction

Before a catalytic testing, a blank test was carried out with the absence of catalyst. The ethanol conversion was obtained (see Table 6.1). The $NaHCO_3$ in the solution could serve as a base catalyst to convert ethanol to acetaldehyde, butyraldehyde, crotonaldehyde, crotylalcohol, 2-butanol and *n*-butanol (Ndou et al., 2003).

By using 1 g of nickel nanoparticle catalyst, the ethanol conversion was more than two fold higher than the blank test. Therefore, nickel catalyst could be a

hydrogen borrowing for dehydrogenation and hydrogenation. Both reactions produced two molecules of aldehyde (intermediate), butanal (intermediate) and butanol (Riittonen et al., 2012; Zhang et al., 2013).

As the presence of their acid/base properties are shown in Chapter V and section 6.4.2, the effect of 0.4 g of supports (MCM-41 and Mod AC) was investigated. The aldol condensation of intermediates was possibly catalyzed via both acid and base catalyst (Nielsen et al., 1968). Thus, the ethanol conversion of MCM-41 and Mod AC slightly increased comparing to the blank test. However, there was no evidence to confirm these phenomena clearly about the role of the bare supports.

Nickel incorporated MCM-41 (0.4 g) as a catalyst was tested to see the possibility as a hydrogen borrowing catalyst from weak hydrogen adsorption on partial charge of surface (Carraro et al., 2014). NiMCM-41 (MW) gave ethanol conversion two times higher than the bare MCM-41. This result assumed that the partial charge on mesopore created by insertion of nickel atom could be a hydrogen borrowing site.

The catalytic testing of nickel impregnated on MCM-41 and Mod AC was carried out to see effect of metal dispersion. The supported catalysts showed higher ethanol conversions than the nanoparticles. The role of support material on nickel catalyst resulted to improve catalytic conversion.

The approximated *n*-butanol selectivity was the highest from nickel nanoparticle. However, the selectivity from Ni-MCM-41 (IMP) and Ni-Mod AC was higher that from the parent support because of the presence of nickel nanoparticles. The lower selectivity might imply that the side reactions happened by the imbalance of acidic and basic catalyst of support and $NaHCO_3$ (Jordison et al., 2015).

Table 6.1 Ethanol conversion (%) and approximated *n*-butanol on catalyst screening.

Catalyst	Ethanol conversion (%)		Peak area of *n*-butanol
		Per mmole of Ni	
None	6.1	-	0.071
Nickel nanoparticle	15.9	2.3	0.50
MCM-41	7.7	-	0.149
Mod AC	8.7	-	0.098
NiMCM-41 (MW)	14.7	21.6	0.144
Ni/MCM-41 (IMP)	23.1	33.9	0.173
Ni/Mod AC	19.2	28.2	0.103

6.5 Conclusions

Nickel incorporated MCM-41 was confirmed by the diffraction peak shift of (100) plane of MCM-41 structure. The acid/base properties of MCM-41 were increased by nickel insertion. Moreover, the hydrogen consuming and releasing on NiMCM-41 was higher than MCM-41 and implied to be a hydrogen borrowing catalyst. In case of Ni-MCM-41 (IMP), the presence of nickel nanoparticle and MCM-41 structure was observed by XRD. Likewise, Ni-Mod AC also confirmed nickel catalyst.

The activity of *n*-butanol synthesis from ethanol conversion via Guerbet process was lower than that from other works. However, the multifunctional active site containing metal and acid/base is promising to improve the catalytic reaction by re-modification of catalyst.

6.6 References

Azzi Rios, R.R.V., Alves, D.E., Dalmázio, I., Bento, S.F.V., Donnici, C.L. and Lago, R.M. (2003). Tailoring Activated Carbon by Surface Chemical Modification with O, S, and N Containing Molecules. **Materials Research**. 6(2): 129 – 135.

Carraro, P., Elías, V., García Blanco, A.A., Sapag, K., Eimer, G. and Olive, M. (2014). Study of hydrogen adsorption properties on MCM-41 mesoporous materials modified with nickel. **International Journal of Hydrogen Energy**. 39: 8749 – 8753.

Dharmaraj, N., Prabu, P., Nagarajan, S., Kim, C.H., Park, J.H. and Kim, H.Y. (2006). Synthesis of nickel oxide nanoparticles using nickel acetate and poly(vinyl acetate) precursor. **Materials Science and Engineering: B**. 128(1-3): 111 – 114.

Fidalgo, B., Zubizarreta, L., Bermúdez, J.M., Arenillas, A. and Menéndez, J.A. (2010). Synthesis of carbon-supported nickel catalysts for the dry reforming of CH_4. **Fuel Processing Technology**. 91: 765 – 769.

González Vargas, O.A., de los Reyes Heredia, J.A., Wang, J.A., Chen, L.F., Montesinos Castellanos, A. and Llanos, M.E. (2013). Hydrogen production over Rh/Ce-MCM-41 catalysts via ethanol steam reforming. **International Journal of Hydrogen Energy**. 38(32): 13914 – 13925.

Jordison, T.L., Lira, C.T. and Miller D.J. (2015). Condensed-phase ethanol conversion to higher alcohols. **Industrial & Engineering Chemistry Research**. 45: 10991 – 11000.

Karnjanakom, S., Guan, G., Asep, B., Du, X., Hao, X., Samart, C. and Abuliti, A. (2015). Catalytic steam reforming of tar derived from steam gasification of sunflower stalk over ethylene glycol assisting prepared Ni/MCM-41. **Energy Conversion and Management**. 98: 359 – 368.

Motuzas, J., Drobek, M., Diniz da Costa, J.C. and Julbe, A. (2014). Novel microwave assisted approach to large scale nickel nanoparticle fabrication. **Chemical Engineering Journal.** 240: 155 – 160.

Ndou, A.S., Plint, N. and Coville, N.J. (2003). Dimerisation of ethanol to butanol over solid-base catalysts. **Applied Catalysis A: General**. 251: 337 – 345.

Nielsen, A.T. and Houlihan., W.J. (1968). The Aldol Condensation. **Organic Reactions** 16: 1 – 438.

Park, S.J. and Lee, S.Y. (2010). A study on hydrogen-storage behaviors of nickel-loaded mesoporous MCM-41. **Journal of Colloid Interface Science.** 346(1): 194 – 198.

Qin, J., Li, B., Zhang, W., Lv, W., Han, C. and Liu, J. (2015). Synthesis, characterization and catalytic performance of well-ordered mesoporous Ni-MCM-41 with high nickel content. **Microporous and Mesoporous Materials**. 208: 181 – 187.

Ramachandran, S., Ha, J.-H. and Kim, D.K. (2007). Hydrogen storage characteristics of metal oxide doped Al–MCM-41 mesoporous materials. **Catalysis Communications**. 8(12): 1934 – 1938.

Riittonen, T., Eränen, K., Mäki-Arvela, P., Shchukarev, A., Rautio, A.-R., Kordas, K., Kumar, N., Salmi, T. and Mikkola, J. (2015). Continuous liquid-phase valorization of bio-ethanol towards bio-butanol over metal modified alumina. **Renewable Energy**. 74: 369 – 378.

Riittonen, T., Toukoniitty, E., Madnani, D.K., Leino, A.-R., Kordas, K., Szabo, M., Sapi, A., Arve, K., Wärnå, J. and Mikkola, J.-P. (2012). One-pot liquid-phase catalytic conversion of ethanol to 1-butanol over aluminium oxide - the effect of the active metal on the selectivity. **Catalysts**. 2: 68 – 84.

Rios, R.R.A., Alves, D.E., Fernando, D.S., Bento, V., Donnici, L. and Lago, R.M. (2003). Tailoring Activated Carbon by Surface Chemical Modification with O, S, and N Containing Molecules. **Material research**. 6: 129 – 135.

Tanaka, M., Itadani, A., Kuroda, Y. and Iwamoto, M. (2012). Effect of Pore Size and Nickel Content of Ni-MCM-41 on Catalytic Activity for Ethene Dimerization and Local Structures of Nickel Ions. **The Journal of Physical Chemistry C.** 116(9): 5664 – 5672.

Tanggarnjanavalukul, C., Donphai, W., Witoon, T., Chareonpanich, M. and Limtrakul, J. (2015). Deactivation of nickel catalysts in methane cracking reaction: Effect of bimodal meso–macropore structure of silica support. **Chemical Engineering Journal**. 262: 364 – 371.

Tran, N.T.T., Uemura, Y., Chowdhury, S. and Ramli, A. (2016). Vapor-phase hydrodeoxygenation of guaiacol on Al-MCM-41 supported Ni and Co catalysts. **Applied Catalysis A: General**. 512: 93 – 100.

Vasu, A.E. (2008). Surface Modification of Activated Carbon for Enhancement of Nickel(II) Adsorption. **E-Journal of Chemistry**. 5(4): 814 – 819.

Wojcieszak, R., Monteverdi, S., Mercy, M., Nowak, I., Ziolek, M. and Bettahar, M. M. (2004). Nickel containing MCM-41 and AlMCM-41 mesoporous molecular sieves characteristics and activity in the hydrogenation of benzene. **Applied Catalysis A: General**. 268(1–2): 241 – 253.

Wojcieszak, R., Zieliński, M. and Bettahar, M.M. (2006). Study of nickel nanoparticles supported on activated carbon prepared by aqueous hydrazine reduction. **Journal of Colloid Interface Science.** 299(1): 238 – 248.

Yao, S., Yang, C., Tan, Y. and Han, Y. (2008). Deactivation and regeneration of an activated carbon-supported nickel catalyst for methanol carbonylation in the vapor phase. **Catalysis Communications**. 9(11–12): 2107 – 2111.

Zhang, F., Chen, Y., Zhao, J. and Li, H. (2004). Preparation of Nanosized Nickel Particles by Hydrothermal Method. **Chemistry Letters**. 33(2): 146 – 147.

Zhang, X., Liu, Z., Xu, X., Yue, H., Tian, G. and Feng, S. (2013). Hydrothermal synthesis of 1-butanol from ethanol catalyzed with commercial cobalt powder. **ACS Sustainable Chemistry & Engineering**. 1: 1493 – 1497.

CHAPTER VII

CONCLUSIONS AND RECOMMENDATION

In this work, [Si]MCM-41 was synthesized under microwave irradiation. The MCM-41 with high quality was obtained from a gel composition of $3.34SiO_2$:4.46NaOH :1CTAB:$1.16H_2SO_4$:$225H_2O$ at 100 °C for 90 min. The less CTAB:SiO_2 mole ratio led to incomplete formation of hexagonal structure. In contrast, the excess CTAB:SiO_2 mole ratio caused phase transformation and was not sufficient for the formation of the hexagonal structure. In addition to NaOH:SiO_2 mole ratio, the mesopore wall thickness increased with an increase of NaOH concentration. Finally, the hexagonal phase began to form at 15 min and high order was obtained at 90 min. Under those suitable parameters, [Si]MCM-41 had $a_0 \approx 44.80$ Å, uniform pore diameter of 27.40 Å, BET surface area of 1138 $m^2.g^{-1}$ and high thermal stability to 1100 °C. The obtained [Si]MCM-41 was further employed as a catalysts support. However, studies on parameters like silicate concentration, type of basic solution, pH, temperature, power of microwave etc. were needed to improve the quality of [Si]MCM-41 synthesized under microwave irradiation.

CTA^+ removal from the as-synthesized [Si]MCM-41 was investigated by ion exchange. The appropriate condition was performed at 30 °C for 15 min under sonication with NH_4Cl methanolic solution to give 77% removal. The obtained [Si]MCM-41 after an ion exchange from the suitable condition did not collapse. Unlike other conditions, the ordering hexagonal phase of [Si]MCM-41 changed

or lost by alkaline or basic salt solution. Although the suitable temperature and time in this study was mild, an increase of both parameters led to increase on ion exchange behavior. Furthermore, the CTA^+ recovery in this work resulted in partially oxidized sample and mixed compound from both extracted CTA^+ and waste powder. The recovery process is interesting for a further study to make the recycle possible.

Another catalyst support was a modified activated carbon from *M. calabura*. The physical treatment by air zero was used to activate the charcoal. Then, a further physical treatment by CO_2 was used to increase acid functional groups as adsorption sites. The modified activated carbon had more acid sites than the parent one. The decrease of BET surface area was probably caused by pore collapse and blocking from an increasing of functional groups. Moreover, the thermal stability of the activated carbon rose up to 550 °C after modification. However, the properties of activated might be further enhanced by varying time and temperature during physical treatment. The acid and basic species could be accurately determined by Boehm titration.

Finally, nickel catalysts supported on [Si]MCM-41 and modified activated carbon were prepared. Catalyst screening for all nickel catalysts on the synthesis of *n*-butanol from ethanol by Guerbet reaction showed 6 – 23% of ethanol conversion with a low approximated *n*-butanol selectivity. Nickel catalyst supported on [Si]MCM-41 and modification had a higher ethanol conversion than the unsupported nanoparticles. In addition, nickel incorporated [Si]MCM-41 resulted in a twofold higher ethanol conversion than the bare [Si]MCM-41. This case implied that nickel might play an important role as hydrogen borrowing sites. So, the re-modification of multifunctional catalyst is promising to improve the catalytic activity.

APPENDICES

APPENDIX A

EFFECT OF Na^+ AND K^+ WITH DIFFERENT ANIONS AND EXTRACTION BY PURE METHANOL

A 1 Effect of Na^+ and K^+ with different anions

The TGA thermograms and percent CTA^+ removal of detemplated [Si]MCM-41 (MW) after extraction with sodium salts containing different anions (OAc^-, NO_3^-, Cl^- and Br^-) in methanol are showed in Figure A 1 and Table A 1. The highest efficient CTA^+ removal was obtained from $NaNO_3$ solution. In the event of NaCl and NaBr solution, they showed the low CTA^+ removal because both of bond dissociation energy of Na-Cl and Na-Br (410 and 370 kJ/mol, respectively) are more than Na-O(-Si) (Cottrell, 1958). Consequently, the exchange between Na^+ and CTA^+ was not favorable. In case of NaOAc solution, the CTA^+ removal was the lowest because base species were generated by acetate anion and then compete for interaction with other cations.

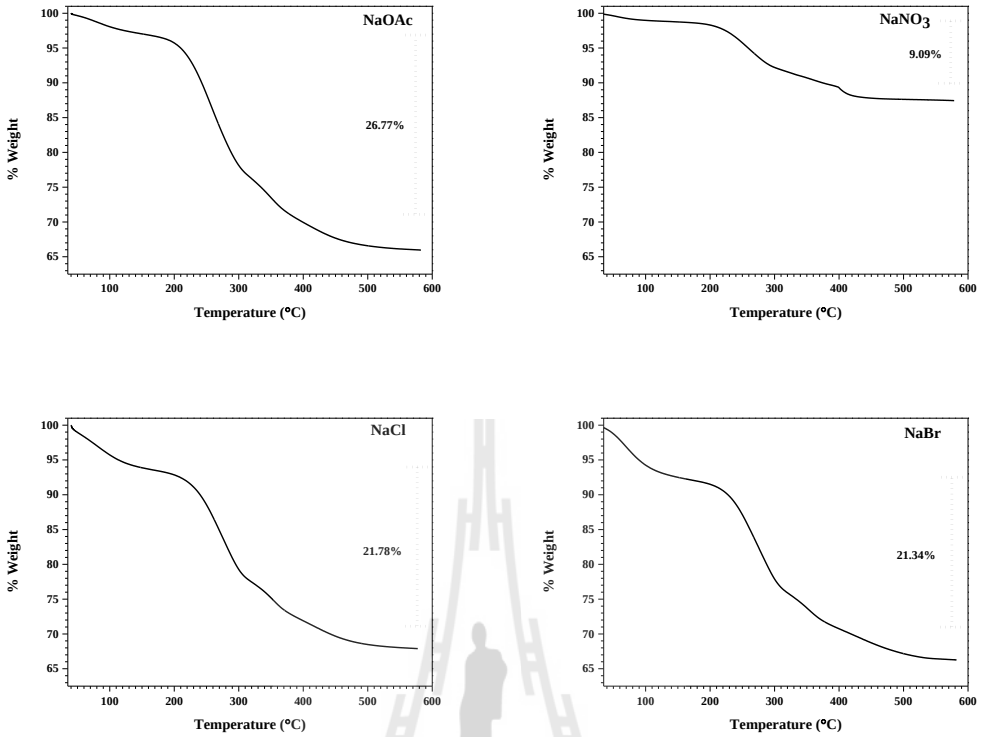

Figure A 1 Thermograms of detemplated [Si]MCM-41 (MW) after extraction with sodium salts containing different anions (OAc^- , NO_3^-, Cl^- and Br^-) in methanol.

Table A 1 The percent CTA^+ removal of detemplated [Si]MCM-41 (MW) after extraction with sodium salts containing different anions (OAc^-, NO_3^-, Cl^- and Br^-) in methanol.

	% Weight loss	% CTA^+ removal
Na(OAc)	26.77	36.40
$NaNO_3$	9.09	78.40
NaCl	21.78	48.25
NaBr	21.34	49.30

By fixing K^+ cation, the TGA thermograms and percent removal are shown in Figure A 2 and Table A 2, respectively. All potassium salts displayed the similar CTA^+ removal. The reason can be explained by same way as sodium salts. The different anions of potassium salt could not improve the removal efficiency.

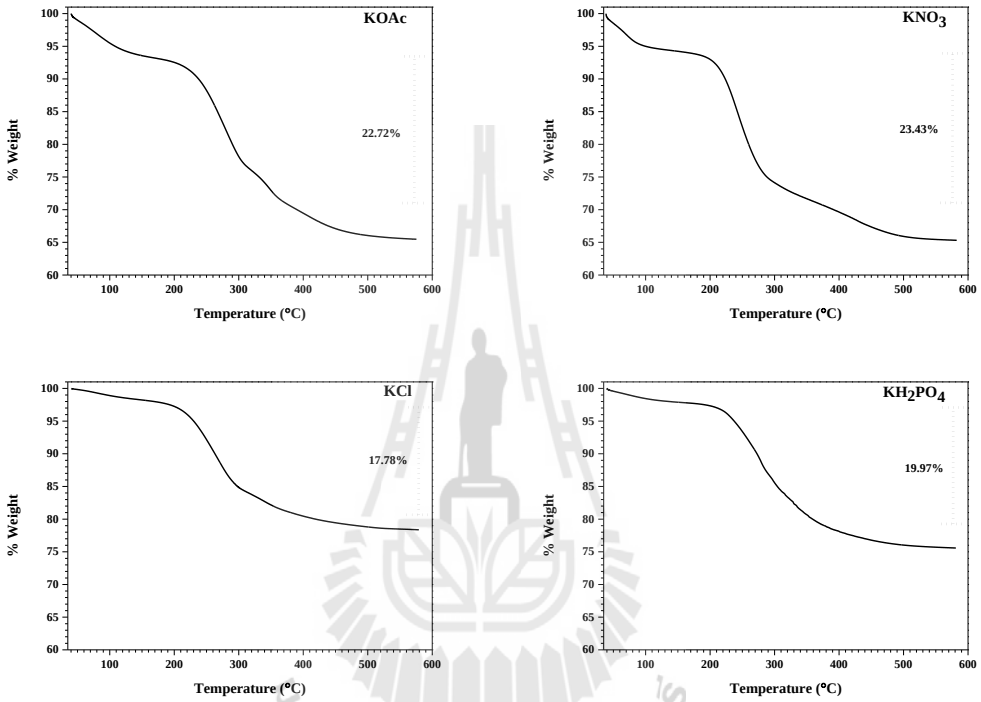

Figure A 2 Thermograms of detemplated [Si]MCM-41 (MW) after extraction with potassium salts containing different anions (OAc^-(A), NO_3^-(B), Cl^-(C) and $H_2PO_4^-$(D)) in methanol.

Table A 2 The percent CTA^+ removal of detemplated [Si]MCM-41 (MW) after extraction with potassium salts containing different anions (OAc^-, NO_3^-, Cl^- and $H_2PO_4^-$) in methanol.

	% Weight loss	% CTA^+ removal
K(OAc)	22.72	46.02
KNO_3	23.43	44.33
KCl	17.78	57.75
KH_2PO_4	19.97	52.55

Furthermore, the [Si]MCM-41 structure of detemplated [Si]MCM-41 (MW) after extraction with sodium or potassium salts containing different anions in methanol was characterized by XRD (Figure A 3 and A 4. Almost sodium and potassium salts lead to destroy [Si]MCM-41 structure during ion exchange even in other anions condition. The formation of alkaline oxide on the pore wall was still occurred. Moreover, base species from acetate ion, it would directly broke down [Si]MCM-41 structure by depolymerization (Hitz and Prins, 1997). In case of $KHPO_4$ solution, $H_2PO_4^-$ ions can dissociate to H^+, HPO_4^{2-} and PO_4^{3-} . For this reason, the one species of those is proton (H^+) which is the smallest cation size and easiest to exchange with CTA^+. [Si]MCM-41 structure could not be broke off by KH_2PO_4.

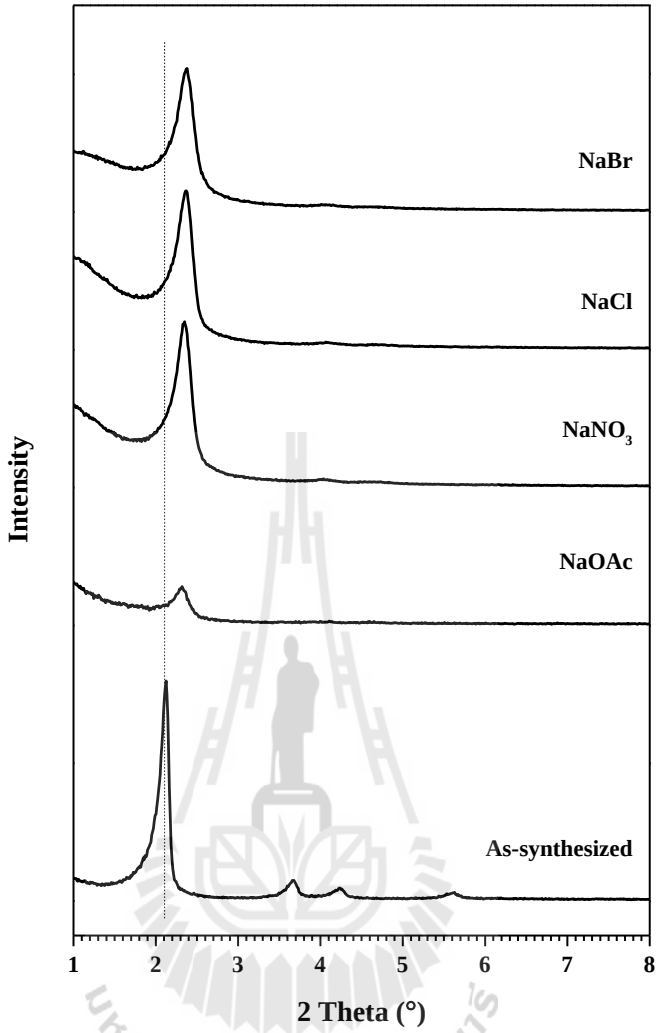

Figure A 3 XRD patterns of detemplated [Si]MCM-41 (MW) after extraction with sodium salts containing different anions (OAc^-, NO_3^-, Cl^- and Br^-) in methanol.

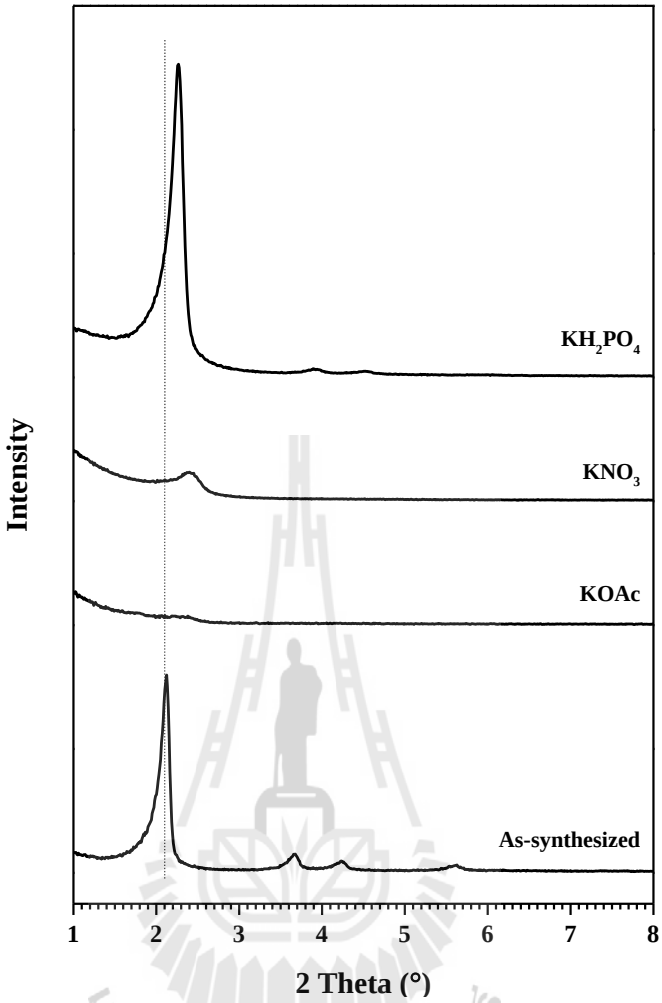

Figure A 4 XRD patterns of detemplated [Si]MCM-41 (MW) after extraction with potassium salts containing different anions (OAc^-, NO_3^-, Cl^- and $H_2PO_4^-$) in methanol.

A 2 Extraction by pure methanol

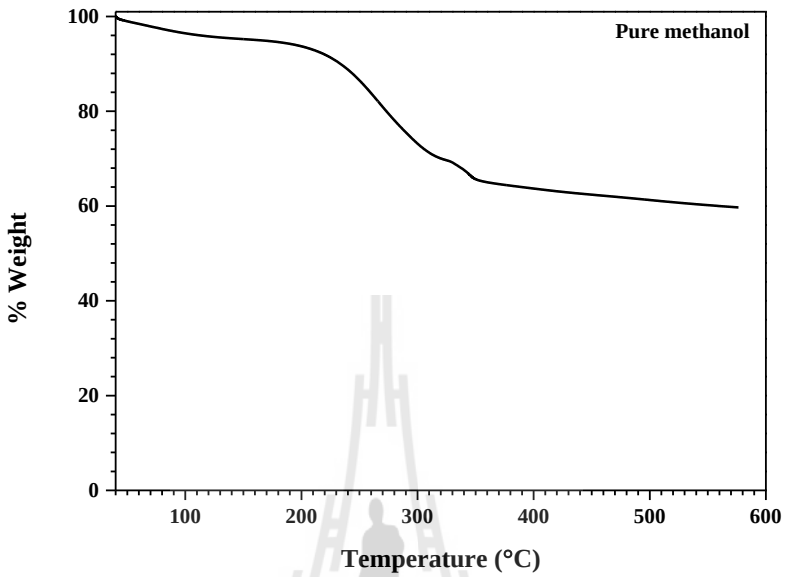

Figure A 5 Thermogram of detemplated [Si]MCM-41 (MW) after extraction with pure methanol.

APPENDIX B

ADDITIONAL INFORMATION OF NICKEL CATAL AND CATALYTIC TESTING

B 1 Characterizations of NiMCM-41 (MW)

The XRD pattern of Ni-MCM-41 is shown in Figure B 1. The sample shows characteristic peaks of MCM-41 at 2.00, 3.50, 4.00 and 5.40 degree corresponding to (100), (200) and (220) planes. Comparing to the parent MCM-41, all diffraction peaks of NiMCM-41 shifted to lower angles corresponding to pore expansion because the longer Ni-O bond distance (1.94 Å) than Si-O (1.63 Å) implied to increase framework of pore along with (100) plane (Tanaka et al., 2012). Moreover, the sample did not show diffraction peaks corresponding to NiO or Ni metallic form (Figure B 2). Therefore, it can be concluded that nickel was successfully inserted into MCM-41 structure.

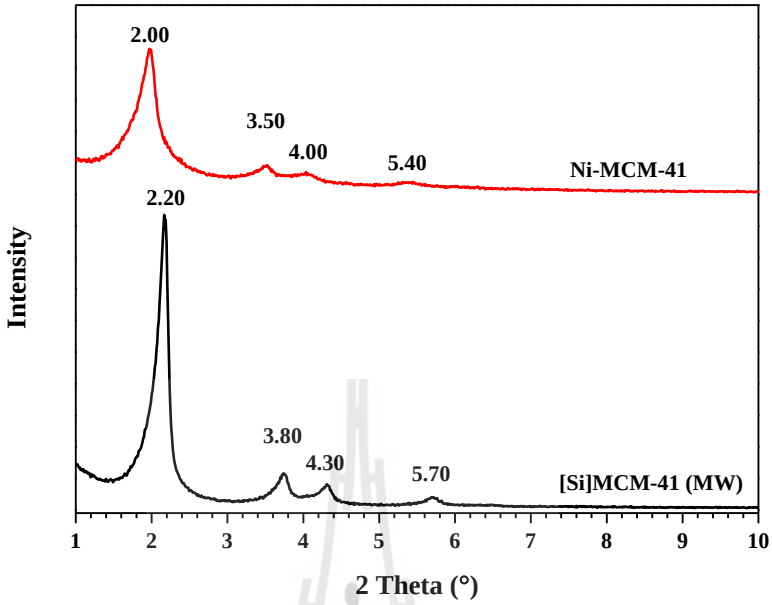

Figure B 1 XRD patterns of [Si]MCM-41 (MW) and Ni-MCM-41.

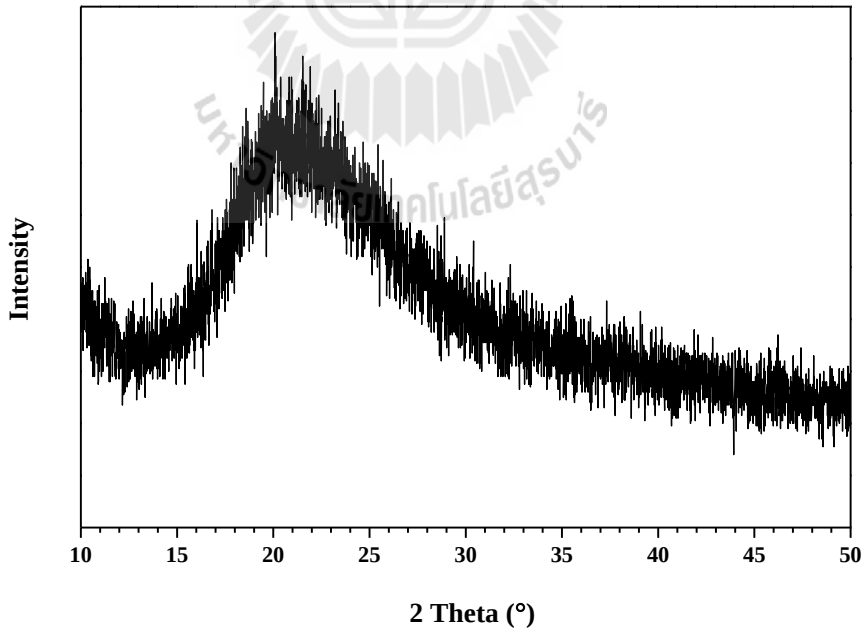

Figure B 2 XRD pattern of NiMCM-41 (MW) of 10 - 50 degree.

CO_2-TPD profiles and total basicity of [Si]MCM-41 (MW) and Ni-MCM-41 are shown in Figure B 3 and Table B 1. The [Si]MCM-41 (MW) illustrated a broad peak around 100-400 °C related to weak basicity from physisorbed CO_2 . For the nickel incooperated MCM-41, a broad peak also displayed between 100-400 °C. However, peak at 200 °C showed significantly increasing. This would explain that nickel phyllosicate induced the higher partial negative charge on oxygen atom than pristine MCM-41. Similar to Chen et al. (2007), they added a metal with a lower oxidation state than silicate into siliceous mesoporous material. The basicity of their material was higher value than that of the parent material.

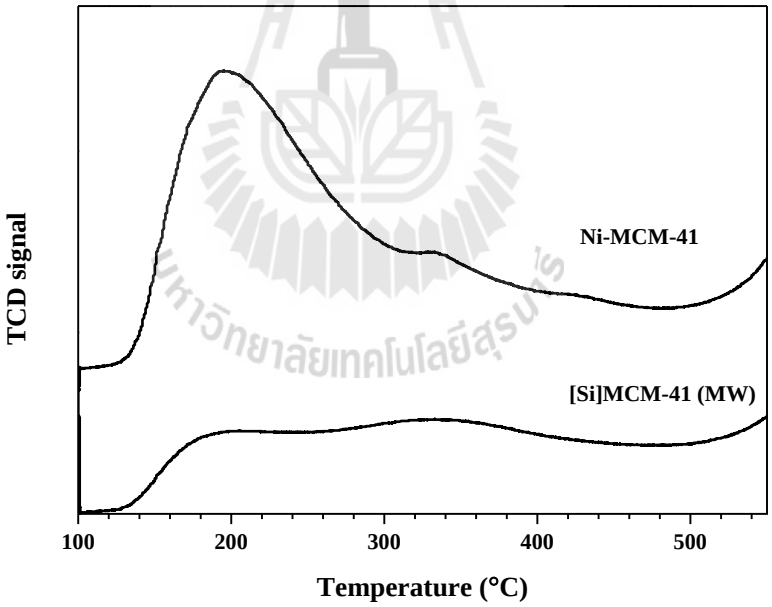

Figure B 3 CO_2-TPD profiles of [Si]MCM-41 (MW) and Ni-MCM-41.

NH_3-TPD profiles and total acidity of [Si]MCM-41 (MW) and Ni-MCM-41 are shown in Figure B 4 and Table B 1. The [Si]MCM-41 (MW) illustrated a broad peak

around 300 °C which corresponded to Brönsted acid site from silanol group. The presence of various location of silanol group resulted in a broad peak (Chen et al., 1995; Zhao et al., 1997). For the nickel incooperated MCM-41, a broad peak displayed between 100-500 °C. It seemed to composed of two acid sites (Lehmann et al., 2012). The broad peak at around 100 °C referred to Lewis acid site from nickel phyllosilicate and around 300 °C referred to Brönsted acid site. In this case the addition of nickel inserted to MCM-41 structure led to an increase of Lewis and Brönsted acid sites.

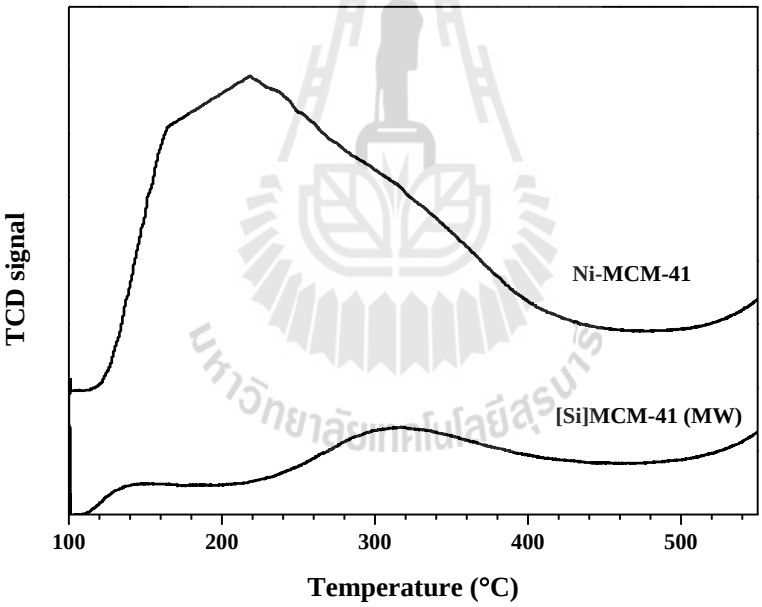

Figure B 4 NH_3-TPD profiles of [Si]MCM-41 (MW) and Ni-MCM-41.

Table B 1 Total basicity and acidity of [Si]MCM-41 (MW) and Ni-MCM-41.

	Total basicity (mmol/g)	Total acidity (mmol/g)
[Si]MCM-41 (MW)	0.086	0.085
Ni.MCM-41	0.137	0.345

The invert-TPR profiles of [Si]MCM-41 (MW) and Ni-MCM-41 are shown in figure B.5. The [Si]MCM-41 (MW) sample showed a hydrogen consumption peak at 146 °C from the water desorption which probably influenced the methane formation. The release of hydrogen peaks around 414 and 456 °C corresponded to physisorbed hydrogen. The Ni-MCM-41 sample showed hydrogen consumption peaks at 139 °C and at 185 °C. Again, the hydrogen evolution at 396 °C related to hydrogen desorption from nickel species. Furthermore, a huge broad peak around 542 °C could be assigned to reduction of Ni^{2+} to Ni^{0}. From these data, the [Si]MCM-41 (MW) and Ni-MCM-41 could be used as borrowing hydrogen material.

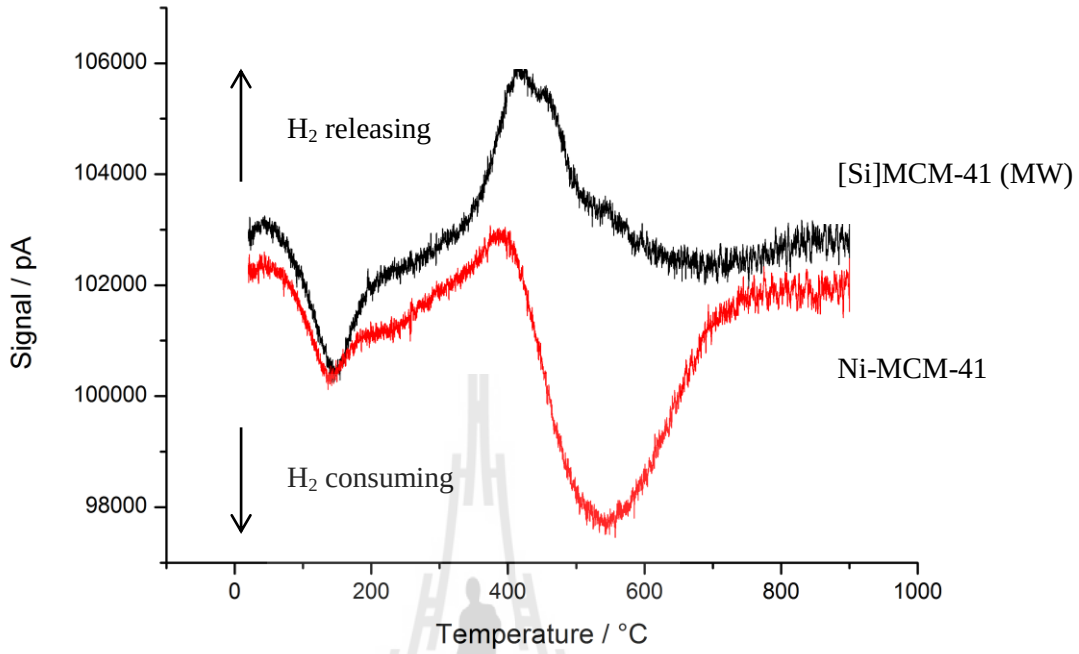

Figure B 5 Invert-temperature program reduction (i-TPR) profiles of [Si]MCM-41 (MW) and Ni-MCM-41.

B 2 Additional information on catalytic testing

Table B 2 The ratio of peak height of ethanol and *n*-butanol with %volume of ethanol.

Peak high of ethanol	Peak high of *n*-heptanol	%Volume	Ratio of peak height
6245	5353	0.70	1.167
4312	5005	0.50	0.8615
2845	5285	0.30	0.5383
2376	5250	0.25	0.4526
2280	6202	0.20	0.3676
1704	6094	0.15	0.2796
1070	5393	0.10	0.1984

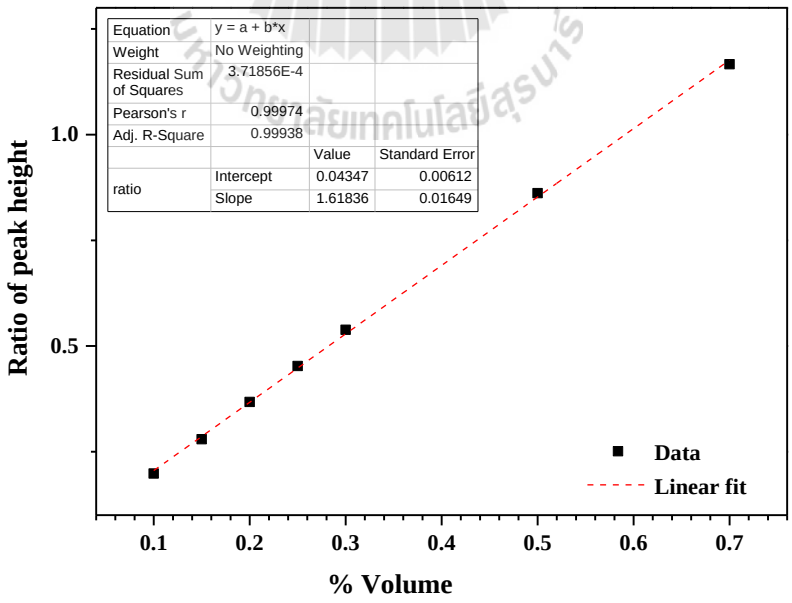

Figure B 6 The standard curve of % volume of ethanol.

CURRICULUM VITAE

Mr. KRITTANUN DEEKAMWONG

Education

2015	Research at Pohang University of Science and Technology (POSTECH), South Korea for 6 months
2013-2016	M.Sc. Candidate (Chemistry) at Suranaree University of Technology, Thailand
2012	B.Sc. (Chemistry, 1st class honors) Khon kaen University, Thailand

International Publications

Rongchapo, W., **Deekamwong, K.**, Loiha, S., Prayoonpokarach, S. and Wittayakun, J. (2015). Paraquat adsorption on NaX and Al-MCM-41. Water Science & Technology. 71(9): 1347 – 1353.

Deekamwong, K. and Wittayakun, J. (2016). Template removal from as-synthesized siliceous MCM-41 from microwave-assisted method. Microporous and Mesoporous materials. (Manuscript)

National Publications

Pantupho, W., **Deekamwong, K.,** Prayoonpokarach, S., Wittayakun, J. and Loiha, S. (2016). Effects of Iron Species on Catalytic Performance for Phenol Hydroxylation of Fe-MCM-41. KKU Science Journal. 44(1): 175 – 188.